Deep mantle structure as a reference frame for movements in and on the Earth

Trond H. Torsvik[a,b,c,d,1], Rob van der Voo[b,e], Pavel V. Doubrovine[a,b], Kevin Burke[b,d,f], Bernhard Steinberger[a,b,g], Lewis D. Ashwal[d], Reidar G. Trønnes[a,b,h], Susan J. Webb[d], and Abigail L. Bull[a]

[a]Centre for Earth Evolution and Dynamics, University of Oslo, 0316 Oslo, Norway; [b]Centre for Advanced Study, 0271 Oslo, Norway; [c]Geodynamics, Geological Survey of Norway, 7491 Trondheim, Norway; [d]School of Geosciences, University of the Witwatersrand, WITS 2050 Johannesburg WITS 2050, South Africa; [e]Department of Earth and Environmental Sciences, University of Michigan, Ann Arbor, MI 48109; [f]Department of Geosciences, University of Houston, Houston, Texas 77204; [g]Helmholtz Centre Potsdam, GFZ German Research Centre for Geosciences, 14473 Potsdam, Germany; and [h]Natural History Museum, University of Oslo, 0318 Oslo, Norway

Edited by John Suppe, National Taiwan University, Taipei, Taiwan, and approved May 8, 2014 (received for review September 27, 2013)

Earth's residual geoid is dominated by a degree-2 mode, with elevated regions above large low shear-wave velocity provinces on the core–mantle boundary beneath Africa and the Pacific. The edges of these deep mantle bodies, when projected radially to the Earth's surface, correlate with the reconstructed positions of large igneous provinces and kimberlites since Pangea formed about 320 million years ago. Using this surface-to-core–mantle boundary correlation to locate continents in longitude and a novel iterative approach for defining a paleomagnetic reference frame corrected for true polar wander, we have developed a model for absolute plate motion back to earliest Paleozoic time (540 Ma). For the Paleozoic, we have identified six phases of slow, oscillatory true polar wander during which the Earth's axis of minimum moment of inertia was similar to that of Mesozoic times. The rates of Paleozoic true polar wander (<1°/My) are compatible with those in the Mesozoic, but absolute plate velocities are, on average, twice as high. Our reconstructions generate geologically plausible scenarios, with large igneous provinces and kimberlites sourced from the margins of the large low shear-wave velocity provinces, as in Mesozoic and Cenozoic times. This absolute kinematic model suggests that a degree-2 convection mode within the Earth's mantle may have operated throughout the entire Phanerozoic.

plate reconstructions | thermochemical piles

Two equatorial, antipodal, large low shear-wave velocity provinces (Fig. 1) in the lowermost mantle (1) beneath Africa (termed Tuzo) (2) and the Pacific Ocean (Jason) are prominent in all shear-wave tomographic models (3–7) and have been argued to be related to a dominant degree-2 pattern of mantle convection that has been stable for long times (3). Most reconstructed large igneous provinces and kimberlites over the past 300 My have erupted directly above the margins of Tuzo and Jason, which we term the plume generation zones (1, 2, 5). This remarkable correlation suggests that the two deep mantle structures have been stable for at least 300 My. Stability before Pangea (before 320 Ma) is difficult to test with plate reconstructions because the paleogeography, the longitudinal positions of continents, and the estimates of true polar wander are uncertain (8). It is similarly challenging to reproduce such long-term stability in numerical models (9). However, if the correlation between the eruption sites of large igneous provinces, kimberlites, and the plume generation zones observed for the past 300 Ma has been maintained over the entire Phanerozoic (0–540 Ma), it can provide a crucial constraint for defining the longitudinal positions of continental blocks during Paleozoic time (250–540 Ma).

Here we show that a geologically reasonable kinematic model that reconstructs continents in longitude in such a way that large igneous provinces and kimberlites are positioned above the plume generation zones at the times of their formation (Fig. 2*A* and *SI Appendix*, Fig. S2) can be successfully defined for the entire Phanerozoic. This model requires that Tuzo and Jason remain nearly stationary from the early Cambrian (540 Ma) in the large-scale convection within the Earth's mantle.

Plume Generation Zones

Previous work (1, 2, 5, 10) and numerical models (9, 11) suggest that the most likely candidates for the plume generation zones in the lower mantle are those areas that correspond to the largest lateral gradients of the shear-wave velocity directly above the core–mantle boundary. Although the distribution of plume generation zones depends on the particulars of the seismic tomography model used to define them, the differences between alternative definitions are typically small (5). Torsvik and colleagues (1) used the 1% slow-velocity contour in the lowermost layer of the mean Shear-wave tomographic model SMEAN (6) to define the plume generation zones. This contour corresponds to the steepest lateral gradients of shear-wave velocity, and 80% of reconstructed large igneous provinces of the past 300 My plot within 10° of it (Fig. 1*B*).

A perhaps more robust definition of the plume generation zones can be deduced from the recently published cluster analysis of five global shear-wave tomography models (7). In this work, a "voting" map was produced that described whether a geographical location was above a seismically slower-than-average velocity region in the mantle below 1,000 km depth. The voting map (Fig. 1*B*) shows how many of the five tomographic models agree on the classification of the data point. Within contour 5, all five tomographic models show slower-than-average

Significance

Since the Pangea supercontinent formed about 320 million years ago, plumes that sourced large igneous provinces and kimberlites have been derived from the edges of two stable thermochemical reservoirs at the core–mantle boundary. We test whether it is possible to maintain this remarkable surface-to-deep Earth correlation before Pangea through the development of a new plate reconstruction method and find that our reconstructions for the past 540 million years comply with known geological and tectonic constraints (opening and closure of oceans, mountain building, and more). These results have important implications for Earth history, including the style of mantle convection in the deep past and the long-term stability of mantle reservoirs.

Author contributions: T.H.T., R.v.d.V., and P.V.D. designed research; T.H.T. and R.v.d.V. performed research; T.H.T., P.V.D., and B.S. contributed new reagents/analytic tools; T.H.T., P.V.D., K.B., B.S., L.D.A., R.G.T., S.J.W., and A.L.B. analyzed data; and T.H.T., R.v.d.V., P.V.D., K.B., B.S., L.D.A., R.G.T., S.J.W., and A.L.B. wrote the paper.

The authors declare no conflict of interest.

This article is a PNAS Direct Submission.

[1]To whom correspondence should be addressed. E-mail: t.h.torsvik@geo.uio.no.

This article contains supporting information online at www.pnas.org/lookup/suppl/doi:10.1073/pnas.1318135111/-/DCSupplemental.

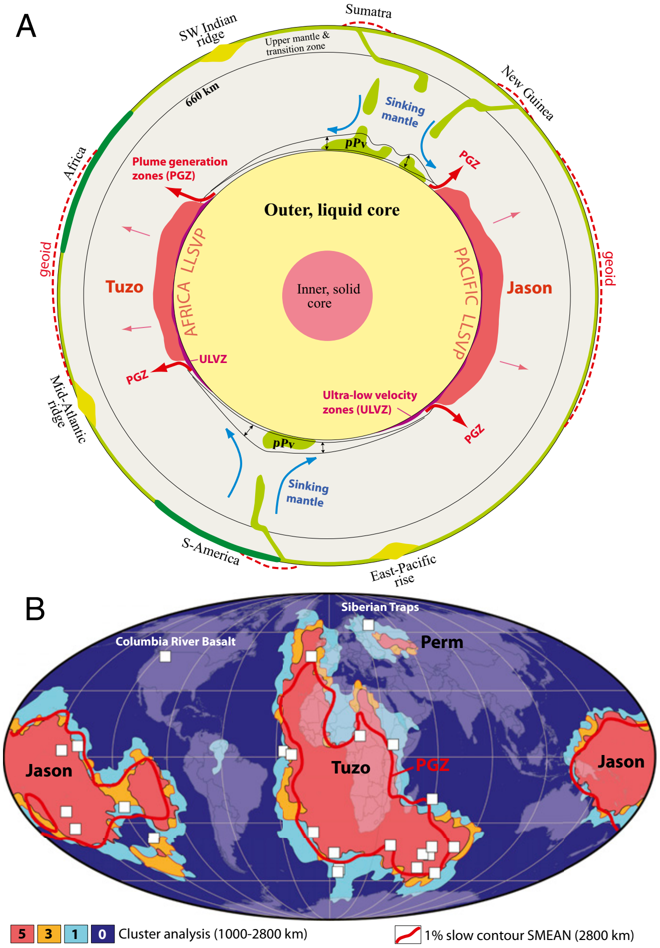

Fig. 1. (*A*) Schematic cross-section of the Earth as seen from the South Pole. The Earth's lower mantle is dominated by two antipodal large low shear-wave velocity provinces (LLSVPs) beneath Africa (Tuzo) and the Pacific (Jason). These dominate the elevated regions of the residual geoid (dashed red lines), and their margins, the plume generation zones (PGZs), are the principal source regions for large igneous provinces and kimberlites (1). The thin arrows above Tuzo and Jason are shown to indicate that the residual geoid (15) is largely a result of buoyant upwellings overlying these hot and dense mantle structures. The "pPv" (between the two lines separated by up–down arrows) indicates lenses of postperovskite (40). (*B*) Reconstructed large igneous provinces for the past 300 My (1) and the 1% slow SMEAN (6) contour (2,800 km depth) used as a proxy for the plume generation zones. Also shown are the "voting" map contours of ref. (7). Contours 5–1 (only 5, 3, and 1 are shown for clarity) define Tuzo and Jason (seismically slow regions) in addition to a smaller Perm anomaly. The Columbia River Basalt (17 My) is the only anomalous large igneous province (located above faster regions, contour 0) in these global tomographic models.

seismic velocities, whereas, for example, contour 3 outlines the area in which three of five models are in agreement. Contour 3 is similar to the 1% slow SMEAN contour (80% of large igneous provinces within 10° from both of them); however, contours 5 and 4 match the distribution of reconstructed large igneous provinces better. The cluster analysis also suggests that the ~251 Ma Siberian Traps originated from the plume generation zone of a smaller anomaly (12), now dubbed Perm (7); this anomaly is also discernible in the SMEAN model (~0.5% slow in Fig. 2*A*). For ease of comparison with earlier studies (1, 2, 5), we here use the 1% slow contour of the SMEAN model as a proxy for the plume generation zones, but we also present relevant summaries for the comparisons with the contours defined by the cluster analysis (7).

Paleozoic Plate Model

The Early Paleozoic (8) was dominated by the great continent of Gondwana. Other continents included Laurentia and Baltica (Fig. 2*A*), which fused together with the Avalonia microcontinent to form Laurussia, the second largest Paleozoic continent, after the closure of the Iapetus Ocean in the Silurian (~430 My). By the late Carboniferous (~320 My), Gondwana and Laurussia had amalgamated, forming the supercontinent of Pangea. Relative fits within Gondwana, Laurussia, and later, Pangea are reasonably well known; the sources of these reconstructions have been documented in a recent review by Torsvik and colleagues (8). In contrast, absolute Paleozoic reconstructions have remained uncertain because longitudes of continental blocks cannot be derived from paleomagnetic data (although latitudes and azimuthal orientations can). Our plate model is mainly based on apparent polar wander paths for Gondwana, Siberia, Laurentia/Baltica (Laurussia after 430 My), and their later combinations into Pangea (8). Of these paths, the Gondwana path during the Mid-Paleozoic is probably the most controversial. Euler poles were calculated from the apparent polar wander paths, and continents were reconstructed in latitude and azimuthal orientation.

Paleogeographic reconstructions relate the past configurations of continents to the Earth's spin axis (8). However, correlating the reconstructed positions of large igneous provinces and kimberlites to the plume generation zones requires reconstructions relative to the Earth's mantle. The two reference frames (paleogeographic, which we also refer to as "paleomagnetic," and the mantle frames) generally differ because over time, the solid Earth (mantle and crust) can slowly rotate with respect to the spin axis, driven by the redistribution of density heterogeneities within the solid Earth, resulting in changes of the planetary moment of inertia. This process is known as true polar wander (13). The estimates for Cenozoic and Mesozoic times (8, 14–16) suggest that the direction of true polar wander is largely controlled by the mass of the two antipodal large low shear-wave velocity provinces associated with persistent degree-2 residual geoid highs. True polar wander is therefore mainly confined to the circumpolar belt of high shear-wave velocities between Tuzo and Jason that remain close to the equator. Assuming that these deep mantle bodies have been stable over a longer time scale, we expect a similar pattern of Paleozoic polar motion, dominantly confined to the great circle passing through the geographic poles at approximately the same distance from the two large low shear-wave velocity provinces. Massive slabs, such as under North America (17), probably can contribute geoid signals of comparable magnitude, so that the pole can also move some distance toward or away from Tuzo and Jason (16).

To define the longitudes in our paleogeographic reconstructions, using the correlation between the eruption localities of large igneous provinces/kimberlites and the plume generation zones, we adopted an approach that incorporates the estimates of true polar wander that is based on the work of Steinberger and Torsvik (14) but is extended to earlier times. We compiled all dated kimberlites and large igneous provinces for the Paleozoic (*SI Appendix*, Fig. S1). For our initial model, continental longitudes in the paleomagnetic frame were defined both according to geological constraints and so that large igneous provinces or kimberlites were located directly above a plume generation zone, ignoring any possible true polar wander (and plume advection) in the Paleozoic. The next step from this idealized model was estimating true polar wander and correcting the paleogeographic reconstruction, using the obtained true polar wander rotations.

The method we used to derive the true polar wander rotations (8, 14) requires that the longitudes of the continents in the paleomagnetic frame are specified before estimating true polar wander. Because these are a priori unknown, we developed an iterative approach for defining a paleomagnetic frame, corrected

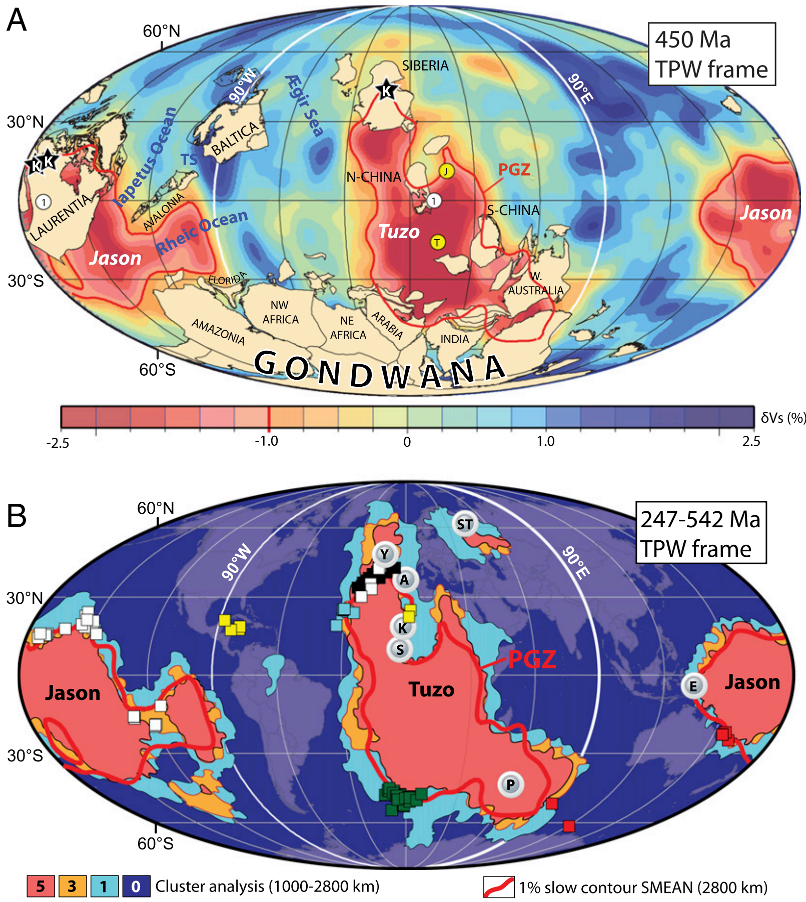

Fig. 2. (*A*), 450-My true polar wander (TPW)-corrected mantle frame reconstruction draped on the SMEAN tomographic model (6) and the plume generation zones (PGZs; 1% slow SMEAN contour). Yellow dots (marked T and J) are the center of mass (12) for Tuzo and its antipode for Jason. Open white circles (marked 1) show the preferred axis (0°N, 11°E and 169°W) for Paleozoic TPW and approximate the longitude of the minimum moment of inertia (I_{min}) axis associated with the Tuzo and Jason large low shear-wave velocity provinces, as well as the geotectonic bipolarity axis proposed by Pavoni (41). Kimberlite locations (Canada and Siberia, black stars) dated 445–455 Ma fall vertically above the plume generation zones. The 450 My reconstruction is only an example, and a paleogeographic cavalcade (*SI Appendix*, Figs. S7–S36), reconstruction parameters (*SI Appendix*, Table S1), and a GPlates (www.gplates.org) rotation file (GPlates Data File) are found in the *SI Appendix*. (*B*) Paleozoic large igneous provinces (annotated gray circles with white rings; 251–510 My) and kimberlites (colored and black and white squares; 247–542 My) reconstructed in a TPW-corrected reference frame to the exact eruption time (sixth and final iteration). Kimberlites are plotted with white (Laurentia), yellow (Baltica: Russia), black (Siberia), light blue (China blocks), green (Gondwana: South Africa), and red (Gondwana: Australia) colors. K, Kalkarindji (510 My, Australia); A, Altay-Sayan (400 My, Siberia); Y, Yakutsk (360 My, Siberia); S, Skagerrak (297 My, Europe); P, Panjal Traps (285 My, India/NW Himalaya; allochthonous); E, Emeishan (258 My, South China); ST, Siberian Traps (251 My). Background map as in Fig. 1*B*.

for true polar wander (*SI Appendix*, Fig. S3). Using our initial idealized Paleozoic reconstructions with no true polar wander, we computed net rotations of continents at 10 My steps, which were decomposed into component rotations along three orthogonal axes (8, 14). Axis 1 is at the equator at 11°E, which corresponds to the longitude axis of minimum moment of inertia of Tuzo and Jason (Fig. 2*A*). Episodes of coherent rotations about this axis were interpreted as a true polar wander signal (i.e., we assume that a dominant contribution from the stable large low shear-wave velocity provinces to the overall moment of inertia of the Earth stabilizes the orientation of the true polar wander axis over geologic time). Because the true polar wander corrections would generally degrade the large igneous province and kimberlite fits to the plume generation zones (*SI Appendix*, Fig. S3), the longitudes in the paleomagnetic frame were then redefined to produce an optimal fit after the true polar wander correction. This produced the second approximation for the longitude-calibrated paleomagnetic frame. The entire procedure of true polar wander analysis and longitude refinements was repeated six times until no further improvement was observed in the true polar wander-corrected frame. Our final iterations yielded six episodes (5–10 in Fig. 3*A*) of Paleozoic true polar wander along a great circle around an equatorial axis at 11°E; this iterative procedure generates two sets of Paleozoic reconstructions: one that describes configurations of continents relative to the spin axis (paleogeography) and one in which paleogeographic reconstructions were corrected for true polar wander (Fig. 2*A*), describing plate motions relative to the Earth's mantle (*SI Appendix*, Figs. S7–S36). As an example of the latter, we show a 450 Ma reconstruction at a time when the continents were spread over a large part of the globe (Fig. 2*A*). At this time, the Iapetus Ocean separated Baltica and Avalonia from Laurentia, which itself was separated from Gondwana by the wide Rheic Ocean.

Source Regions for Paleozoic Large Igneous Provinces and Kimberlites

In our final model (*SI Appendix*, Table S1), North American and Russian (Baltican) kimberlites were sourced from the Jason plume generation zone in the early-mid Paleozoic, whereas the Late Paleozoic (~290–250 Ma) kimberlites were sourced from the Tuzo plume generation zone (*SI Appendix*, Figs. S7–S36). Conversely, Cambrian large igneous provinces and kimberlites

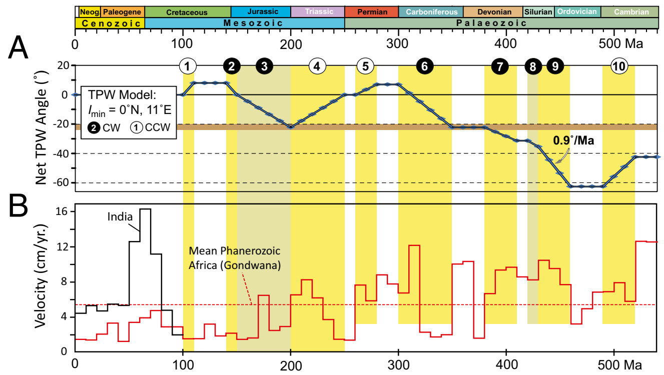

Fig. 3. (*A*) We model 10 Phanerozoic phases of clockwise (CW) and counter clockwise (CCW) rotations (TPW, true polar wander) around 0°N, 11°E: (1) 110–100 My: +8°; (2) 150–140 My: −8°; (3) 200–150 My: −22°; (4) 250–200 My: +22°; (5) 280–260 My: +7°; (6) 350–300 My: −29°; (7) 410–380 My: −9°; (8) 430–420 My: −4°; (9) 460–430 My: −27°; (10) 520–490 My: +20°. TPW phases 1–4 updated from refs. 8 and 14. The brown belt corresponds to a pole location near the I_{max} axis of both large low shear-wave velocity provinces (15). (*B*) Phanerozoic plate velocities for a central location in Africa/Gondwana (8°N, 19°E), based on Paleozoic (this study) and Mesozoic (8) TPW-corrected reference frames and a moving hotspot frame after 125 Ma (16). Average velocities are higher than for Mesozoic–Cenozoic times, but for comparison, we also show plate velocities for a central location in India (22°N, 76°E) for the past 100 My (16). Between 70 and 60 Ma, India shows a velocity burst of more than 16 cm/y.

from South Africa were sourced by the Tuzo plume generation zone, and a short-lived kimberlite event (380–370 Ma) in Australia was sourced by the Jason plume generation zone. All large igneous provinces and kimberlites from Siberia and China come from the Tuzo and Perm plume generation zone except the Emeishan large igneous province in South China (5), sourced from the Jason plume generation zone at 258 Ma. Whenever possible, large igneous provinces and kimberlites were modeled to be located directly above the plume generation zones, but some positions were selected as a compromise between multiple kimberlite and large igneous province sites. The largest deviation from a plume generation zone was observed for ∼400 Ma Russian kimberlites (yellow squares in Fig. 2*B*) because we fitted similar-aged kimberlites in North America to the Jason plume generation zone. Both areas were part of Laurussia, and our choice maintains more credible plate velocities for Laurussia (*SI Appendix*, Fig. S5*A*). The Panjal Traps (allochtonous) and the Siberian Traps were not modeled (forced) to be located directly above the margins of Tuzo.

In the true polar wander-corrected frame, five of seven Paleozoic large igneous provinces plot within 5° of the plume generation zones, and one (Panjal Traps) plots 11.2° away. Of 231 kimberlites, 98% plot within 10° of a plume generation zone (Fig. 2*B* and *SI Appendix*, Table S2). Although our longitude fitting method used the 1% slow SMEAN contour (6) as a proxy for the plume generation zones, the statistical correlation is similar and even improved compared with the seismic voting map contours (7). As an example, all large igneous provinces (including the Siberian Traps) plot within 10° of contour 4 (Fig. 2*B* and *SI Appendix*, Table S2).

Plate Velocities and Rates of True Polar Wander

Our Paleozoic model is consistent with the geological surface record of the opening and closure of the main Paleozoic Oceans. However, the developing Iapetus Ocean in Cambrian times is uncertain because of poor or absent data (notably from Baltica). Current Cambrian paleogeography and plate velocity estimates should therefore be viewed with caution.

Plate velocities calculated for central locations in Gondwana, Laurentia, Baltica, their later amalgamation into Laurussia, and Siberia are below 20 cm/y (*SI Appendix*, Figs. S4 and S5), but the average velocities are about twice as high (Fig. 3*B*) as those in Mesozoic and Cenozoic times (18, 19). The most extreme velocities in our model are seen for parts of peri-Gondwana and, notably, Australia (*SI Appendix*, Fig. S5*B*). Angular rotations are also high, with Gondwana rotating strongly counterclockwise in the Cambrian and clockwise in Late Ordovician/Silurian times. True polar wander corrections led to smaller/slower angular rotations, but they are still pronounced in our Paleozoic model. Higher-than-normal plate velocities (Fig. 3*B*) may arise from our longitude calibration method or a combination of poor paleomagnetic data (recording north–south velocity only) and inadequate true polar wander corrections. We model 10 phases of slow (≤0.9°/My; ≤10 cm/y) and oscillatory true polar wander for the entire Phanerozoic, but net true polar wander rotations peak at −62° in the Ordovician (Fig. 3*A*). True polar wander estimates before the Carboniferous (360–540 My), however, should be treated with caution because the continental masses were dominantly in the southern hemisphere at polar latitudes (*SI Appendix*, Fig. S6). It is, therefore, difficult to differentiate between north–south plate motion and true polar wander without assuming a specific location of the axis of minimal moment of inertia, I_{min}. For example, Mitchell and colleagues (20) postulated that I_{min} was 90° further to the east during much of the Paleozoic, migrating westward to its present position between 370 and 260 Ma. Their reconstructions, using very different assumptions and "locking" Australia near the equator at 110°E (assumed I_{min} longitude) from 500–390 Ma, may at times show some similarities with ours, but their model features fast plate velocities (except for Australia), and overall, the reconstructed large igneous provinces and kimberlites are uncorrelated with the margins of Tuzo and Jason (only 30% within 10° from their margins).

Before true polar wander correction, absolute plate velocities for a central location in Africa show velocity spikes (∼15 cm/y) in the Late Cambrian, Silurian, and Late Carboniferous (*SI Appendix*, Fig. S4). The latter, however, is linked to north–south motion based on paleomagnetic inclination data alone and, thus, is not a result of longitude calibrations. African (Gondwanan) plate velocities are reduced after true polar wander correction, averaging 7.3 cm/y, and only the Late Carboniferous (320–310 Ma) spike, reduced to ∼12 cm/y, remains (Fig. 3*B* and *SI Appendix*, Fig. S4). For a central location in North America, we note in our true polar wander-corrected reconstructions a Late Silurian–Early Devonian (420–410 Ma) velocity spike (∼17 cm/y; *SI Appendix*, Fig. S5*A*) shortly after the formation of Laurussia (Baltica–Avalonia merging with Laurentia); this peak also occurs in the north–south motion of Laurussia (∼10 cm/y in North America) and is therefore not an artifact of longitude calibrations. Laurussia must have drifted eastward from the Late Devonian to source Late Paleozoic kimberlites, mostly Canadian, and the Skagerrak Centered large igneous province (∼297 Ma) from the Tuzo PGZ. The modeled change from the Jason to the Tuzo plume generation zone requires plate velocities of 10–17 cm/y (370–310 Ma; *SI Appendix*, Fig. S5*A*). These modeled velocities are certainly higher than those that would be normally expected for large continental blocks, except for the high velocities recorded for India in Late Mesozoic/Early Cenozoic times (Fig. 3*B*).

Most large igneous provinces and kimberlites plot within 10° of a plume generation zone in our model (Fig. 2*B* and *SI Appendix*, Table S2). We note that for more recent times after Pangea assembly, when plate motions are better constrained, we are not able to fit all large igneous provinces and kimberlites above the margins of Tuzo and Jason, particularly Late Cretaceous and Early Tertiary kimberlites in North America (1), the Columbia River Basalt, and Siberian Traps (Fig. 1*B*). Likewise, it is possible that some of the earlier large igneous provinces and kimberlites we are fitting here do not originate directly above these margins. Relaxing this constraint to fit most large igneous provinces and kimberlites precisely over the margins of Tuzo and Jason could yield plate reconstructions with slower plate motions. However, we prefer not to take such an approach here because it would introduce arbitrariness.

Another potential source of uncertainty in our reconstructions is the geometry of Pangea in the Late Paleozoic. We model an Early Carboniferous Pangea B type configuration (Laurussia located "west" of Gondwana; *SI Appendix*, Figs. S25–S29), evolving into a Pangea A-type configuration at 320 Ma (19, 21). Conversely, Muttoni and colleagues (22) maintain a Pangea B fit between ~300 and 270 Ma, with Laurussia located 5,000 km "west" of Gondwana (*SI Appendix*, Fig. S37). There are few large igneous provinces, and kimberlites erupted between 320 and 270 Ma, but they do show a better fit to a plume generation zone in a Pangea A configuration. However, a slightly younger transition from Pangea B to A could reduce the Carboniferous velocities for Laurussia.

Sources of True Polar Wander

Adding dense material in the upper mantle at intermediate to high latitudes must be a prime candidate for causing true polar wander, and geoid kernel modeling (15, 23) suggests that the maximum effect is achieved 30–40 My after subduction initiation, when slabs arrive in the transition zone (Fig. 4*A*). The effect of slabs in the lower mantle is expected to be smaller, because thermal expansivity of mantle material becomes smaller with depth. However, this may be partly compensated for by a larger amount of slabs in the lower mantle as a result of lower sinking speeds. The exact shape of geoid kernels depends on viscosity structure and phase boundary parameters (Clapeyron slope, density jump, thermal expansivity); however, a degree-2 kernel that is positive in the upper part of the mantle and negative in its lower part is a robust feature of mantle models that successfully reproduce large-scale features of the geoid (24–26). Hence, we expect that the intermediate- to high-latitude subduction would preferentially induce true polar wander so that subduction zones shift toward the equator, possibly with some time delay (Fig. 4*A*).

Between 520 and 490 My, we find counter-clockwise true polar wander rotation, which could be related to subduction primarily occurring in the lower right quadrant of the maps shown in the top panels of *SI Appendix*, Figs. S9–S12, during those or somewhat earlier times. For the period 460–300 Ma, a clockwise rotation corresponds to subduction occurring in the lower left quadrant (*SI Appendix*, Figs. S15–S29, *Upper*) related to the closure of the Iapetus and Rheic oceans (Fig. 2*A*). In particular, extensive intermediate- to high-latitude peri-Gondwanan subduction in Late Cambrian–Early Ordovician times (Fig. 4*B*) provides a simple explanation for the "high" rates of true polar wander between 460 and 430 Ma (0.9°/My; Fig. 3). However, a systematic study of how subduction zone locations relate to true polar wander (27, 28) would require full plate reconstructions (not just locations of continents) and is not attempted here.

The overall true polar wander signal dating from 540 Ma can be interpreted as oscillatory swings approximately around the same axis (0°N, 11°E), centered on a rotation angle of ~22° (Fig. 3), which corresponds to a pole location near the axis of maximum moment of inertia for the combined masses of Tuzo and Jason. This pole location would be expected if the Earth's moment of inertia were defined by the contribution from Tuzo and Jason alone (15). Deviations from that location can be explained by subduction (15), but because of persistent triaxial shape or lithospheric elasticity (27), the pole would have a tendency to return to its original location after the termination of subduction. This mechanism can complement the true polar wander forced

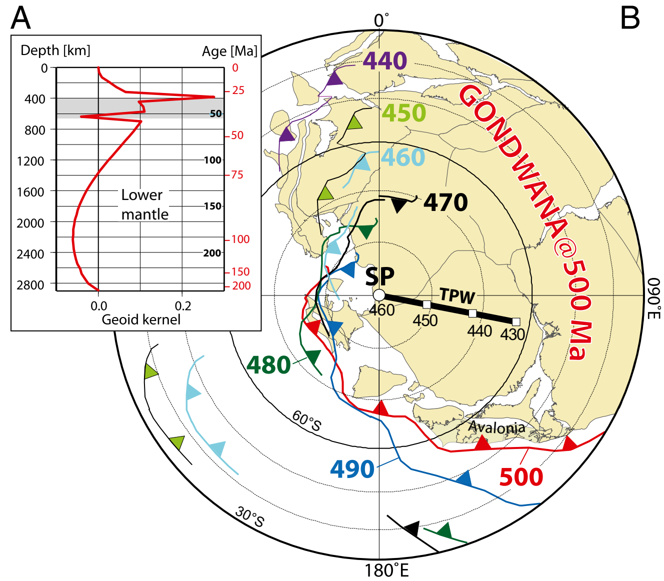

Fig. 4. (*A*) Geoid kernel (Model-I in ref. 15) and the corresponding age–depth relationship for sinking slabs (red numbers). We also show the age–depth relationship (black numbers) suggested by van der Meer and colleagues (42) for Mesozoic–Cenozoic times. Geoid kernels are for total (thermal plus chemical) density anomaly and include the effect of density anomalies themselves and displaced boundaries (surface and core–mantle boundary). Positive geoid associated with large low shear-wave velocity provinces hence implies that the effect of the thermal anomaly, partly in the mantle above and in the form of rising plumes, overcompensates any effect of compositionally heavier material. The transition zone (410–660 km) is shown in dark gray shading. (*B*) The south-pole (SP) of the paleomagnetic frame was located in north Africa in the Late Cambrian (~500 My). Peri-Gondwana subduction is shown as teeth on thin lines and marks trench locations in the paleomagnetic reference frame. The teeth are in the upper plate and indicate the polarity of subduction. Outboard Avalonia, for instance, was adjacent to subduction at high latitudes at 500 Ma (red line and teeth). This pattern of high-latitude subduction continued during the Ordovician but shifted toward lower latitudes (<60°S) by the Early Silurian (~440 My). The trench length, and hence the volume of dense material sinking into the upper mantle, were also reduced during the Ordovician.

by ongoing subduction, providing an explanation for its oscillatory nature in more recent times (16).

Long-Term Stability of Deep Mantle Structures

The two antipodal large low shear-wave velocity provinces, Tuzo and Jason, must impose strong and long-lived control on Earth's thermal, magmatic, magnetic, and rotational dynamics; they may organize the global mantle flow (3, 29), and their edges are favorable sites for the initiation of deep mantle plumes (9–12). A thermochemical constitution of Tuzo and Jason is supported by geochemical observations of multiple chemical reservoirs at depth, strong seismic contrasts, an anticorrelation of shear-wave velocity to bulk sound velocity, and increased density in these regions (4, 30–33). Although a few recent studies argued that all these observations could be explained by thermal anomalies alone (e.g., ref. 34), the long-term stability of Tuzo and Jason is highly unlikely for purely thermal features.

Whereas recycled oceanic crust of basaltic composition may be a candidate material for at least part of Tuzo and Jason, peridotitic materials enriched in iron and perovskite provide a better fit to the seismic properties (35). Magmatic segregations of Fe-rich peridotitic or komatiitic materials could most easily have formed during early magma ocean crystallization or shortly afterward (36–39). Our reconstructions, in which Tuzo and Jason appear to have been stable throughout the Phanerozoic, suggest that a very early origin of these deep mantle structures is a viable hypothesis, and our approach can potentially be paleomagnetically extended to the assembly of Rodinia, about 1 billion years ago.

We would like to stress that the Paleozoic model developed here is a kinematic model for the continents and that the next step in improving it will be developing a global model for the entire lithosphere (including synthetic oceanic lithosphere). This is challenging for the Paleozoic (19) but is essential for assessing whether our model is tectonically and geodynamically plausible, testing the potential longevity of Tuzo and Jason through numerical modeling and comparing the modeled estimates of true polar wander because of subduction with those inferred from comparisons of plate reconstructions in the mantle and paleomagnetic reference frames.

ACKNOWLEDGMENTS. We thank Dennis Kent and two anonymous reviewers for helpful comments. The Centre for Advanced Study (Oslo), the Research Council of Norway, through its Centres of Excellence funding scheme, and the European Research Council, under the European Union's Seventh Framework Programme (FP7/2007-2013)/ERC Advanced Grant Agreement Number 267631 (Beyond Plate Tectonics), are acknowledged for financial support.

1. Torsvik TH, Burke K, Steinberger B, Webb SJ, Ashwal LD (2010) Diamonds sampled by plumes from the core-mantle boundary. *Nature* 466(7304):352–355.
2. Burke K (2011) Plate Tectonics, the Wilson Cycle, and Mantle Plumes: Geodynamics from the Top. *Ann Rev Earth Planet Sci* 39:1–29.
3. Dziewonski AM, Lekic V, Romanowicz BA (2010) Mantle Anchor Structure: An argument for bottom up tectonics. *Earth Planet Sci Lett* 299:69–79.
4. Lay T, Garnero EJ (2011) Deep Mantle Seismic Modeling and Imaging. *Annu Rev Earth Planet Sci* 39:91–123.
5. Torsvik TH, Steinberger B, Cocks LRM, Burke K (2008) Longitude: Linking Earth's ancient surface to its deep interior. *Earth Planet Sci Lett* 276:273–283.
6. Becker TW, Boschi L (2002) A comparison of tomographic and geodynamic mantle models. *Geochem Geophys Geosyst* 3:GC000168.
7. Lekic V, Cottar S, Dziewonski A, Romanowicz B (2012) Cluster analysis of global lower mantle tomography: A new class of structure and implications for chemical heterogeneity. *Earth Planet Sci Lett* 357:68–77.
8. Torsvik TH, et al. (2012) Phanerozoic polar wander, paleogeography and dynamics. *Earth Sci Rev* 114:325–368.
9. Tan E, Leng W, Zhong S, Gurnis M (2011) On the location of plumes and mobility of thermo-chemical structures with high bulk modulus in the 3-D compressible mantle. *Geochem Geophys Geosyst* 12:Q07005.
10. Thorne MS, Garnero EJ, Grand S (2004) Geographic correlation between hot spots and deep mantle lateral shear-wave velocity gradients. *Phys Earth Planet Inter* 146:47–63.
11. Steinberger B, Torsvik TH (2012) A geodynamic model of plumes from the margins of Large Low Shear Velocity Provinces. *Geochem Geophys Geosyst* 13:GC003808.
12. Burke K, Steinberger B, Torsvik TH, Smethurst MA (2008) Plume Generation Zones at the margins of Large Low Shear Velocity Provinces on the Core-Mantle Boundary. *Earth Planet Sci Lett* 265:49–60.
13. Goldreich P, Toomre A (1969) Some remarks on polar wandering. *J Geophys Res* 74: 2555–2569.
14. Steinberger B, Torsvik TH (2008) Absolute plate motions and true polar wander in the absence of hotspot tracks. *Nature* 452(7187):620–623.
15. Steinberger B, Torsvik TH (2010) Toward an explanation for the present and past locations of the poles. *Geochem Geophys Geosyst* 11:GC002889.
16. Doubrovine PV, Steinberger B, Torsvik TH (2012) Absolute plate motions in a reference frame defined by moving hotspots in the Pacific, Atlantic and Indian oceans. *J Geophys Res* 117:B09101.
17. Sigloch K, Mihalynuk MG (2013) Intra-oceanic subduction shaped the assembly of Cordilleran North America. *Nature* 496(7443):50–56.
18. Gurnis M, Torsvik TH (1994) Rapid drift of large continents during the late Precambrian and Palaeozoic: Palaeomagnetic constraints and dynamic models. *Geology* 22: 1023–1026.
19. Domeier M, Torsvik TH (2014) Focus Review Paper: Plate kinematics of the Late Paleozoic. *Geoscience Frontiers* 5:303–350.
20. Mitchell RN, Kilian TM, Evans DAD (2012) Supercontinent cycles and the calculation of absolute palaeolongitude in deep time. *Nature* 482(7384):208–211.
21. Domeier M, Van der Voo R, Torsvik TH (2012) Review Article: Paleomagnetism and Pangea: The Road to reconciliation. *Tectonophysics* 514-517:14–43.
22. Muttoni G, et al. (2009) Opening of the Neo-Tethys Ocean and the Pangea B to Pangea A transformation during the Permian. *GeoArabia* 14:17–48.
23. Hager BH (1984) Subducted slabs and the geoid: Constraints on mantle rheology and flow. *J Geophys Res* 89:6003–6015.
24. Hager BH, Richards MS (1989) Seismic Tomography and Mantle Circulation. *Philosoph Trans R Soc Lond Series A* 328:309–327.
25. Steinberger B, Calderwood A (2006) Models of large-scale viscous flow in the Earth's mantle with constraints from mineral physics and surface observations. *Geophys J Int* 167:1461–1481.
26. Steinberger B, Holme R (2008) Mantle flow models with core-mantle boundary constraints and chemical heterogeneities in the lowermost mantle. *J Geophys Res* 113: B05403.
27. Creveling JR, Mitrovica JX, Chan N-H, Latychev K, Matsuyama I (2012) Mechanisms for oscillatory true polar wander. *Nature* 491(7423):244–248.
28. Evans DAD (2003) True polar wander and supercontinents. *Tectonophysics* 362: 303–320.
29. Conrad CP, Steinberger B, Torsvik TH (2013) Stability of active mantle upwelling revealed by net characteristics of plate tectonics. *Nature* 498(7455):479–482.
30. Hofman AW (1997) Mantle geochemistry: The message from oceanic volcanism. *Nature* 385:219–229.
31. Wang Y, Wen L (2004) Mapping the geometry and geographic distribution of a very low velocity province at the base of the Earth's mantle. *J Geophys Res* 109:B10305.
32. Ishii M, Tromp J (1999) Normal-mode and free-Air gravity constraints on lateral variations in velocity and density of Earth's mantle. *Science* 285(5431):1231–1236.
33. Hernlund JW, Houser C (2008) On the statistical distribution of seismic velocities in Earth's deep mantle. *Earth Planet Sci Lett* 265:423–437.
34. Davies DR, et al. (2012) Reconciling dynamic and seismic models of Earth's lower mantle: The dominant role of thermal heterogeneity. *Earth Planet Sci Lett* 353: 253–269.
35. Deschamps F, Cobden L, Tackley PJ (2012) The primitive nature of large low shear wave velocity provinces. *Earth Planet Sci Lett* 349-350:198–208.
36. Labrosse S, Hernlund JW, Coltice N (2007) A crystallizing dense magma ocean at the base of the Earth's mantle. *Nature* 450(7171):866–869.
37. Stixrude L, de Koker N, Sun N, Mookherjee M, Karki BB (2009) Thermodynamics of silicate liquids in the deep Earth. *Earth Planet Sci Lett* 278:226–232.
38. Lee CT, et al. (2010) Upside-down differentiation and generation of a 'primordial' lower mantle. *Nature* 463(7283):930–933.
39. Liebske C, Frost DJ (2012) Melting phase relations in the MgO–$MgSiO_3$ system between 16 and 26 GPa: Implications for melting in Earth's deep interior. *Earth Planet Sci Lett* 345-348:159–170.
40. Trønnes RG (2010) Structure, mineralogy and dynamics of the lowermost mantle. *Min Petrol* 99:243–261.
41. Pavoni N (1985) Pacific/anti - Pacific bipolarity in the structure of the Earth's mantle. *Eos Trans AGU* 66:497.
42. van der Meer D, Spakman W, van Hinsbergen DJJ, Amaru ML, Torsvik TH (2010) Absolute plate motions since the Permian inferred from lower mantle slab remnants. *Nat Geosci* 3:36–40.

Supporting Information

Torsvik et al.

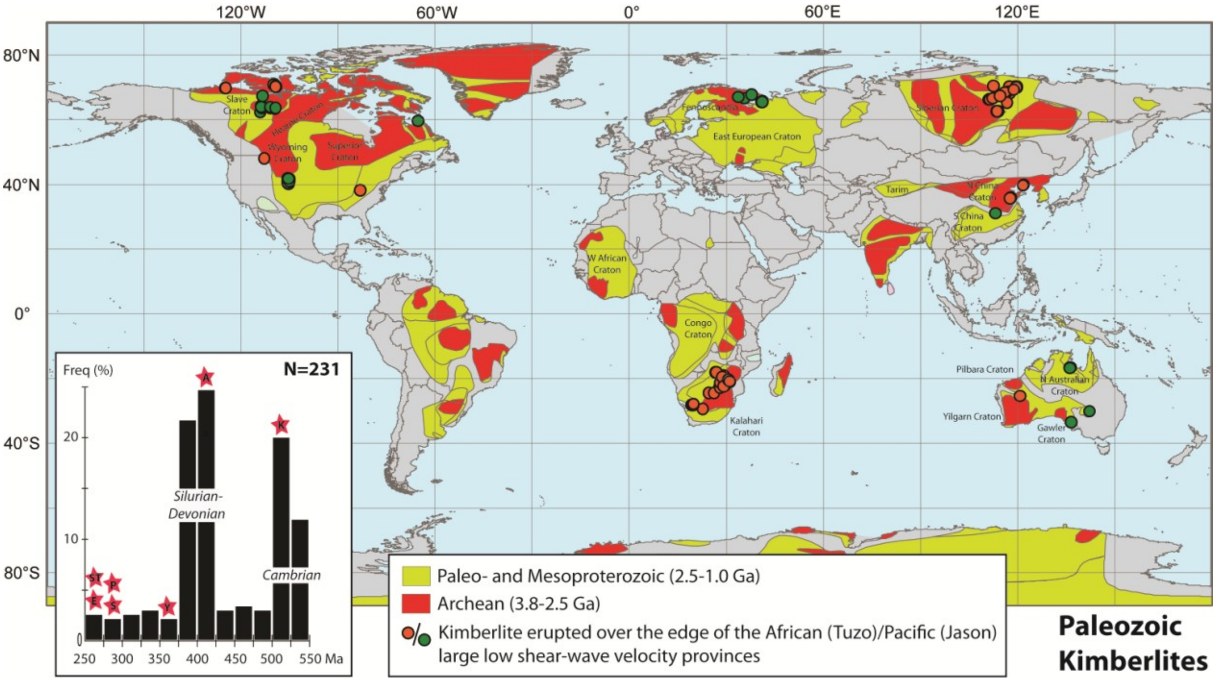

Fig. S1 Kimberlite locations in Laurentia, Baltica, Siberia, Australia, Africa and China (one symbol may represent multiple kimberlite sites), and a general overview of cratons (1) older than 1 Ga. The inset shows the distribution of kimberlites (2) over Phanerozoic time, with red annotated stars denoting occurrences of large igneous provinces. Kimberlites are color coded to indicate if they were sourced by plumes from the edge of the African (red dots) or Pacific (green dots) large slow shear-wave velocity province based on our plate reconstructions (Figs. S7-36). The majority of Paleozoic kimberlites erupted between 400 and 375 Ma (Silurian and Devonian), and between 550 and 500 Ma (Cambrian).

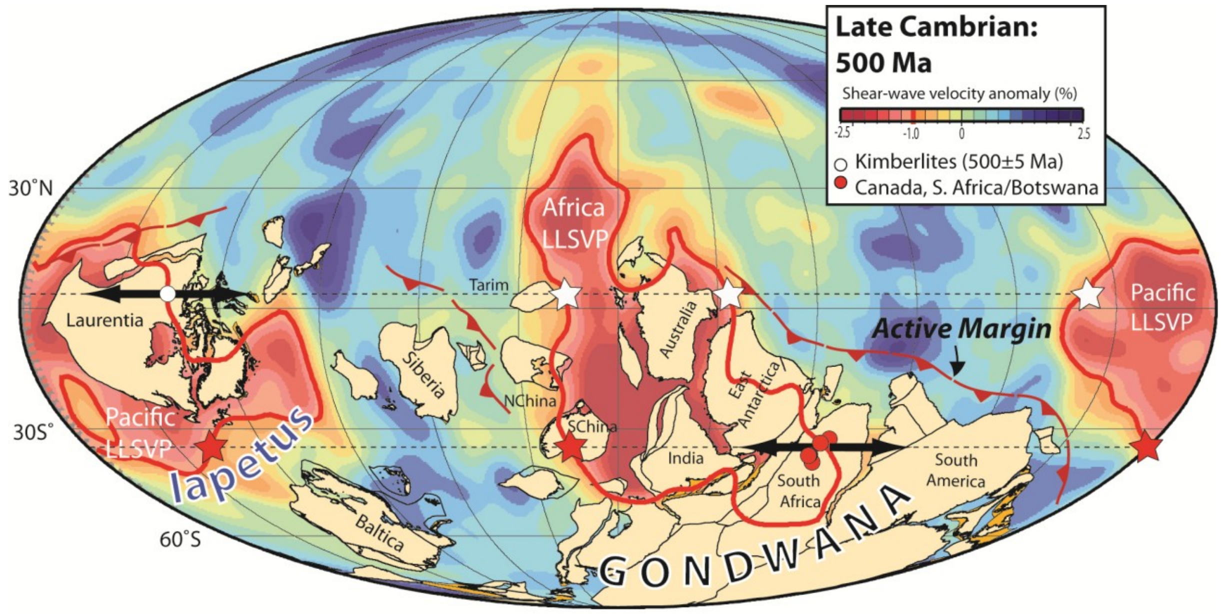

Fig. S2. Late Cambrian reconstruction demonstrating the plume generation zone reconstruction method. We assume a degree-2 mode Earth, stable African (Tuzo) and Pacific (Jason) large slow shear-wave velocity provinces (LLSVPs), and kimberlites in South Africa (part of Gondwana) and Canada (Laurentia) sourced from plumes from their margins, the plume generation zones (3, 4). The 1% low velocity contour (thick red line) in the lowermost layer of the SMEAN tomography model (5) is a good proxy for the plume generation zones (2, 6). There are four longitude options for both Laurentia and Gondwana but our initial option is indicated by the reconstructed kimberlites (white and red dots vs. alternative white and red stars). The reconstruction here is not corrected for true polar wander. True polar wander is the motion of the geographic pole in a reference frame representative of the entire solid Earth (mantle and crust). Both the LLSVPs (mantle) and the crust are affected by true polar wander but the LLSVPs are kept fixed in the mantle in our correlative exercises (Figs. S7-26), and the motion of the continents (crust) ***must*** therefore be corrected for true polar wander.

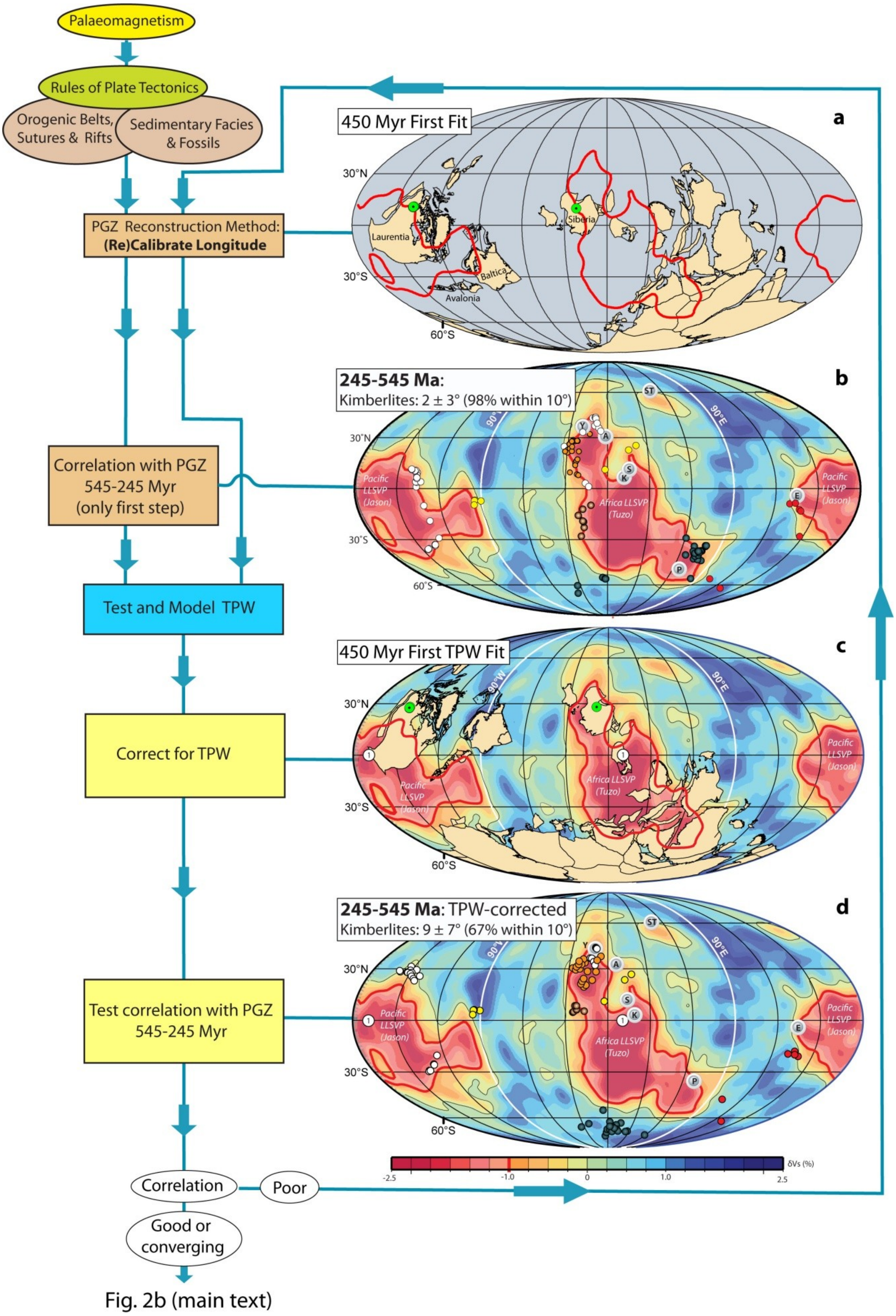

Fig. S3. Workflow for calibrating Paleozoic longitude. **a,** Kimberlite locations (large green circles with black center dots) were used to calibrate continents in longitude so that they fall vertically above the SMEAN 1% low contours (the plume generation zones, PGZs, shown by the thick red lines). In this Late Ordovician (450 Ma) example, kimberlite sites in Canada (part of Laurentia) and Siberia were fitted in longitude above a PGZ. This was our initial ('first') model. Latitude and orientation of the major plates are constrained by paleomagnetic data and the 'first' Paleozoic model attempts to produce a geologically sensible scenario conforming to the rules of plate tectonics.

b, Correlation between the reconstructed positions of Paleozoic large igneous provinces (LIPs) and the PGZs, except the Panjal (P) and Siberian Traps (ST), were used to position continents in longitude. Most kimberlites in this ideal degree-2 Earth model with no TPW were used to reconstruct the continents so that the kimberlites were directly above the PGZ but some fits were defined as a compromise between multiple kimberlite locations and reasonable plate velocities. On average kimberlites plot within 2 ± 3^{o} from a PGZ with 98% within a distance of 10^{o}. Annotated LIPs: K, Kalkarindji (Australia, 510 Ma); A, Altay-Sayan (Siberia, 400 Ma); Y, Yakutsk (Siberia, 360 Ma); S, Skagerrak (Europe, 297 Ma); P, Panjal Traps (India/Himalaya, 285 Ma); E, Emeishan (South China, 258 Ma); ST, Siberian Traps (Siberia, 251 Ma). LIP details in Eldholm & Coffin (8), Torsvik et al. (4, 9), Cauvet et al. (10) (Panjal Traps) and Kuzmin et al. (11) (Altay-Sayan).

c, From our first model we estimated true polar wander (TPW) using a Mesozoic model (12, 13) extended to the Paleozoic, where I_{min} is located at ~11^{o}E and 169^{o}W at equator (white circles denoted 1) and close to the center of the African and the near antipodal Pacific LLSVP. We identified several phases of TPW and produced the first TPW corrected reconstructions, here a 450 Ma example.

d, Reconstruction of all Paleozoic kimberlites (N=231) and LIPs (N=7) based on our first TPW-corrected model. LIPs plot within 2.4 ± 2.1^{o} (except the Siberian Traps) from a PGZ. Kimberlites plot on average 9 ± 7^{o} from a PGZ with 67% within a distance of 10^{o}. This is unmistakably worse than our ideal starting point for a planet with no TPW (a, b) and iteration is required to improve the TPW corrected correlation (d) versus the non-corrected correlation (b). After six iterations, moving the continents in the paleomagnetic reference frame not corrected for TPW (as in (a)) eastward or westward in one million year steps we reached a good and converging correlation in the TPW-corrected frame (see main text and Fig. 2b).

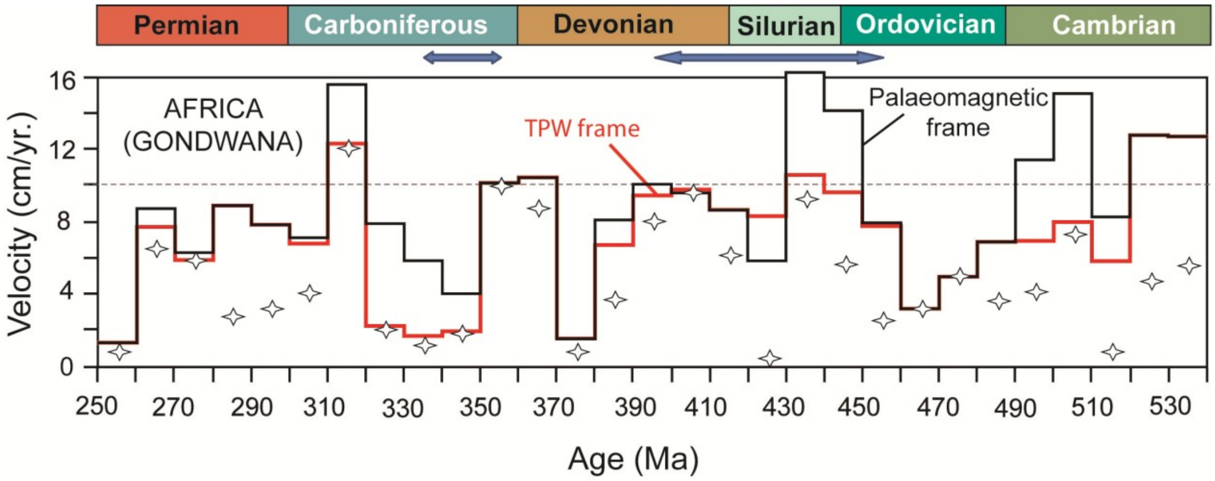

Fig. S4. Paleozoic plate velocities for Africa (Gondwana). Paleozoic time-scale (14) and absolute plate velocity for a central location in Gondwana/Africa (8^{o}N, 19^{o}E). Plate velocity was calculated before (black line) and after (red line) true polar wander (TPW) correction. Before TPW correction, plate velocities show spikes (~15 cm/yr) in the Late Cambrian, Silurian and the Late Carboniferous; only the latter (320-310 Ma) spike remains after TPW correction, but is reduced to ~12 cm/yr. (mean velocity is 7.3 cm/yr). The star symbols show north-south velocities (after TPW correction) based on paleomagnetic inclination data alone (12); these are generally below 10 cm/yr. (average north-south velocity = 4.7 cm/yr.) for a central location in Gondwana. The blue horizontal arrows show times when the paleomagnetic data coverage from Gondwana is poor or non-existing (interpolated).

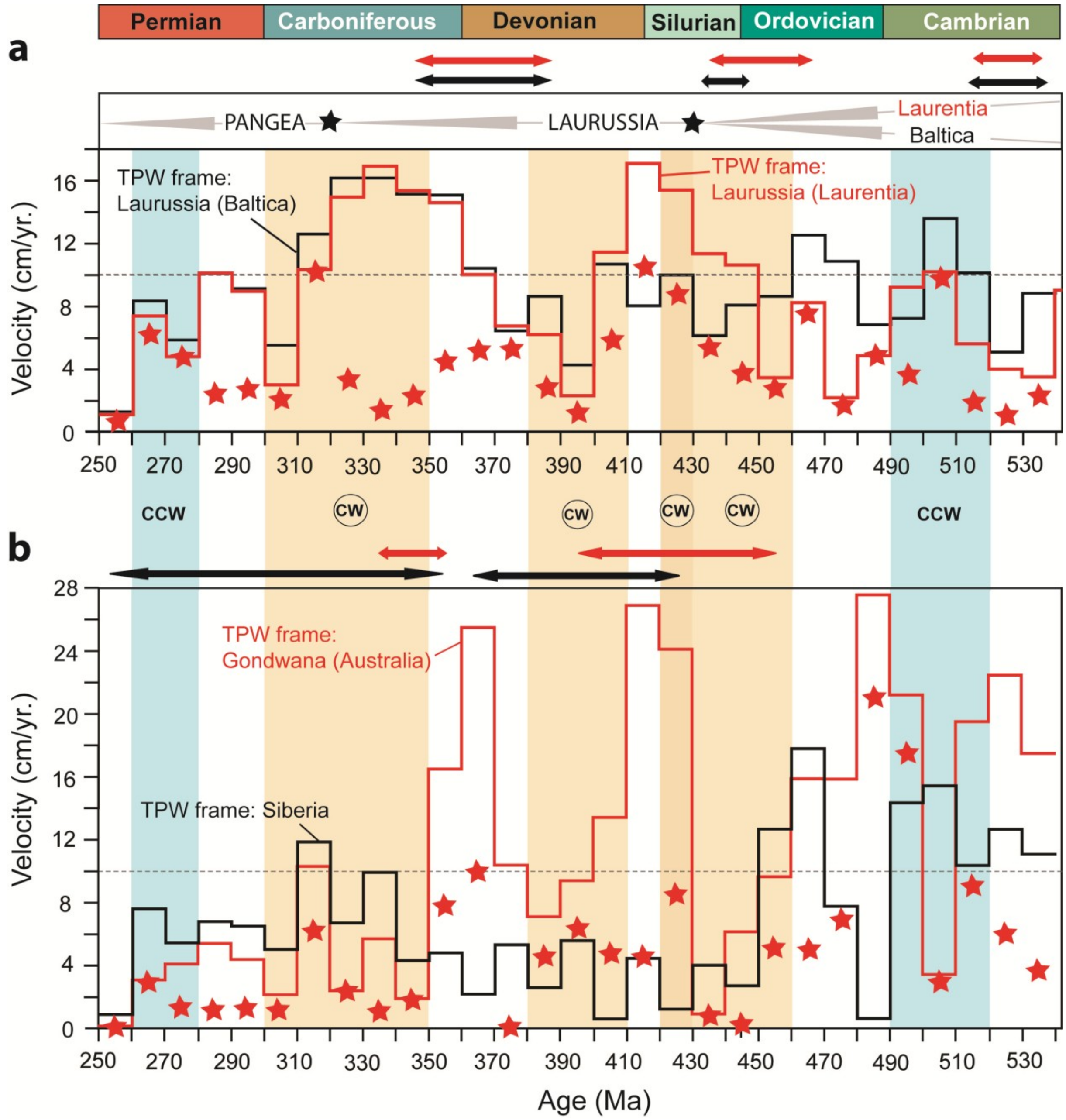

Fig. S5. a. Plate velocity for a central location in North America (57°N, 267°E, red line and average velocity of 8.6 cm/yr) and Baltica (64°N, 36°E, black line) after true polar wander (TPW) correction. Reconstructions before 430 Ma are exclusively based on paleomagnetic data from North America (Laurentia) or Baltica, a combination of North America and Baltica/Europe (Laurussia) data for the 430-320 Ma interval, and a global compilation using 'Pangean' plate-circuits after 320 Myr. Laurussia drifted eastward from the Late Devonian (10-17 cm/yr. between 370 and 310 Ma) in order to source Late Paleozoic kimberlites from the Tuzo PGZ. Note also a Late Silurian-Early Devonian (420-410 Ma) velocity spike (~17 cm/yr) shortly after the formation of Laurussia (Baltica-Avalonia merging with Laurentia); this spike but less pronounced for a geographic location in Baltica (~8 cm/yr) originates from pronounced southward motion of Laurussia (12). The solid red star symbols show Laurentia

(Laurussia/Pangea) north-south velocities (after true polar wander correction and averaging to 4.2 cm/yr) based on paleomagnetic inclination data alone (12).

b. Plate velocity for a central location in Western Australia (22°S, 135°E, red line and average velocity of 11.6 cm/yr) and Siberia (61°N, 109°E) after true polar wander correction. Australia was part of Gondwana and records the highest velocities in our Paleozoic model and the solid red star symbols show north-south velocities for Australia (after true polar wander correction and averaging to 5.0 cm/yr) based on paleomagnetic inclination data alone (12).

The red and blacks horizontal arrows above each panel show times when the paleomagnetic data coverage is poor or non-existing (interpolated). Note the poor data-coverage for Siberia after the Silurian (12). Modelled true polar wander episodes are shaded in light brown (clockwise, CW) and blue (counter-clockwise, CCW) colors.

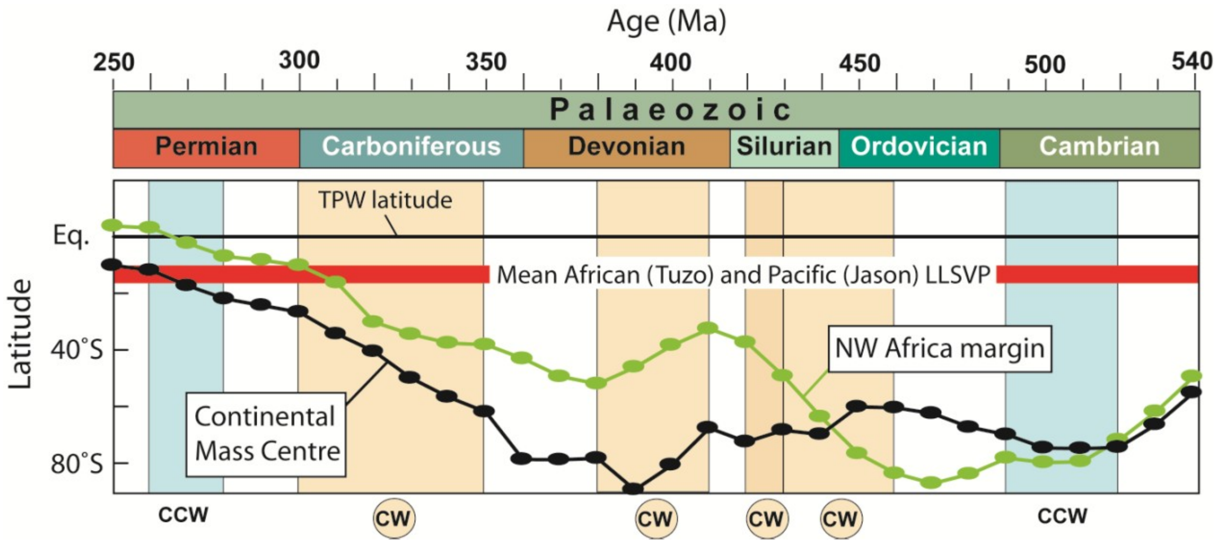

Fig. S6. Latitude of the center of mass of continents in the paleomagnetic, longitude-calibrated frame of our Paleozoic plate model (black curve) (top diagrams in Figs. S7-36). Note the polar mean latitudes (≥60^{o}S) before the Mid-Carboniferous. We also show the latitudes for a location in NW Africa (30^{o}N, 0^{o}E), which was located near peri-Gondwana subduction zones in the Lower Paleozoic, and the mean latitude centers for Tuzo (~16^{o}S) and Jason (~11^{o}S). By definition true polar wander (TPW) must take place around an equatorial location and modelled Paleozoic TPW episodes are shaded in light brown (clockwise, CW) and blue (counter-clockwise, CCW) colors.

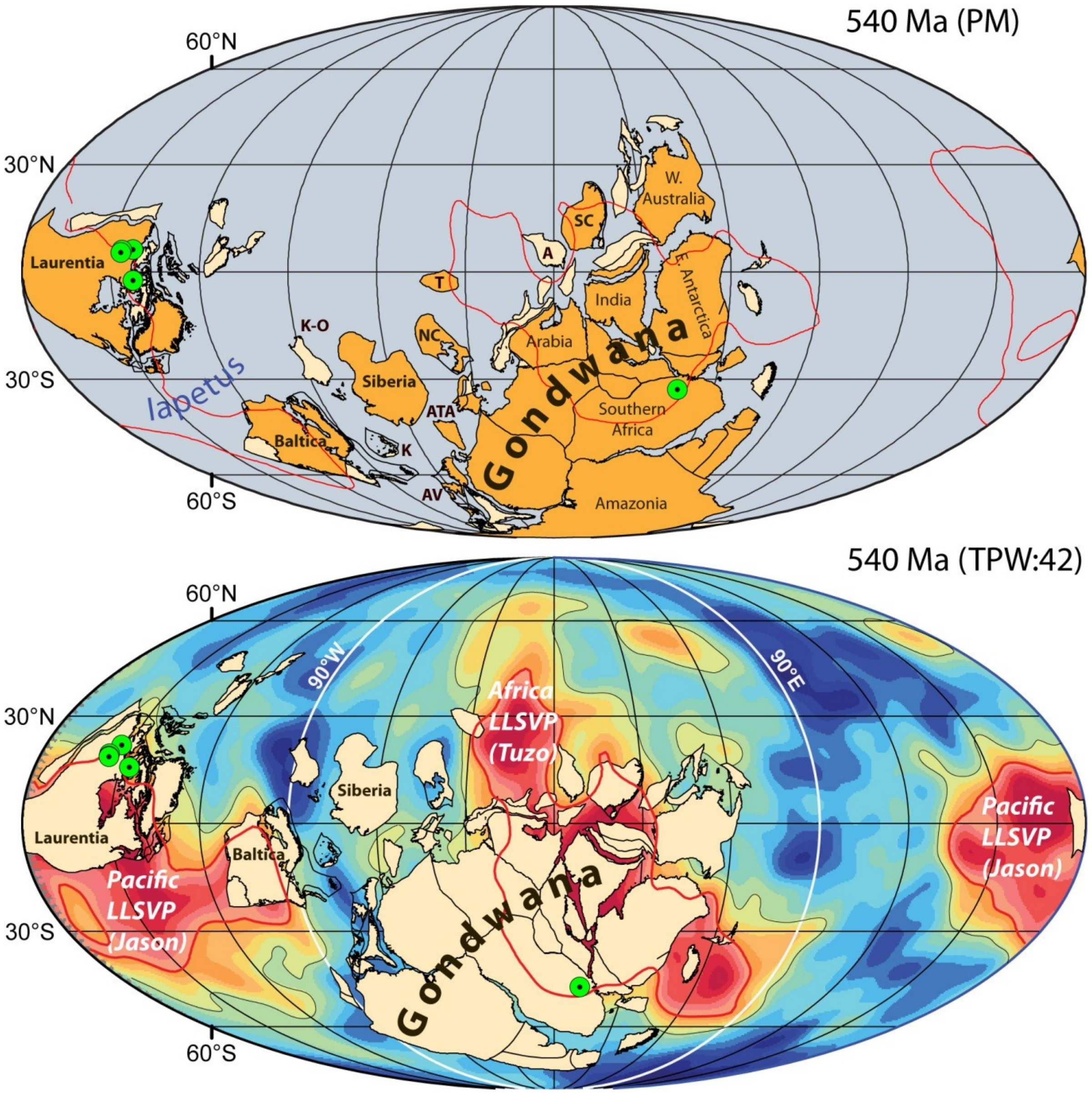

Fig. S7. Early Cambrian reconstruction. In the top panel, continents or smaller blocks from which we have used Paleozoic palaeomagnetic data to locate the continents in latitude and orientation (Figs. S7-36) are shaded in a darker color. The Iapetus Ocean started to form in the Late Precambrian and separated Laurentia (including North America, Greenland, Spitsbergen and the NW British Isles) from Baltica (northern Europe eastward to the Urals) and Gondwana (8, 15-17). Core Gondwana included Africa, South America, Arabia, India, Madagascar, West Australia and East Antarctica. Parts of Paleozoic Gondwana that are now in Europe (e.g. Avalonia (18), AV and the Armorican Terrane Assembly, ATA) and North America (e.g. Florida) are also included, and termed peri-Gondwana. The red line is 1% slow contour in the SMEAN model (5) that approximate the plume generation zone (PGZ). In the lower panels the PGZ is shown as today but in the upper panels the PGZ is rotated according to our TPW model. In all our reconstructions (Figs. S7-36), the large green circles (with a small black central dot) are one or several kimberlite locations with ages within ± 5 Ma from the reconstruction age. Some kimberlites may thus appear further away from the PGZ than we model it because the age does not fully match the reconstruction age. The top panel is our final iterated paleomagnetic model (PM) and the lower panel is the corresponding TPW reconstruction. The number after reconstruction age and TPW is the amount of net TPW at the reconstructed time (in this case 42^{o}; see Fig. 3). SMEAN tomographic color palette in lower panel is the same as in the as scale-bar in Figs. S2-S3. SC, South China; NC, North China; A, Annamia (Indochina); K, Kara (Northern Taimyr, Severnaya Zemlya and surrounding shelf seas); T, Tarim; S, Scotland; AA, Arctic Alaska showed together with Chukotka and Farewell (19). K-O, Kolyma and Omolon.

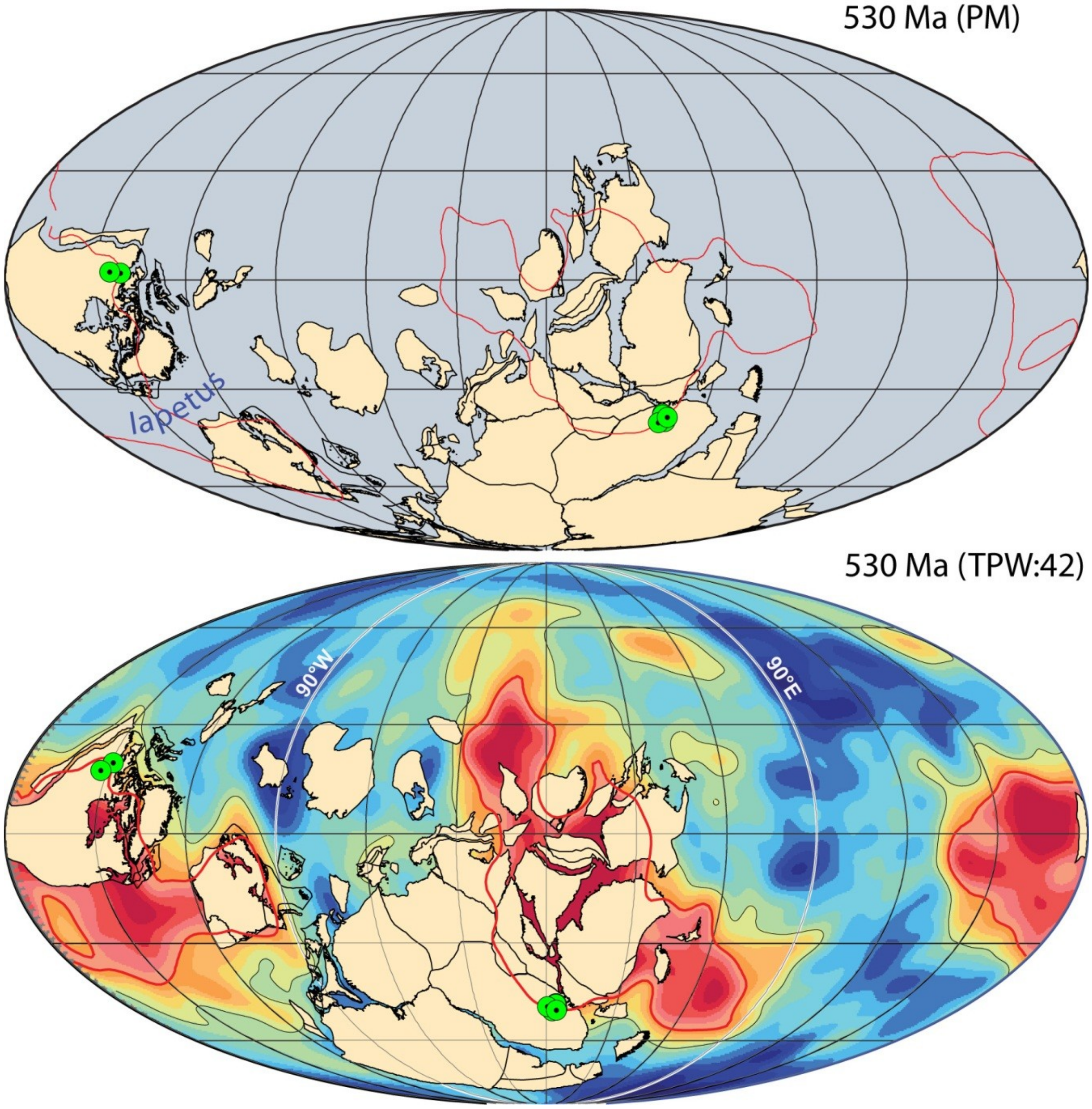

Fig. S8. Early Cambrian reconstruction. See Fig. S7 for legend and more information. The position of Baltica is uncertain for most of the Cambrian (poor or non-existent paleomagnetic data) and there are no known kimberlites and large igneous provinces. Based on paleomagnetic data (12), Gondwana is rotating counter-clockwise of up to 2°/Ma before true polar wander (TPW) correction).

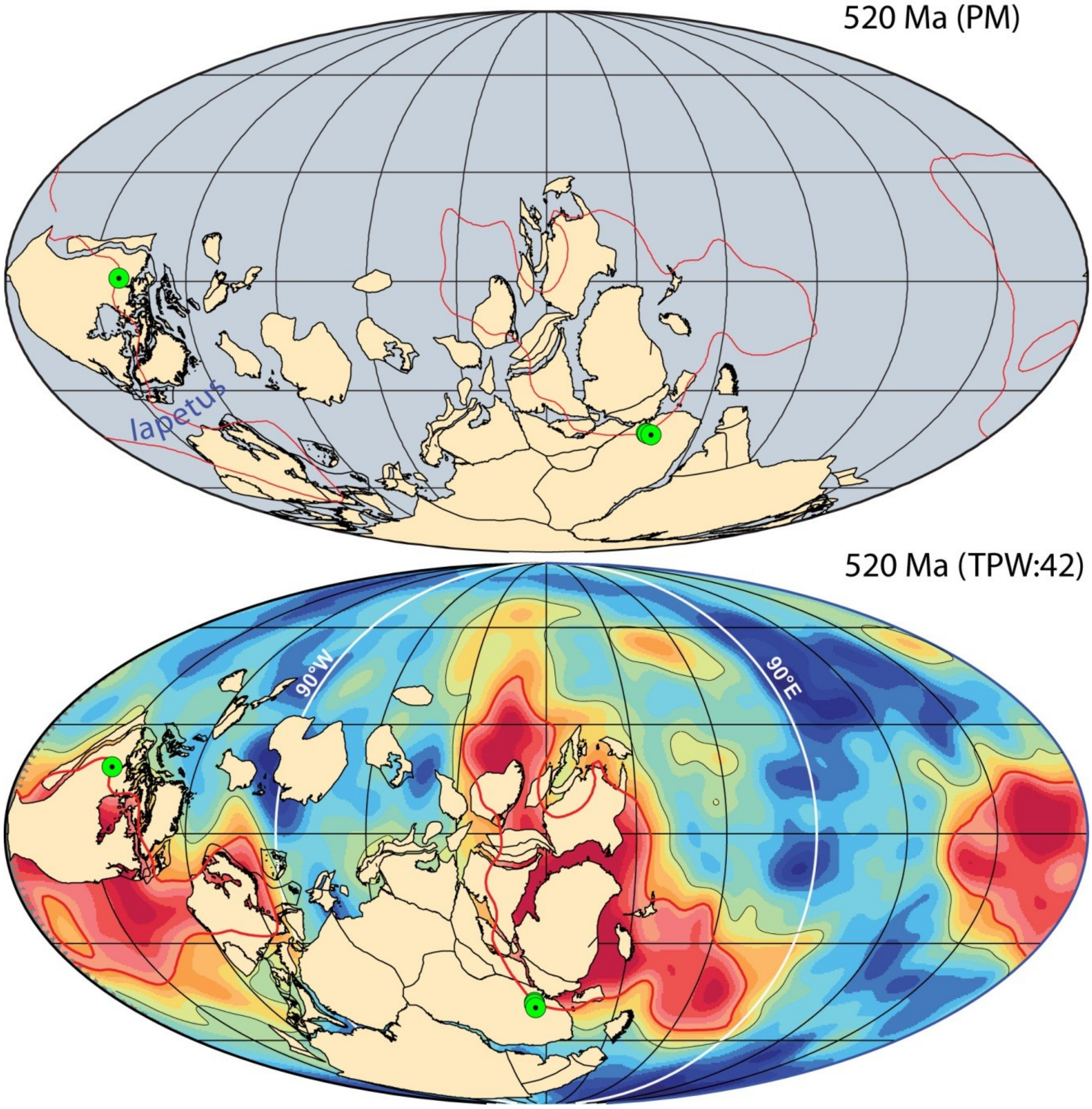

Fig. S9. Early Cambrian reconstruction. See Fig. S7 for legend and more information.

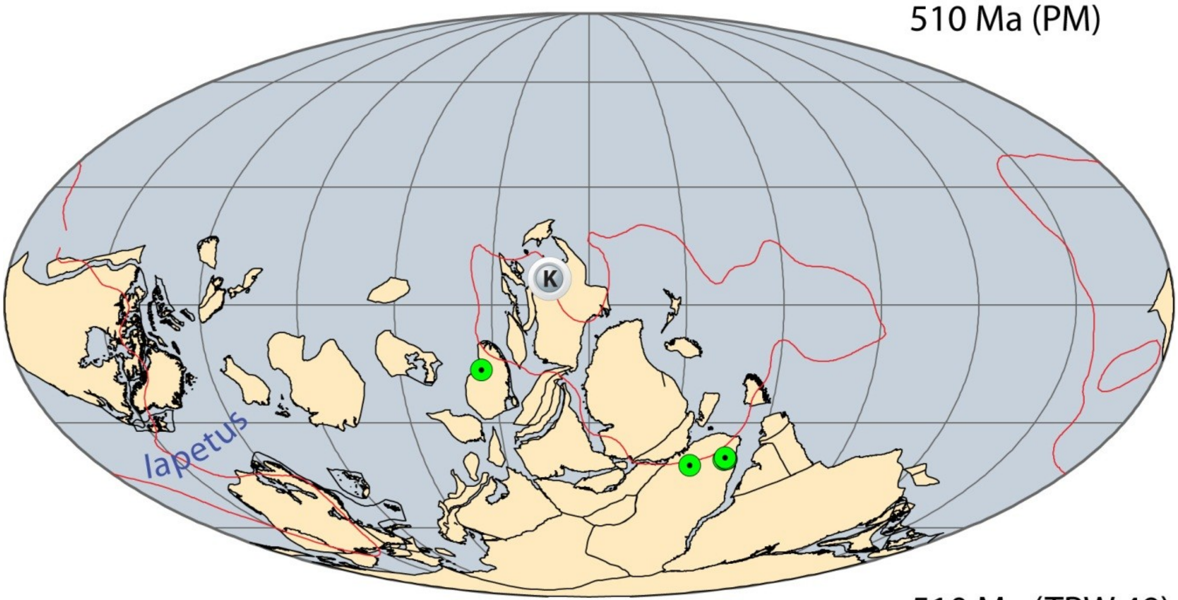

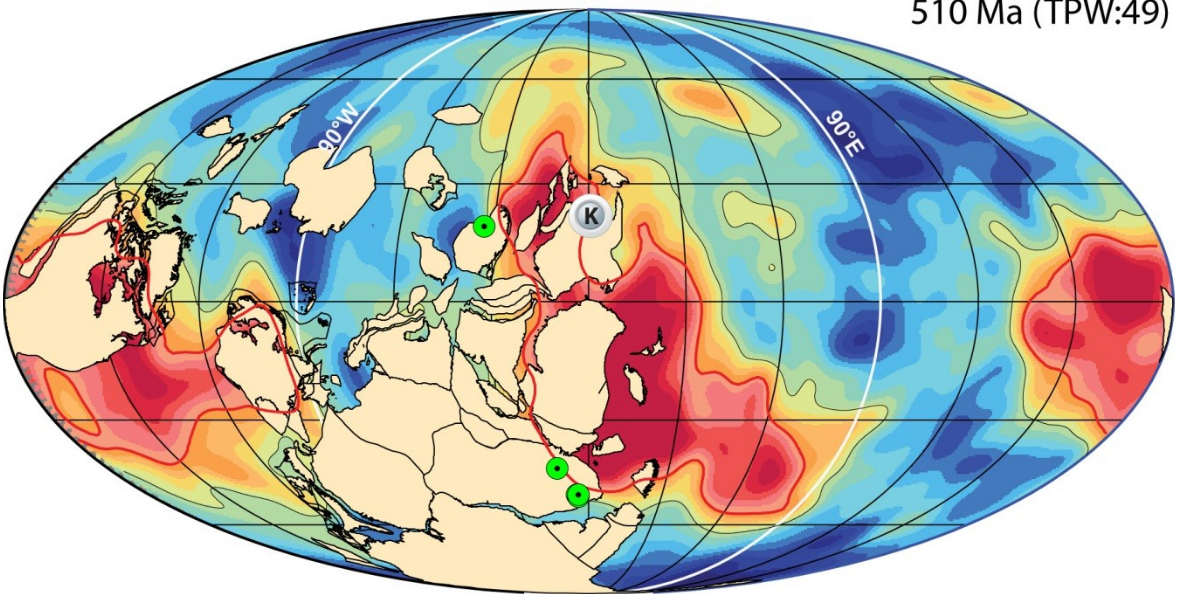

Fig. S10. Middle Cambrian reconstruction. The Kalkarindjii (K) large igneous province (LIP) erupted at ca. 510 Ma and covers about 400,000 km^2 in Western Australia (20, 4). Due to only two and very different Late Cambrian and Early Ordovician poles from South China, we have not used paleomagnetic data to position it in our Cambrian and Ordovician reconstructions. We place South China as in Torsvik et al. (21), relying on faunal data, and we have added Annamia to it. In our reconstruction, the Dahongshan kimberlite in South China plots somewhat west of the PGZ but South China could potentially be moved eastward and closer to the PGZ. Here we use an age of 510 Ma (mean Rb/Sr and Sm/Nd ages) (22) but to complicate matters, a K-Ar age of 326 Ma is also reported from the Dahongshan kimberlite (23). See Fig. S7 for legend and more information.

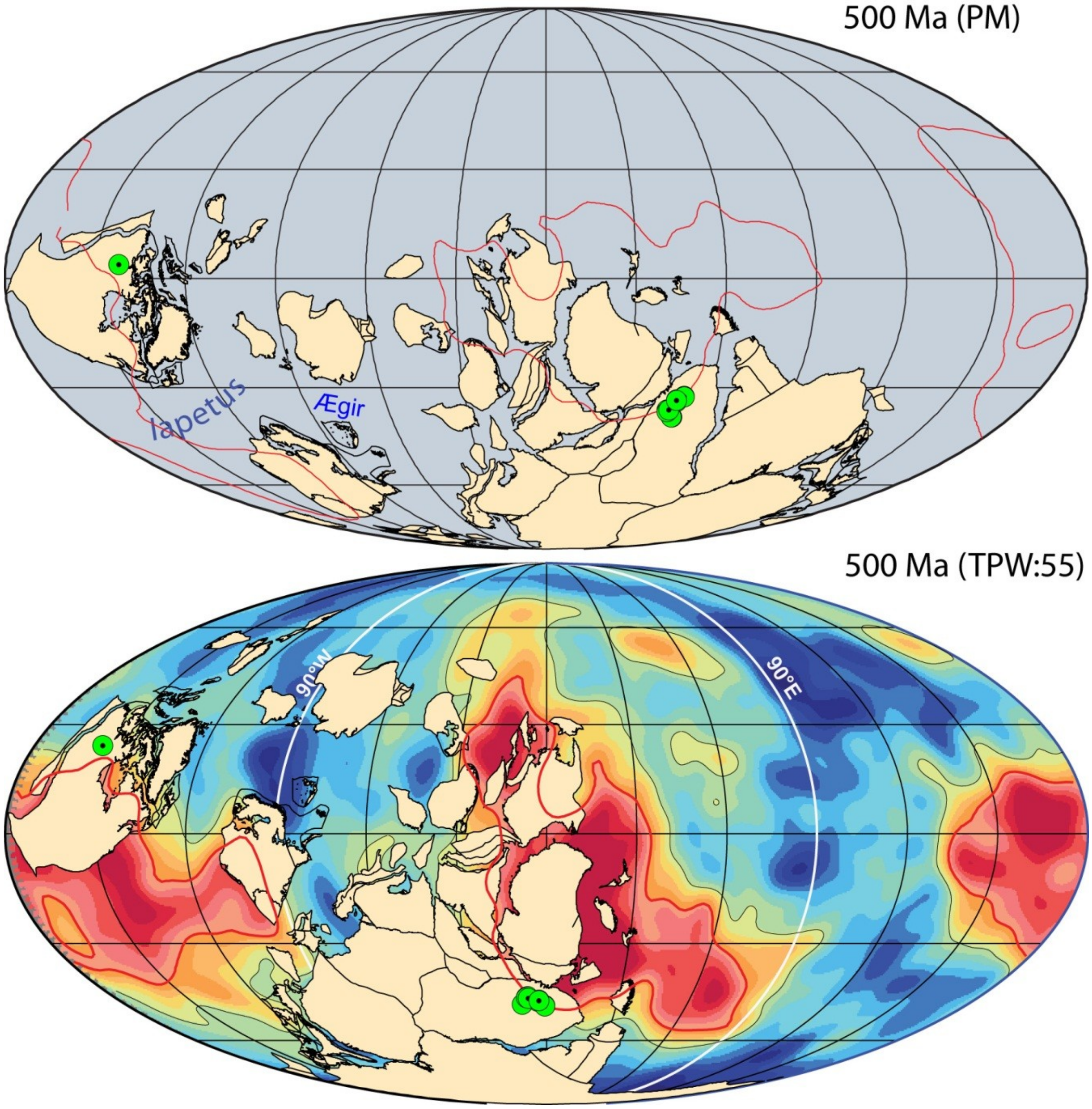

Fig. S11. Late Cambrian reconstruction. See Fig. S7 for legend and more information.

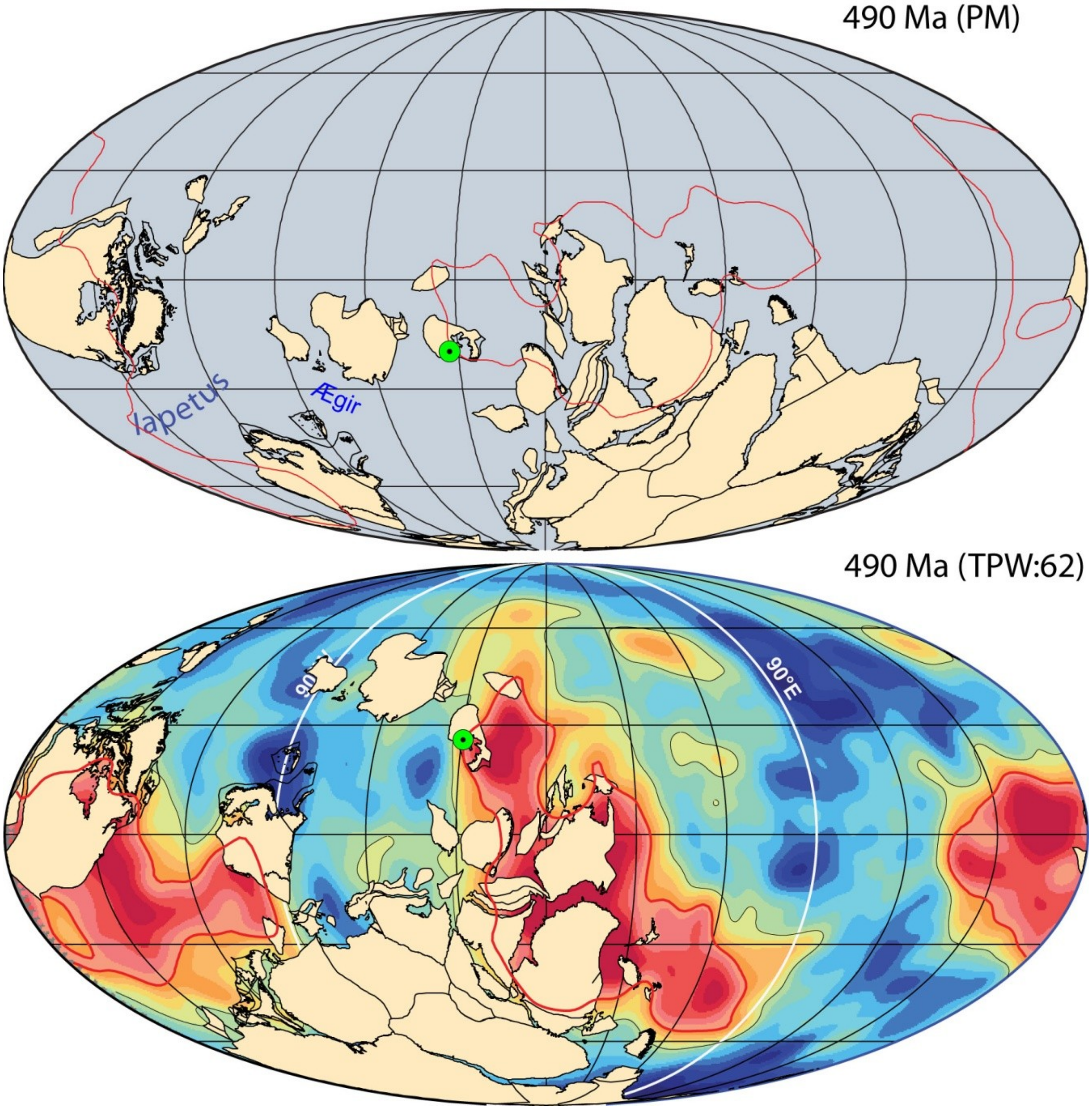

Fig. S12. Late Cambrian reconstruction. North China kimberlites vary between 485 and 474 Ma and the most reliable ages are listed in Li et al. (24). See Fig. S7 for legend and more information.

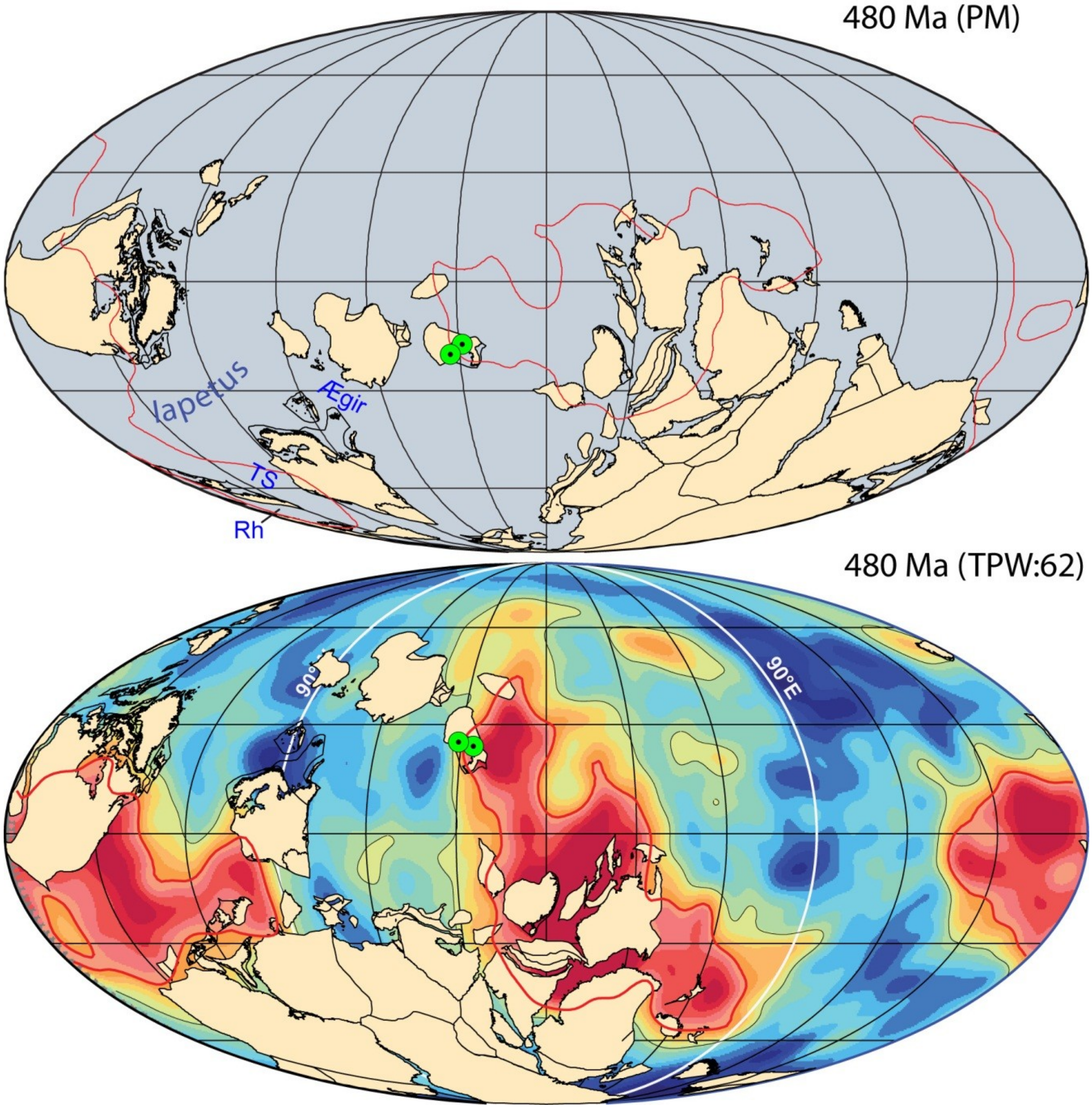

Fig. S13. Early Ordovician reconstruction. The Rheic Ocean (Rh in top panel) opened at Cambrian-Ordovician boundary times (ca. 490 Ma) and Avalonia separated from Gondwana (Florida). The Tornquist Sea (TS in top panel) separated Baltica and Avalonia. Paleomagnetically, Baltica and Siberia are very well constrained for the Ordovician (12). Ordovician data from Gondwana and Laurentia are also mostly of reasonable quality. See Fig. S7 for legend and more information.

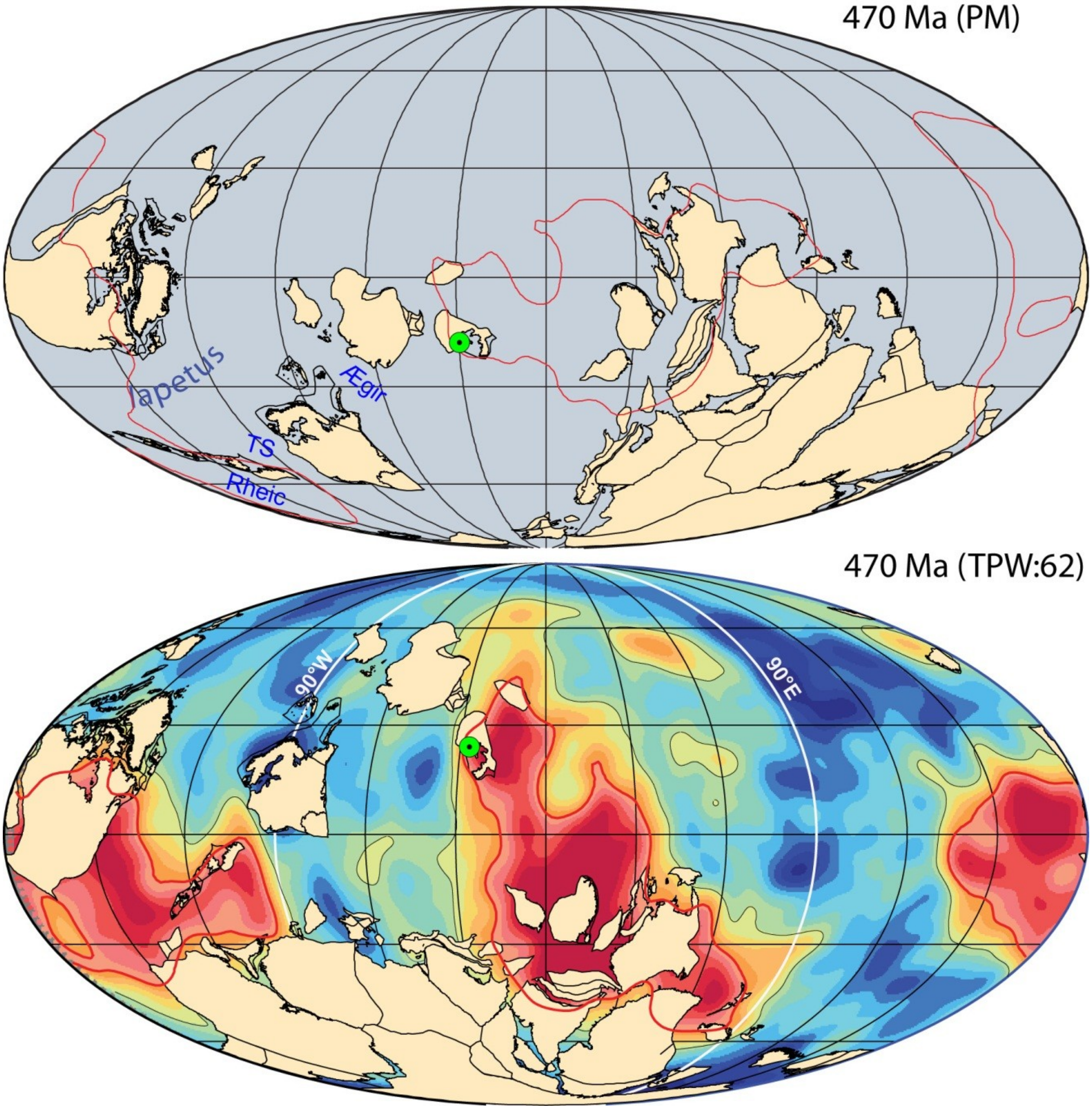

Fig. S14. Early Ordovician reconstruction. See Fig. S7 for legend and more information.

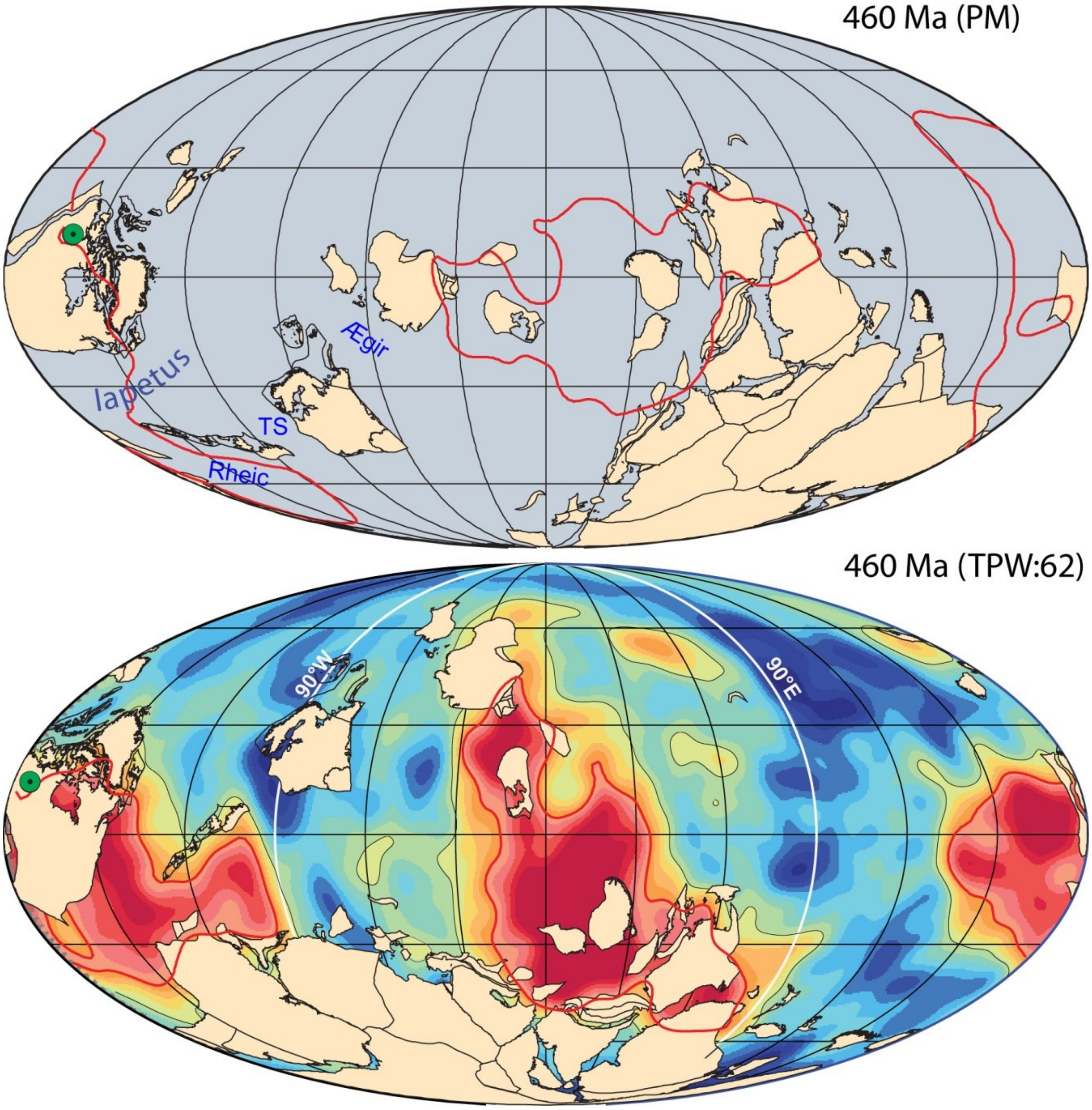

Fig. S15. Late Ordovician reconstruction. See Fig. S7 for legend and more information.

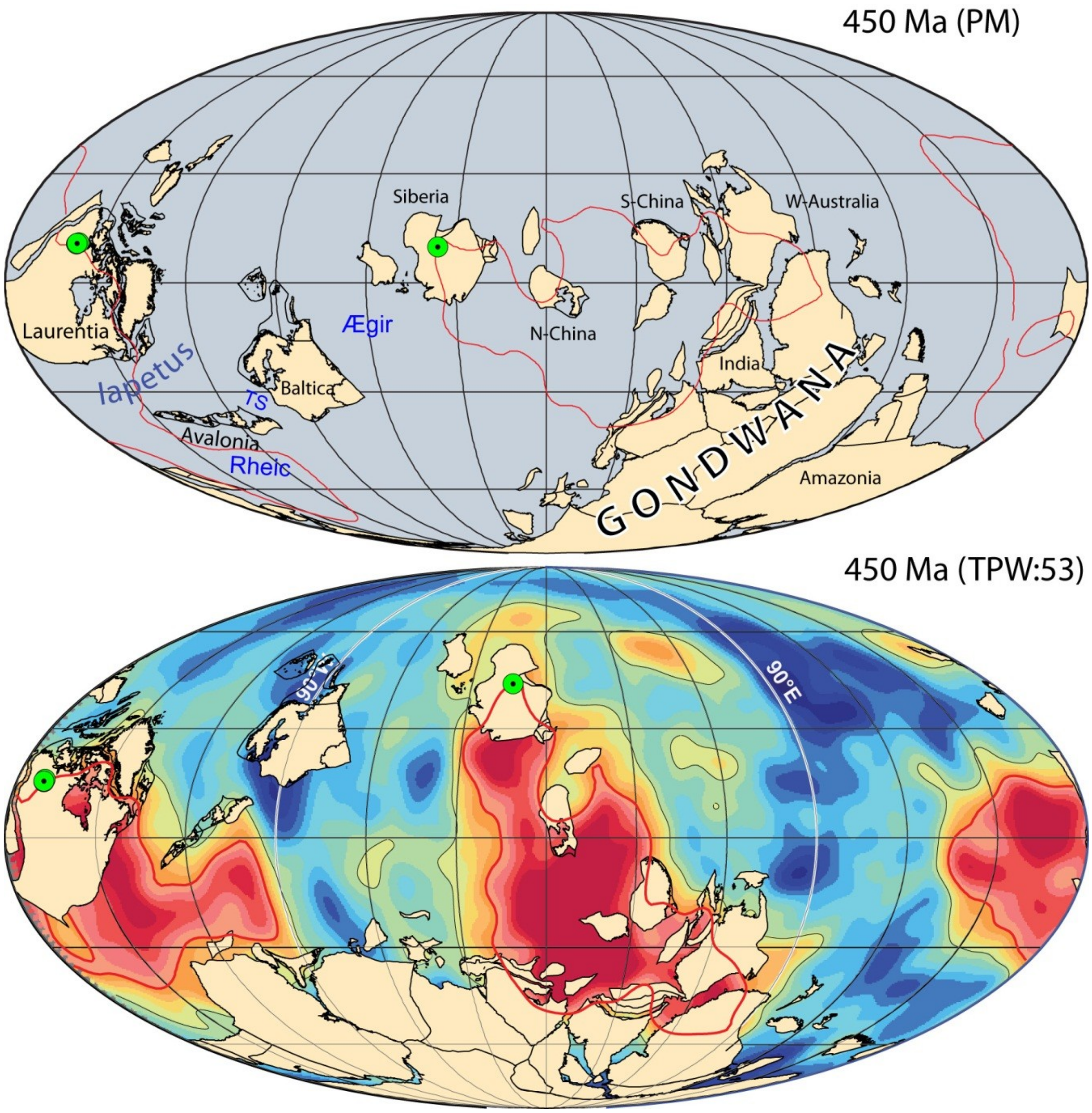

Fig. S16. Late Ordovician reconstruction. The Rheic Ocean is widening at the expense of the Iapetus Ocean and the Tornquist Sea (TS). See Fig. S7 for legend and more information.

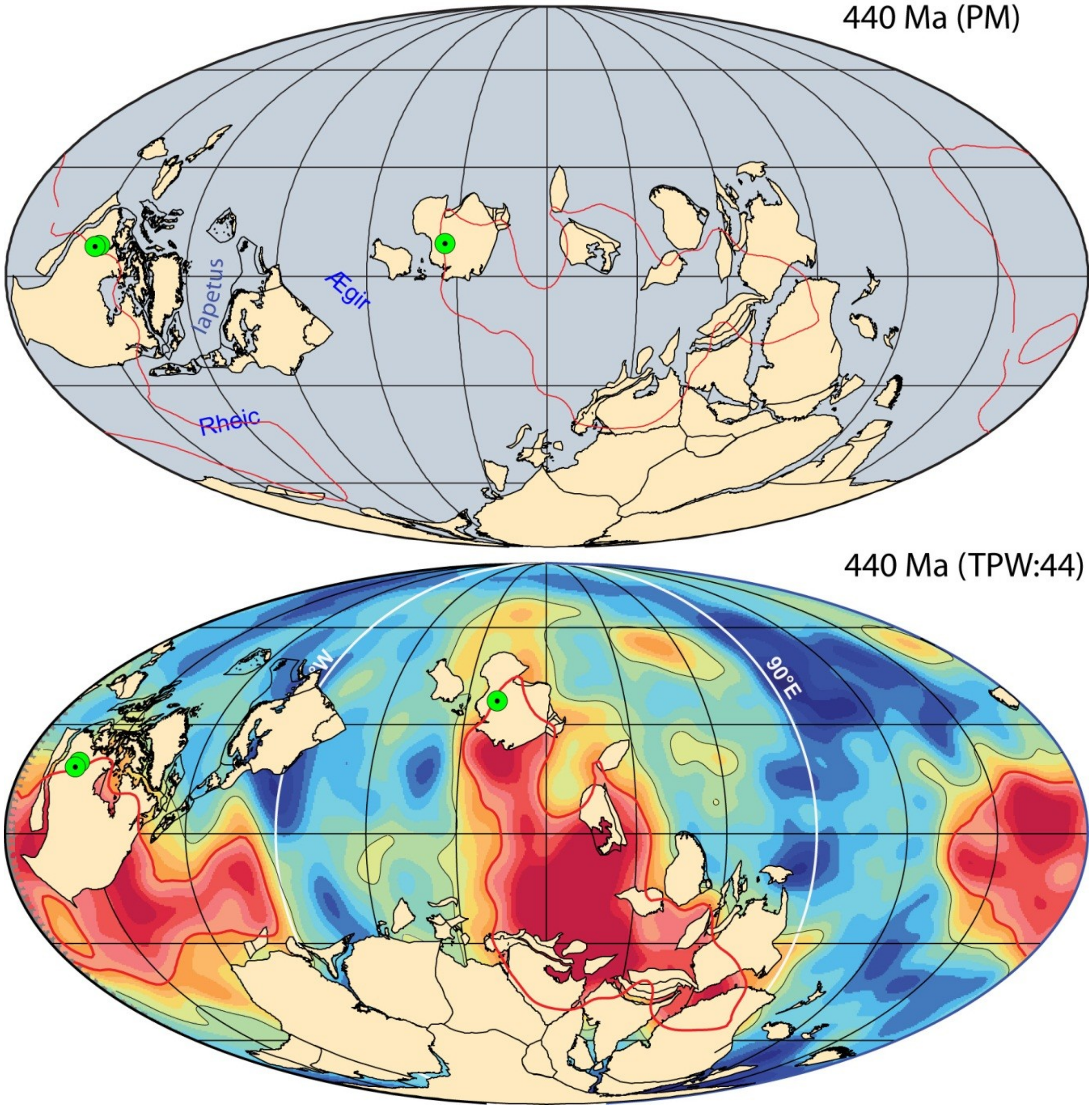

Fig. S17. Early Silurian reconstruction. Avalonia existed as a separate object only during the Ordovician before the closing of the Tornquist Sea to merge with Baltica at around 440 Ma, near the age of the Ordovician-Silurian boundary (25). See Figs. S7 & S16 for legend and more information.

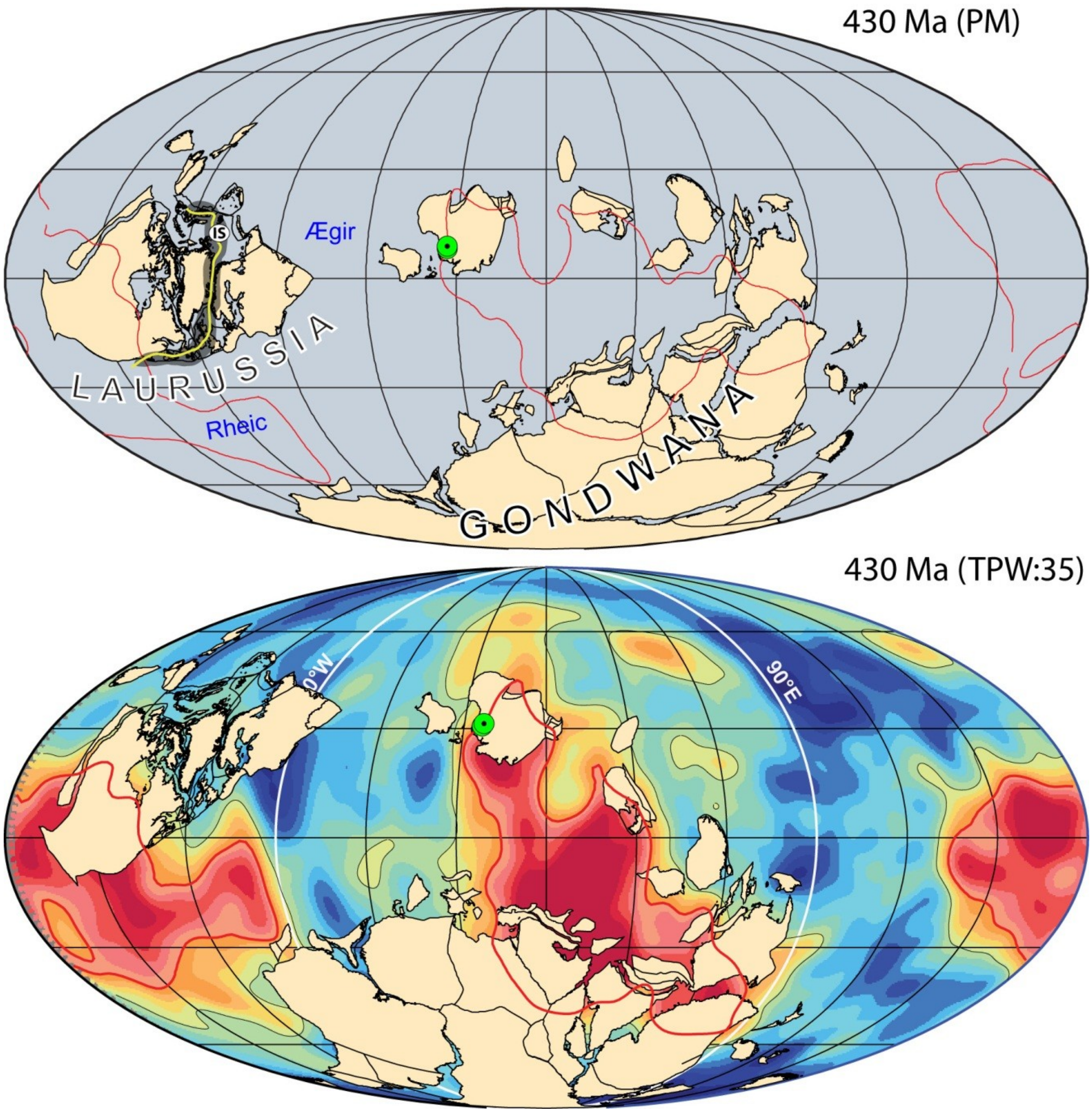

Fig. S18. Mid Silurian reconstruction. United Baltica and Avalonia collided with Laurentia and closed the Iapetus Ocean at around 430-420 Ma (forming Laurussia) in a collision that caused the Appalachian and Caledonian orogenies (dark shading). After the collision, Laurussia drifted southward (until 400 Ma) whilst undergoing counter-clockwise rotation of up to 1.8°/Ma (12) before TPW correction. IS, Iapetus Suture. See Figs. S7 & S16 for legend and more information.

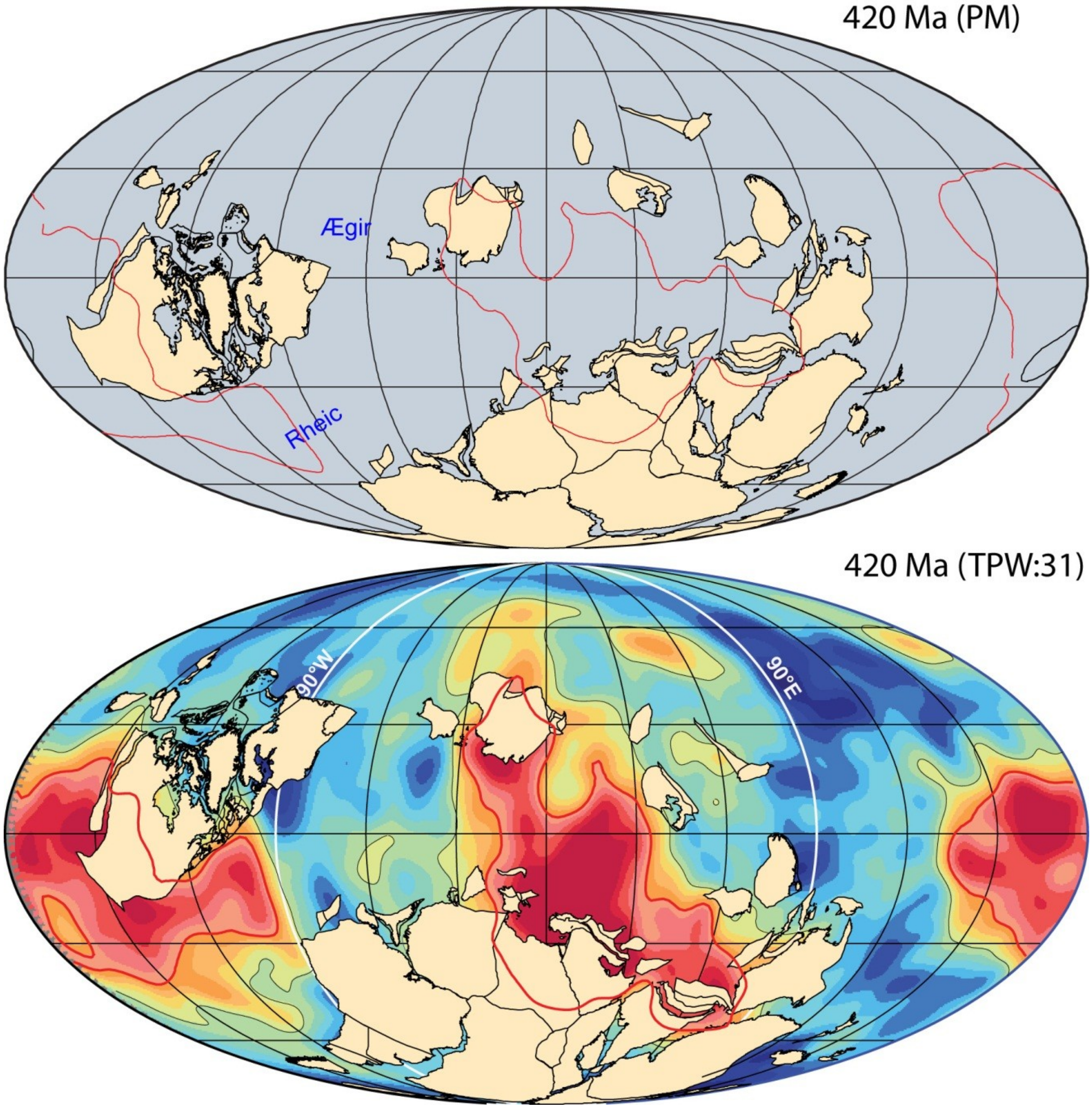

Fig. S19. Late Silurian reconstruction. No known kimberlites or large igneous provinces at this time. See Figs. S7 & S16 for legend and more information.

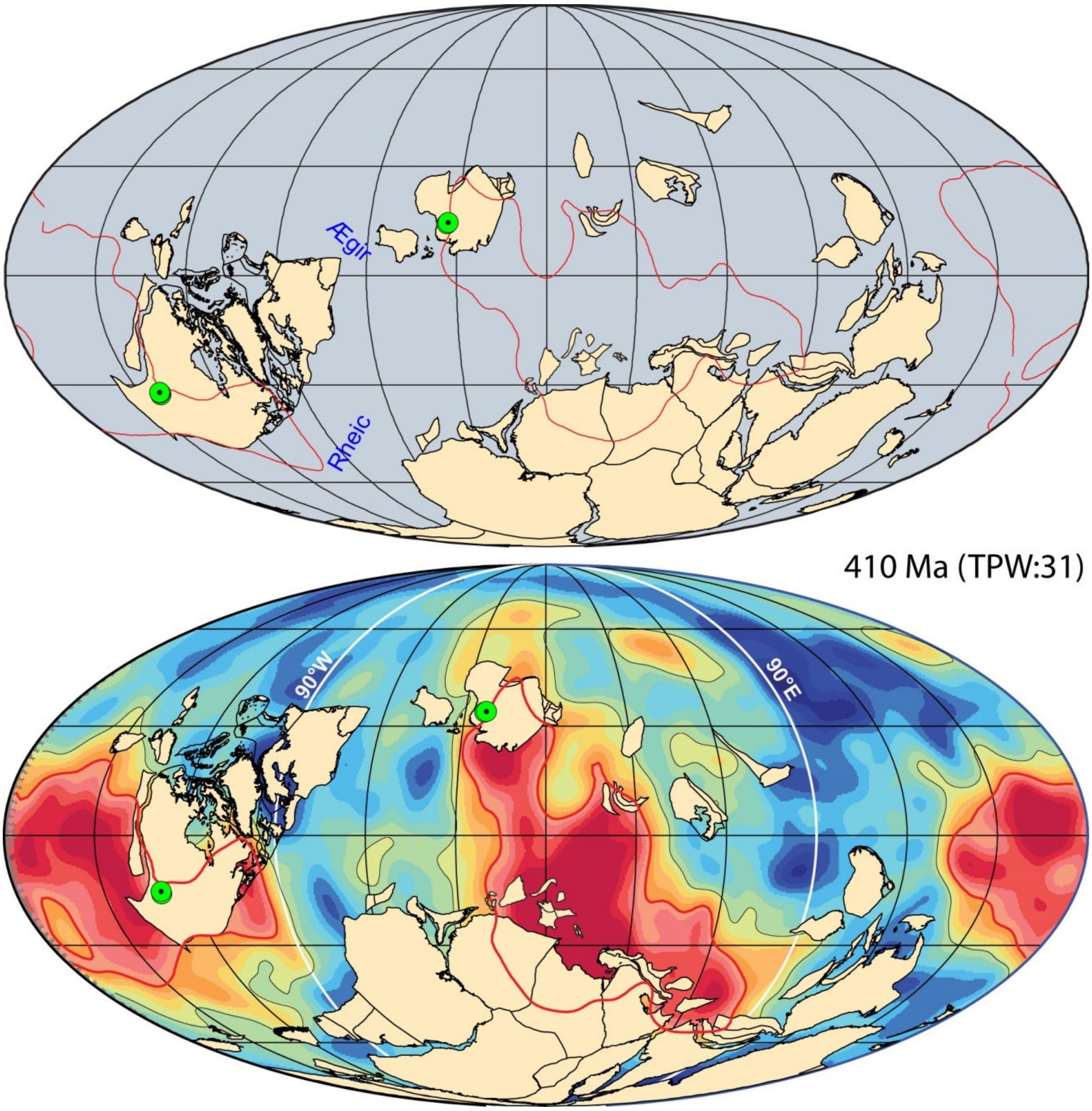

Fig. S20. Early Devonian reconstruction. See Figs. S7 & S16 for legend and more information.

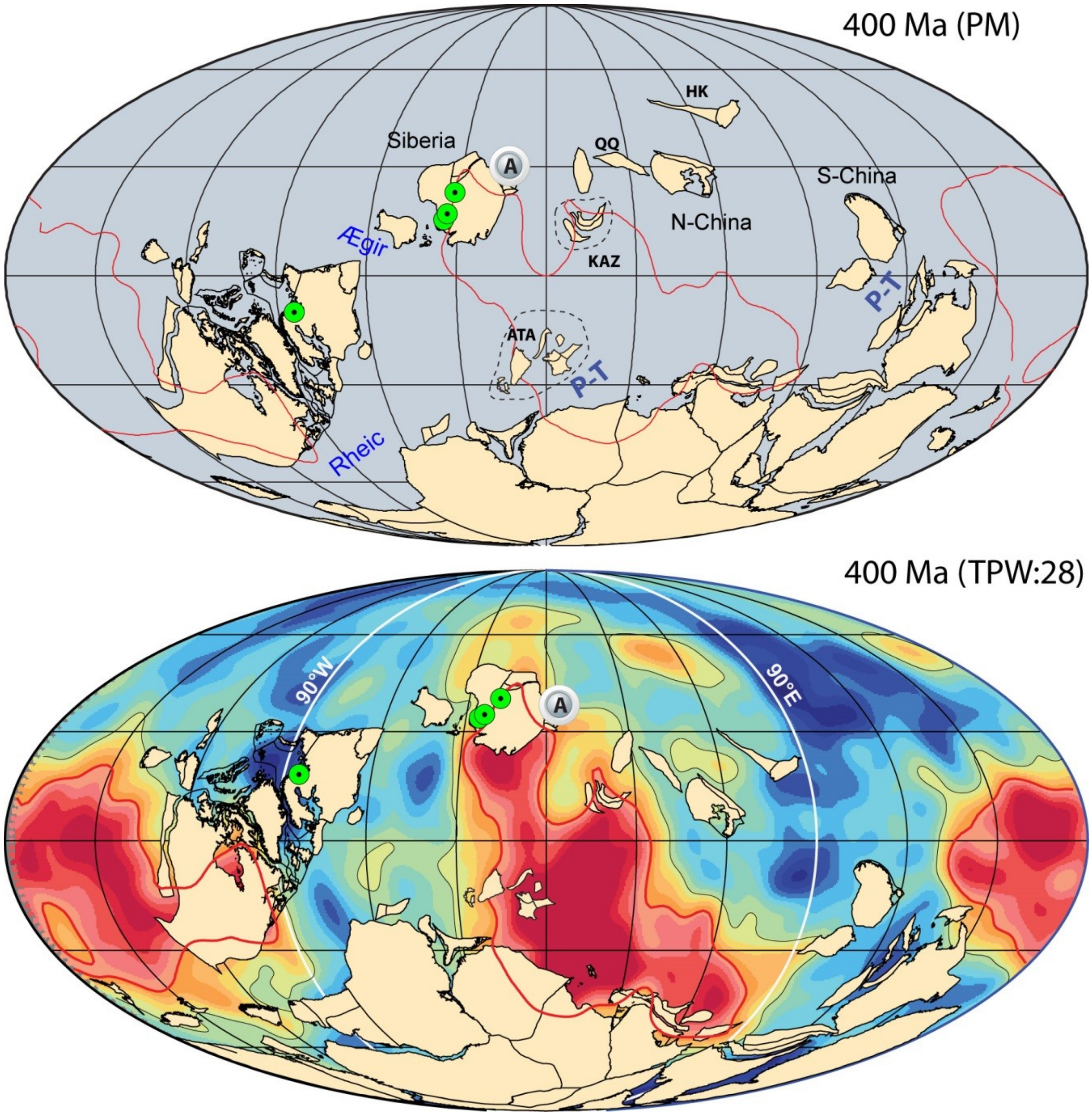

Fig. S21. Early Devonian reconstruction. We place some new blocks on this and subsequent maps. These include KAZ, Kazakhstan; QQ, Qaidam-Qilian; HK, Hutag Uul-Songliao and Khanka-Jiamusi Bureya. At this time, the Armorican Terrane Assembly (ATA) and South China (with Annamia) had drifted off the Gondwana margin and opened the Paleotethys (P-T). A, Altay-Sayan LIP (~400 Ma) in Siberia (11). Note that kimberlites from Russia (Arkhangelsk) in this reconstruction, and in Figs. S22-23, would require a more westerly (ca. 60^{o}) position of Laurentia. This would lead to eastward-directed velocities in excess of 20-25 cm/yr during the Carboniferous and the longitudinal calibration of Laurentia in the Devonian (Figs. S20, S22 & S24) is largely based on North American kimberlites. The position of the Armorican Terrane Assembly after the Early Devonian follows Domeier and Torsvik (26). See Fig. S7 & S16 for legend and more information.

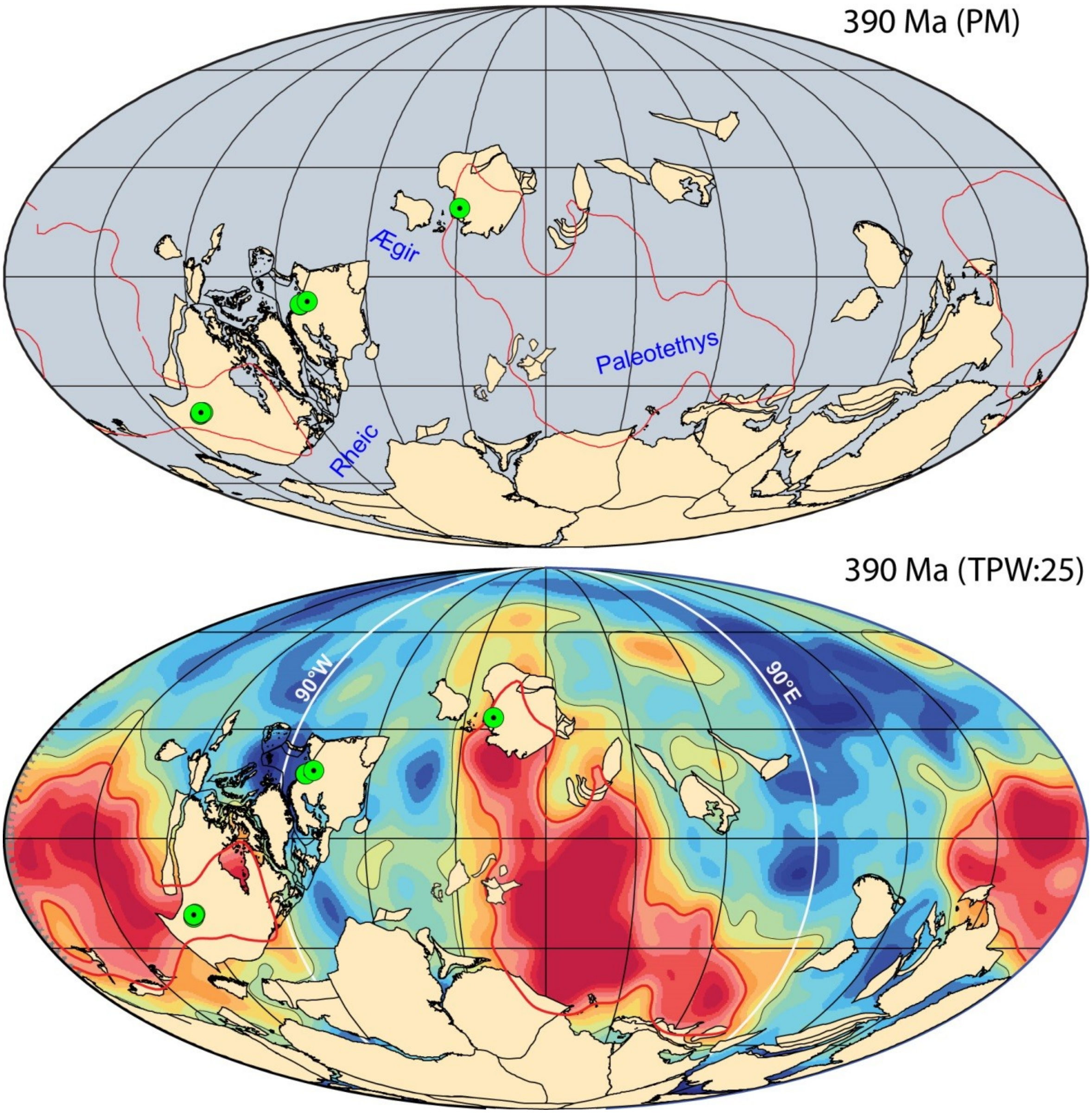

Fig. S22. Mid Devonian reconstruction. See Figs. S7, S16 & S21 for legend and more information.

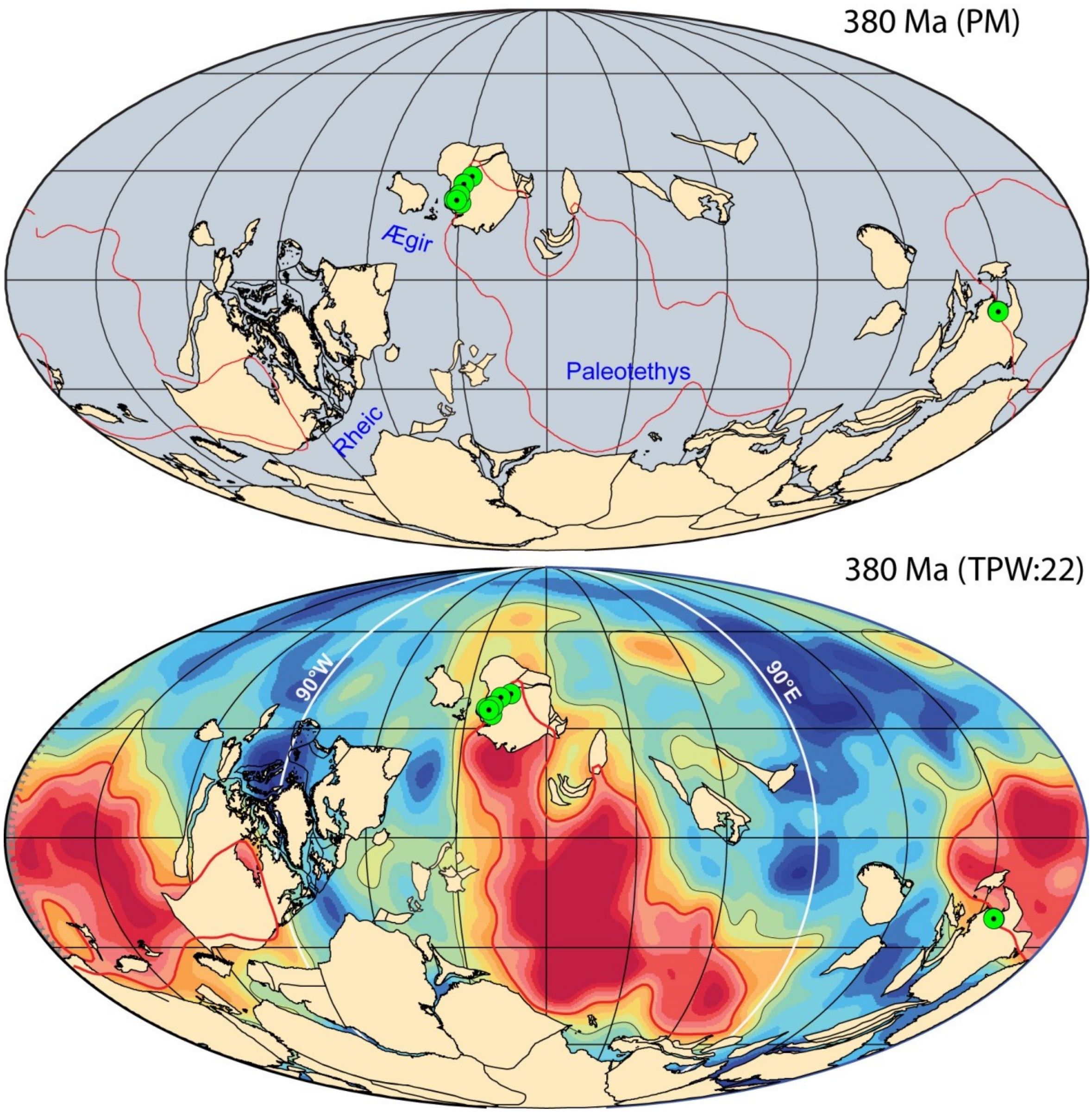

Fig. S23. Late Devonian reconstruction. Note kimberlites in Australia between 382-367 Ma (27). See Figs. S7, S16 & S21 for legend and more information.

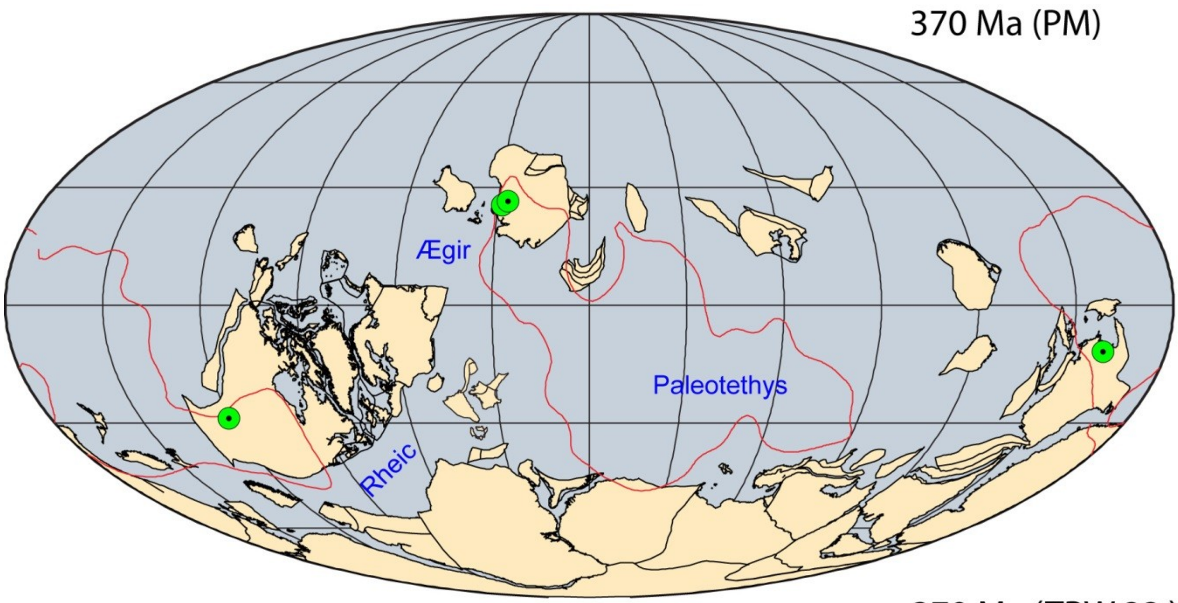

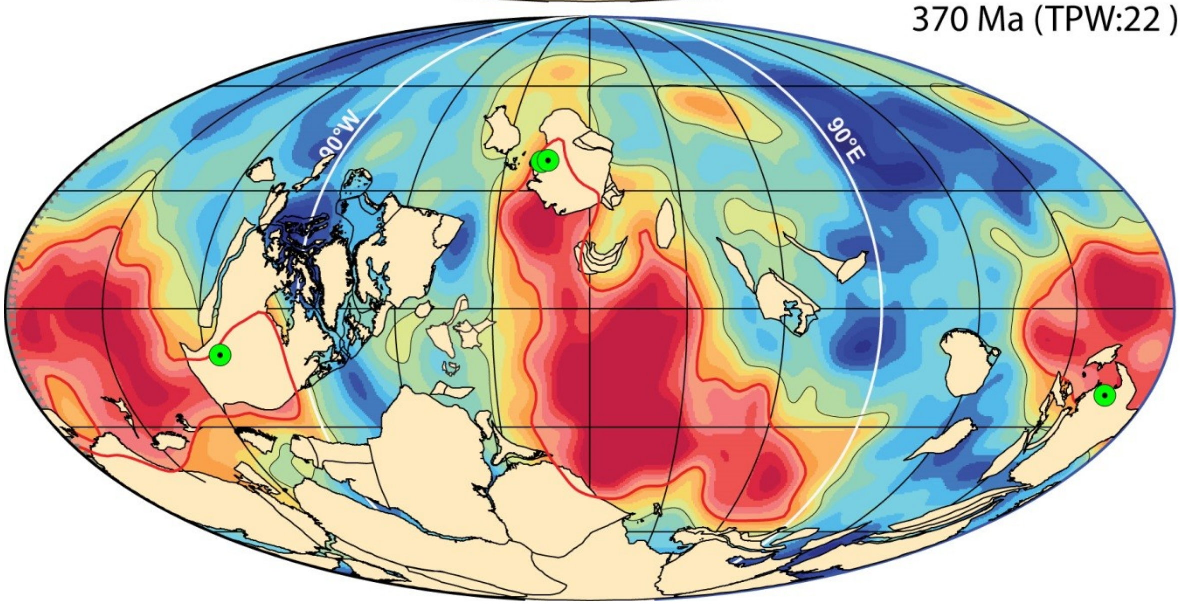

Fig. S24. Late Devonian reconstruction. The Armorican Terrane Assembly is approaching Laurussia and the Rheic Ocean had narrowed considerable. However, there is a peculiarity in our closure model of the Rheic Ocean because Rheic appears to widen between 380 and 370 Ma. This is a consequence of compromising longitude for kimberlites in North America and Russia at 390 Ma (Fig. S22). The apparent narrowing Rheic Ocean between 380 and 370 Ma could potentially be resolved by locating 390 Ma kimberlites in North America at the extreme eastern edge of Jason (ignoring the Russian ones), and doing the same at 370 Ma (no Laurussian kimberlites at 380 Ma). Average velocity for the Armorican Terrane Assembly is 10 cm/yr after detaching from Gondwana (after 410 Ma). See Figs. S7, S16 & S21 for legend and more information.

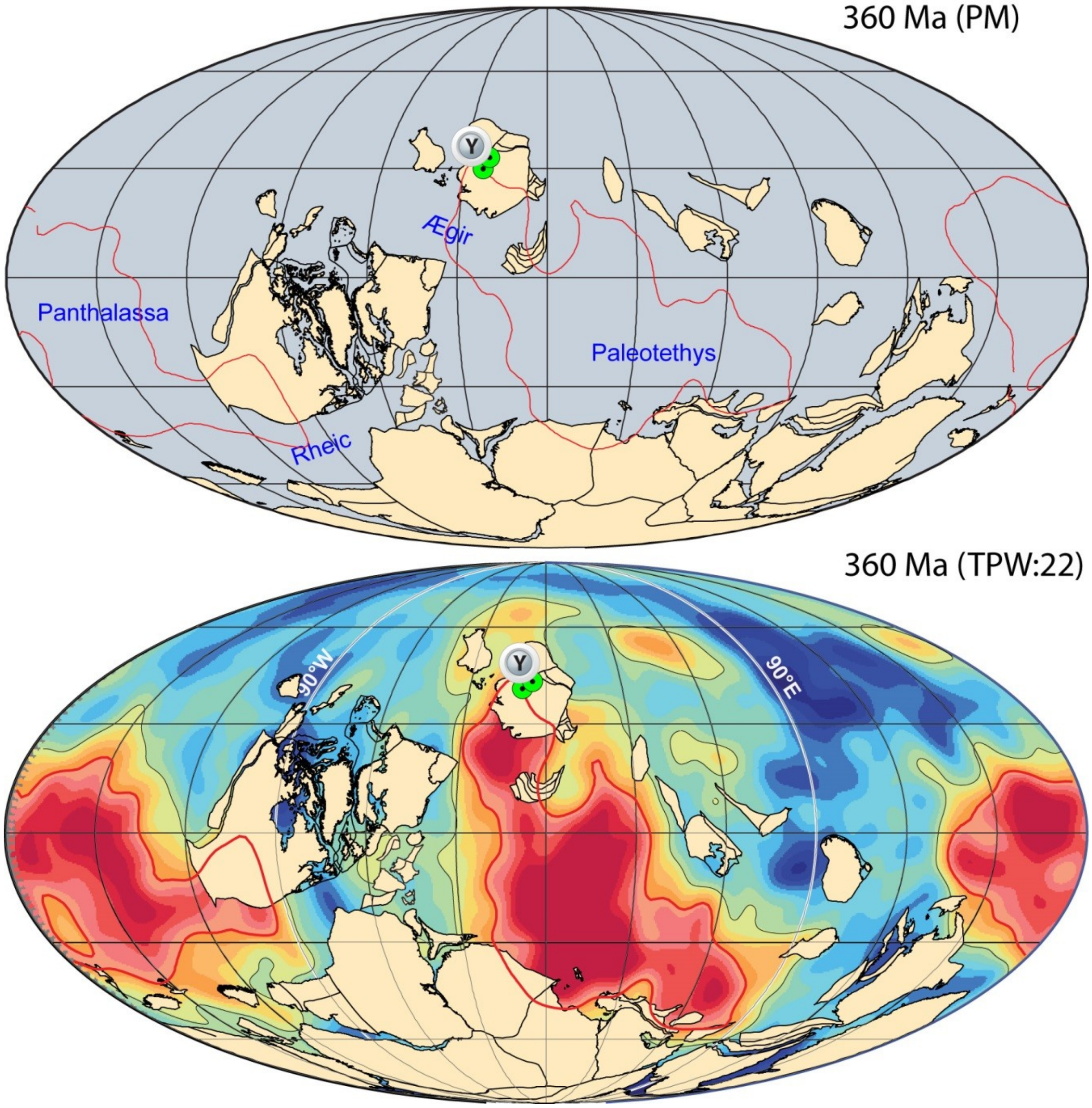

Fig. S25. Late Devonian reconstructions. Y=Yakutsk LIP (ca. 360 Ma) in Siberia (4, 11). See Figs. S7, S16 & S21 for legend and more information.

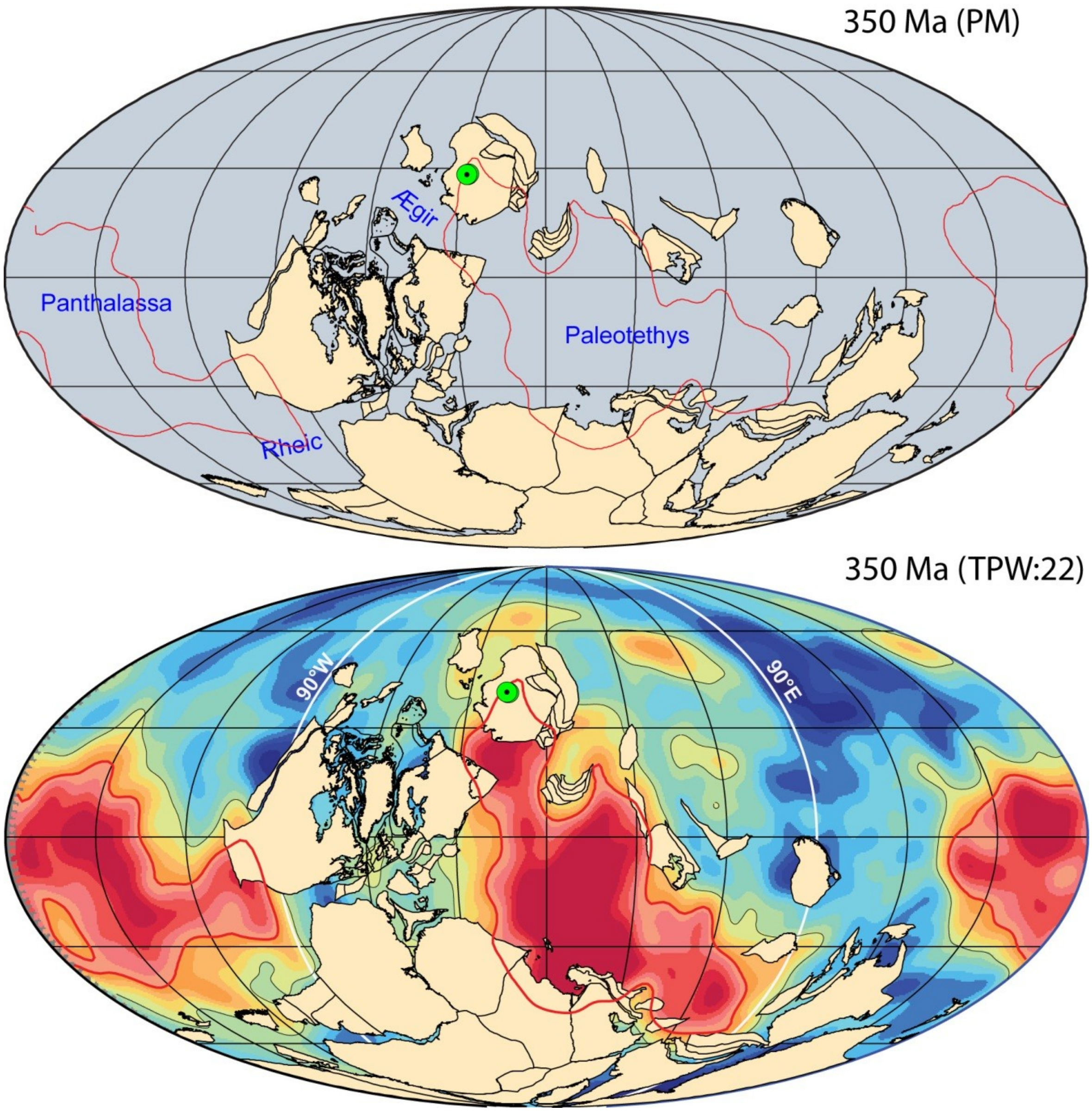

Fig. S26. Early Carboniferous reconstruction. European sector of Rheic almost vanished. Late Devonian and Carboniferous kimberlites are lacking in Laurussia and in our Paleozoic model we shift Laurentia eastward during this time period (Figs. S25-29). See Figs. S7, S16 & S21 for legend and more information.

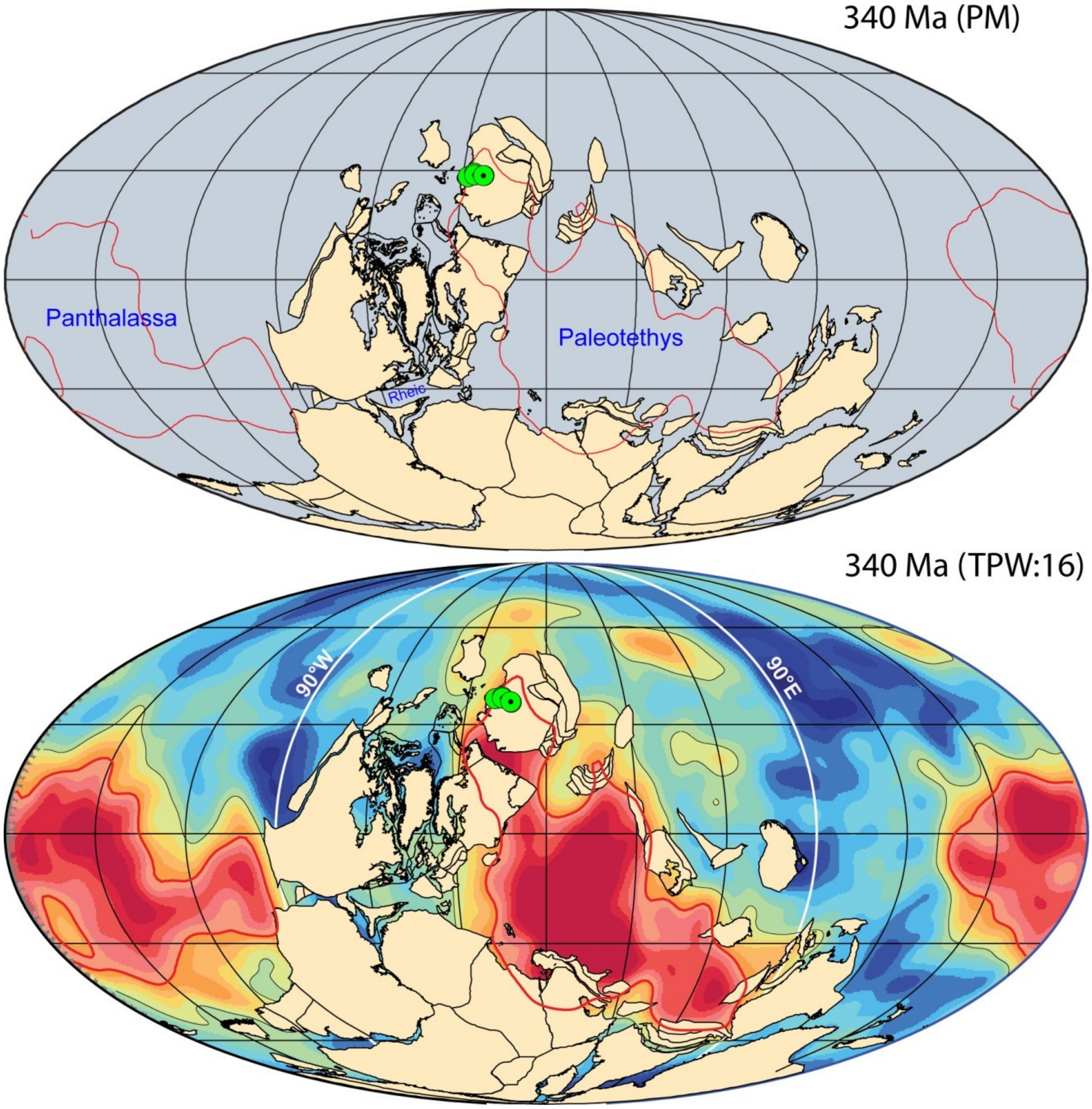

Fig. S27. Mid Carboniferous reconstruction. See Figs. S7, S16 & S21 for legend and more information.

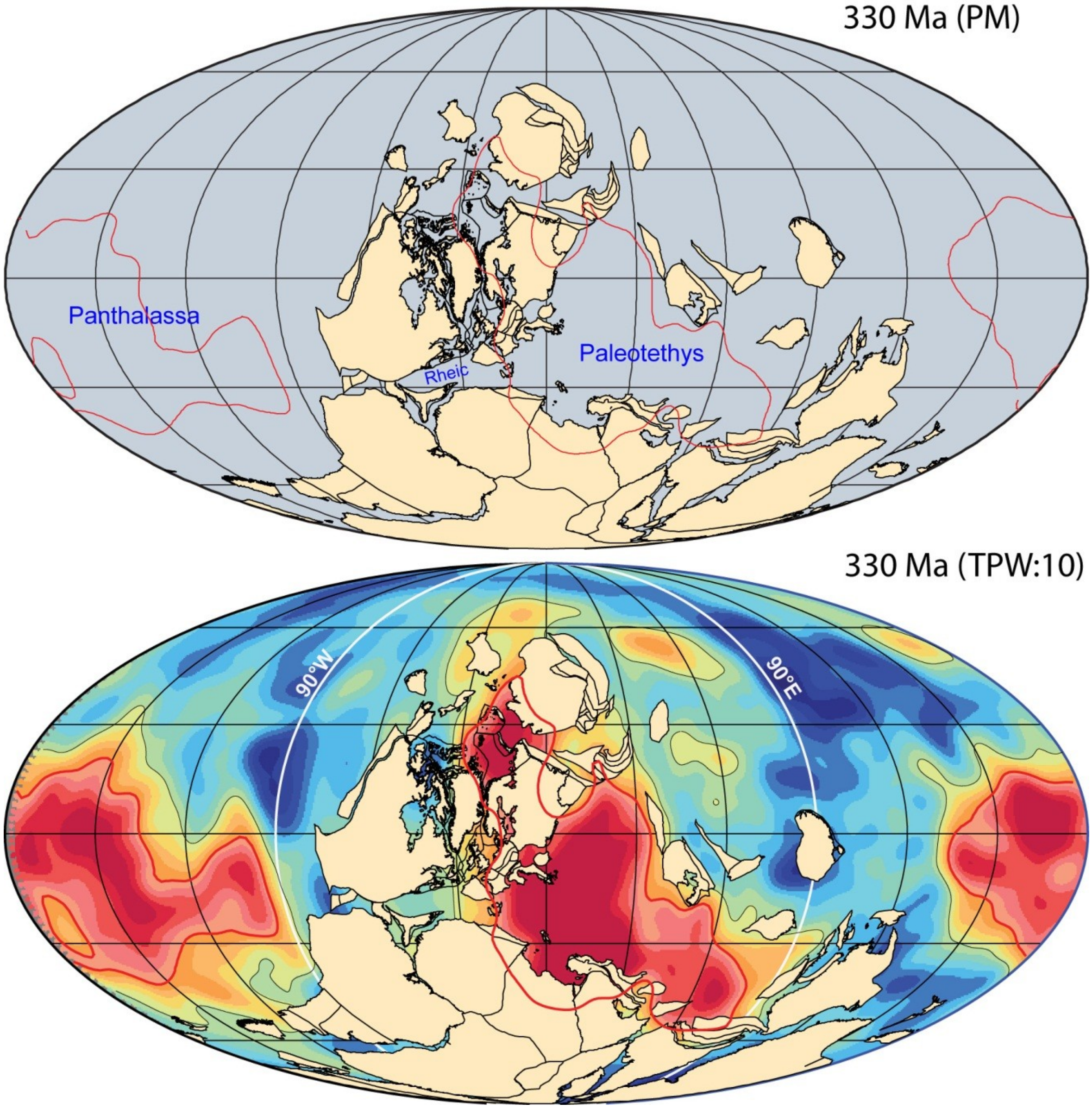

Fig. S28. Mid Carboniferous reconstruction. No known kimberlites or large igneous provinces at this time. See Figs. S7, S16 & S21 for legend and more information.

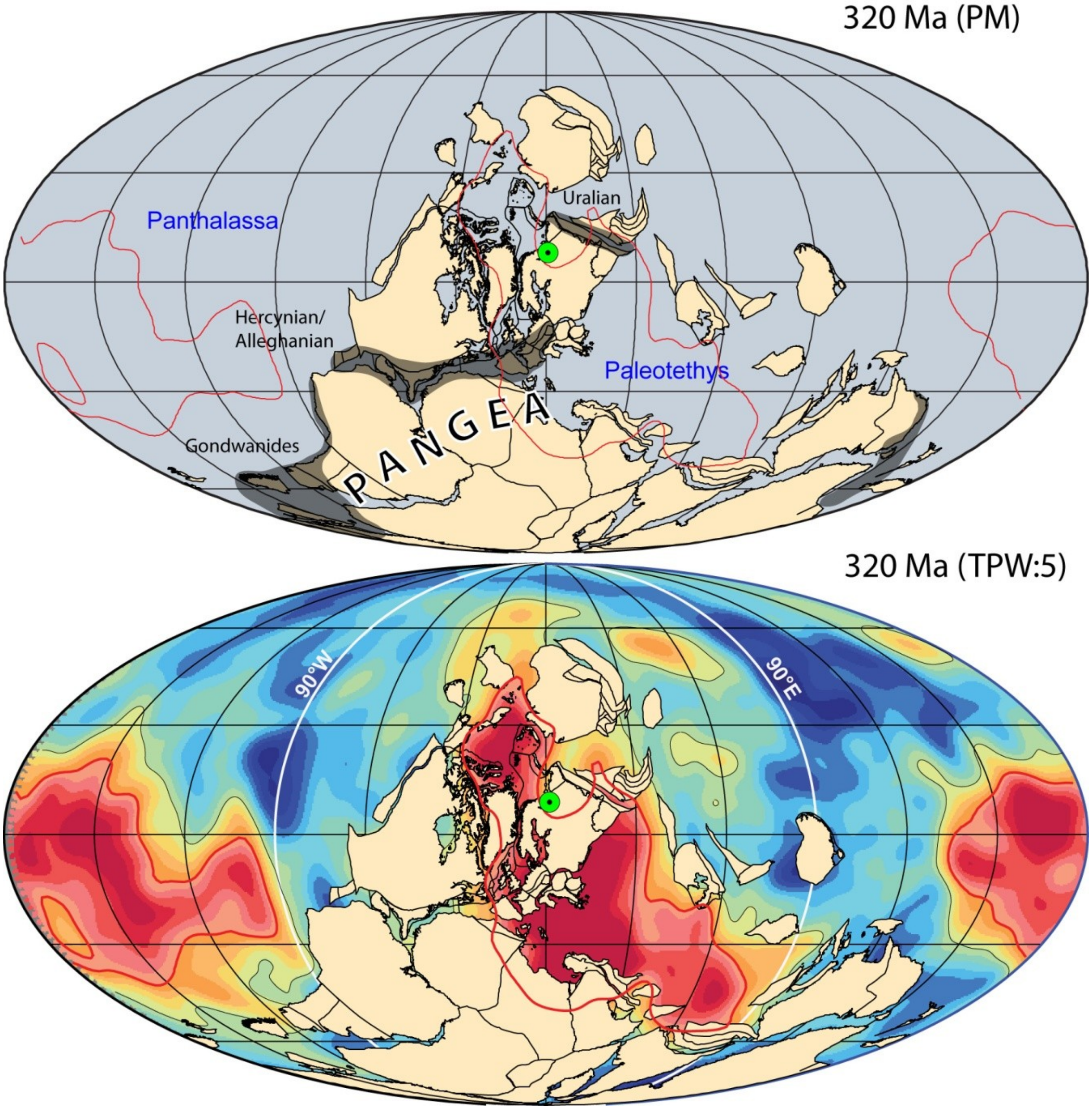

Fig. S29. Late Carboniferous reconstruction. The Rheic Ocean closed in the Carboniferous, during the main Pangea growth phase, which created the Alleghenian (in North America) and the Hercynian/Variscan (in Europe) orogenic belts (grey shading). We have also shaded the Permian-Early Mesozoic Gondwanide orogen. See Figs. S7, S16 & S21 for legend and more information.

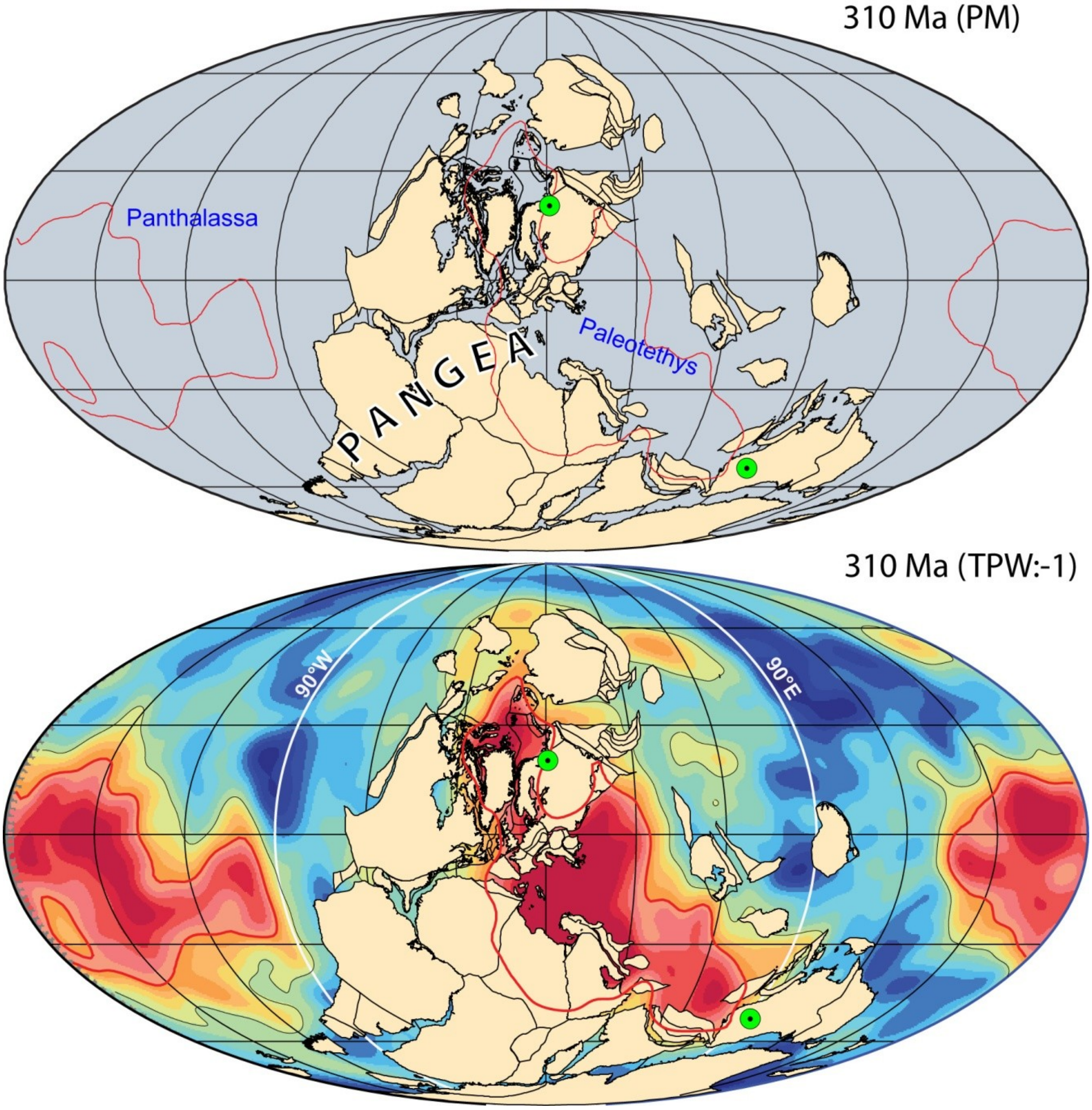

Fig. S30. Late Carboniferous reconstruction. See Figs. S7, S16 & S21 for legend and more information.

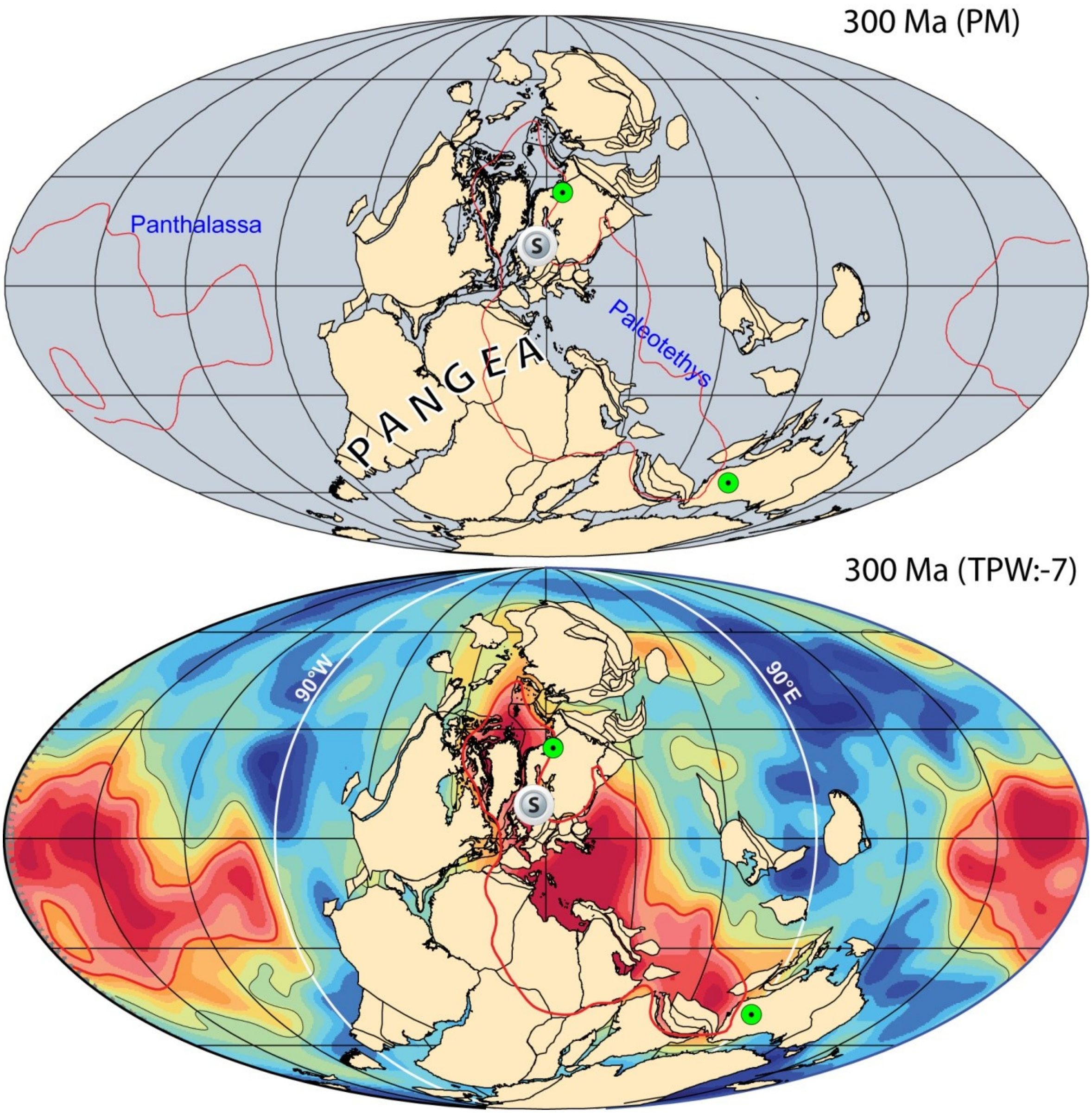

Fig. S31. Late Carboniferous reconstructions. S, Skagerrak Centred LIP in Europe (ca. 297 Ma) (9). See Figs. S7, S16 & S21 for legend and more information.

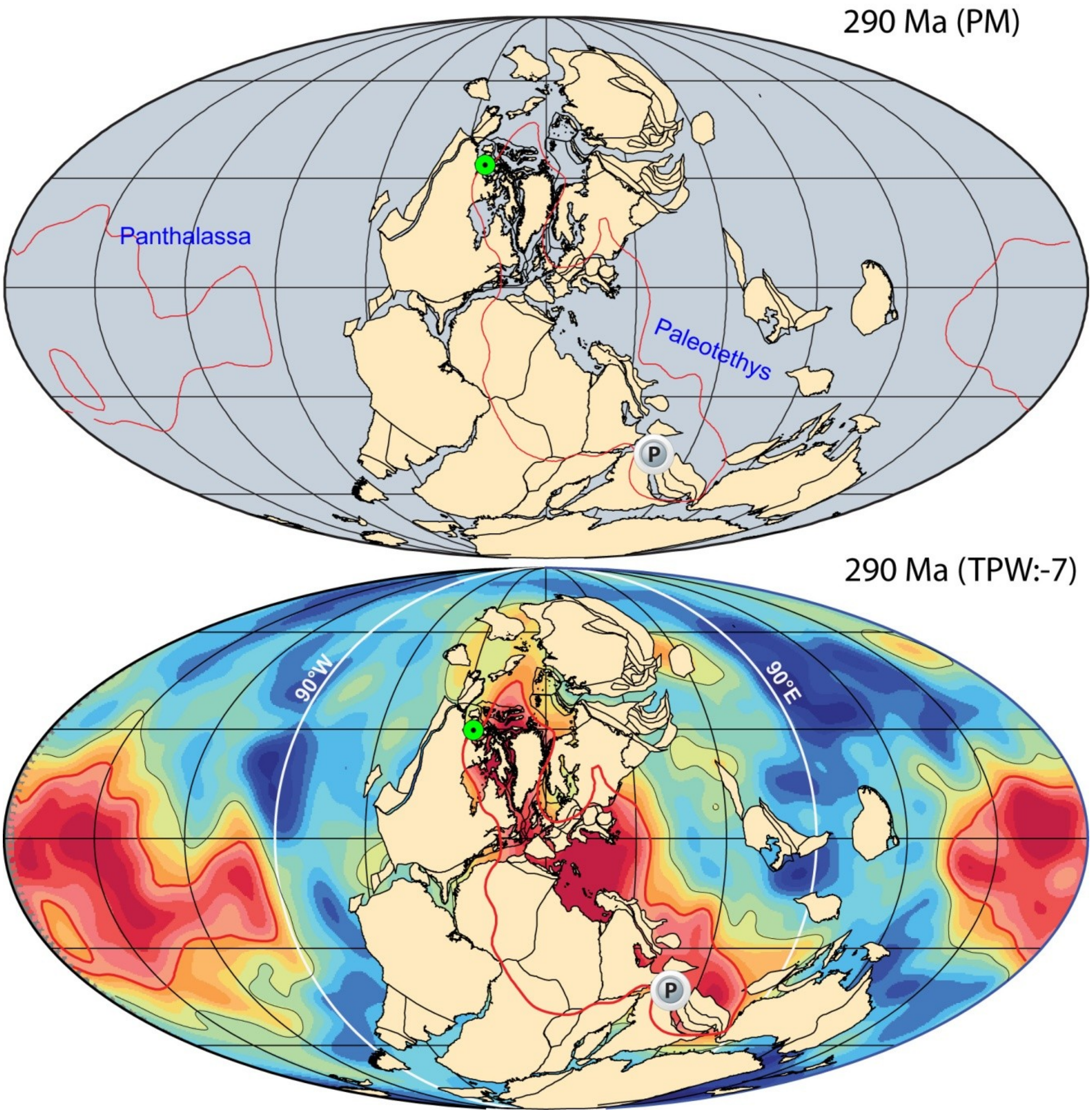

Fig. S32. Early Permian reconstruction. P, Panjal Traps (~285 Ma) in India/NW Himalaya (10, 28). See Figs. S7, S16 & S21 for legend and more information.

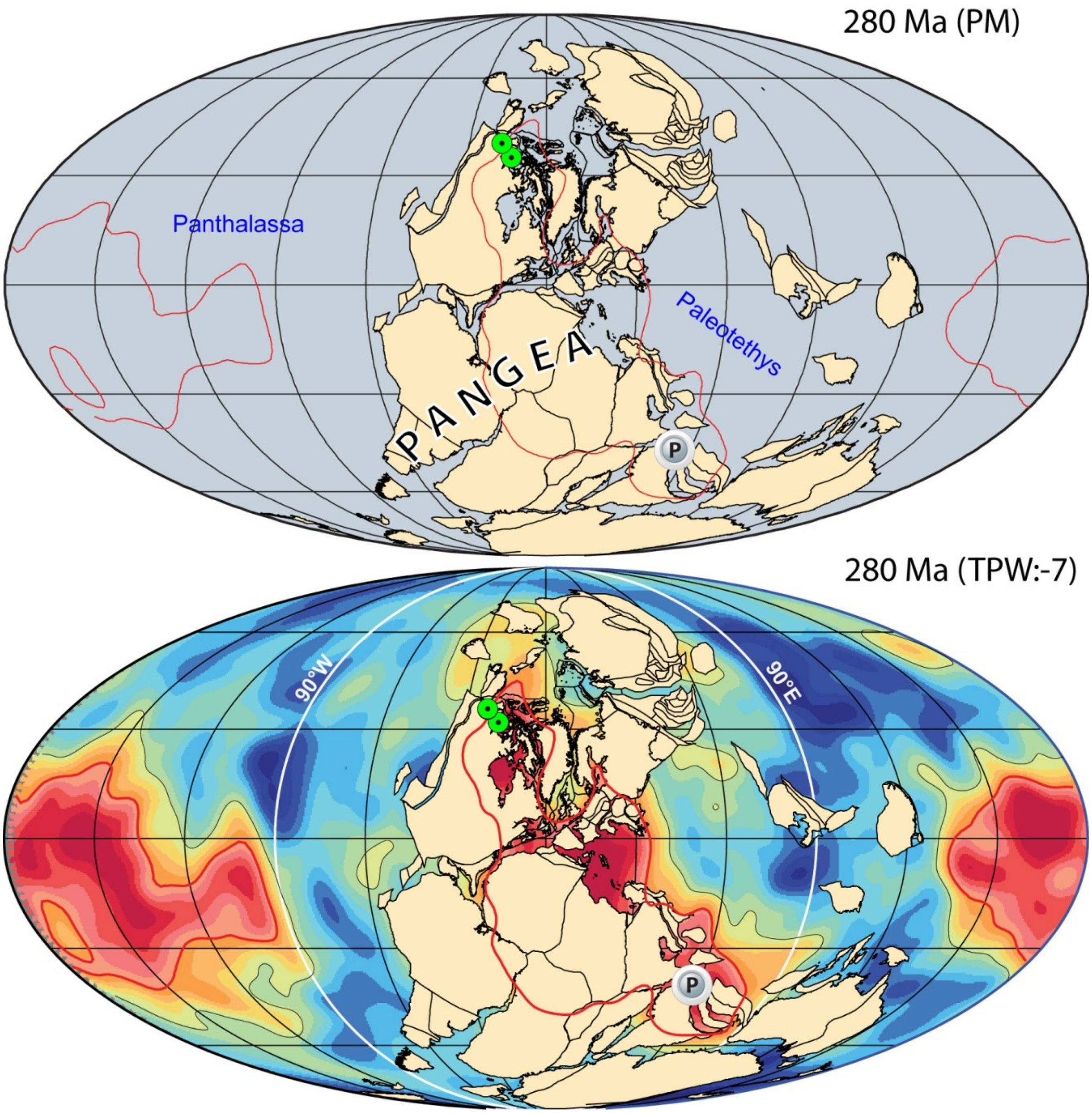

Fig. S33. Early Permian reconstruction. P, Panjal Traps (~285 Ma). See Figs. S7, S16 & S21 for legend and more information.

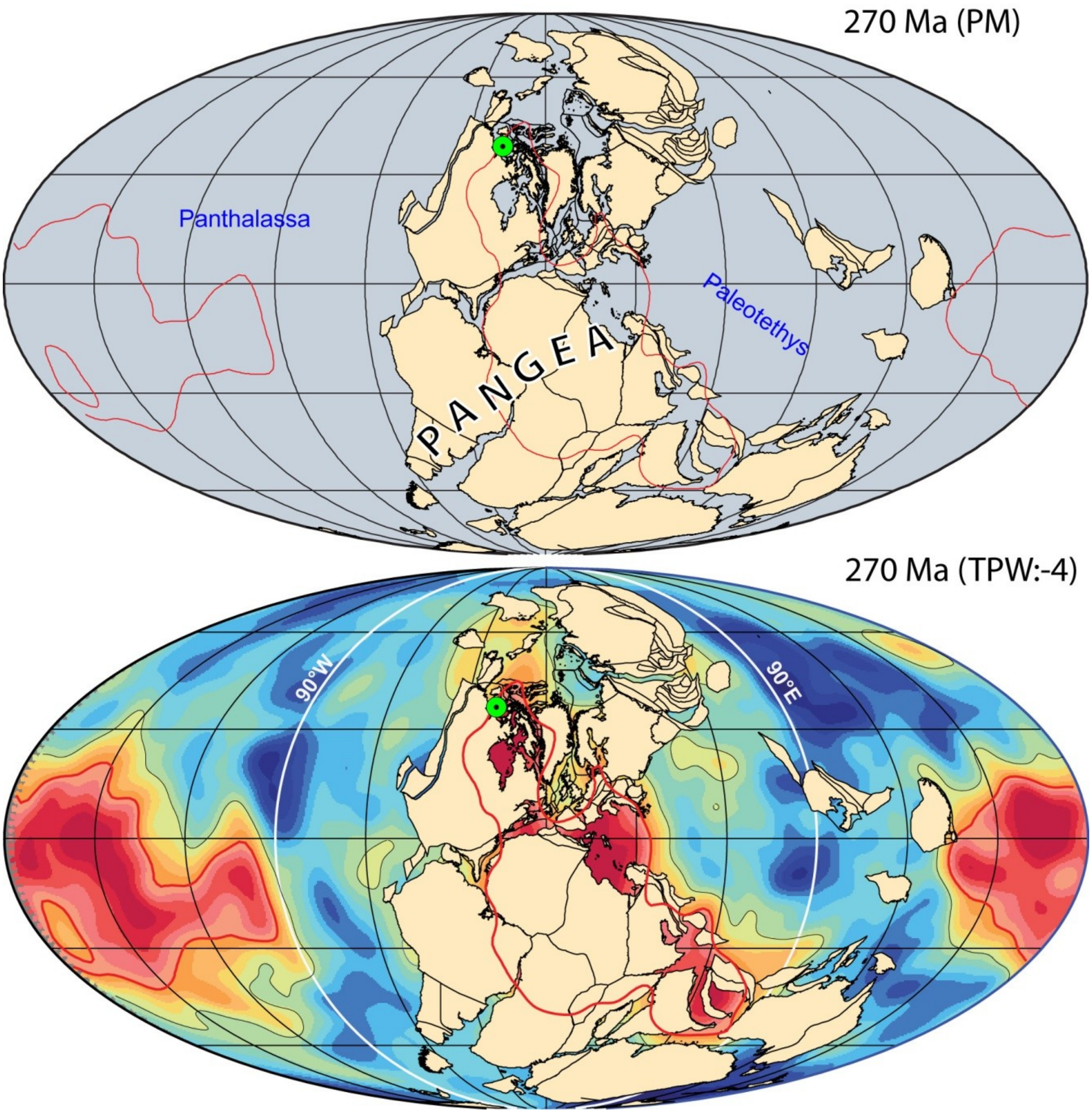

Fig. S34. Mid Permian reconstruction. See Figs. S7, S16 & S21 for legend and more information.

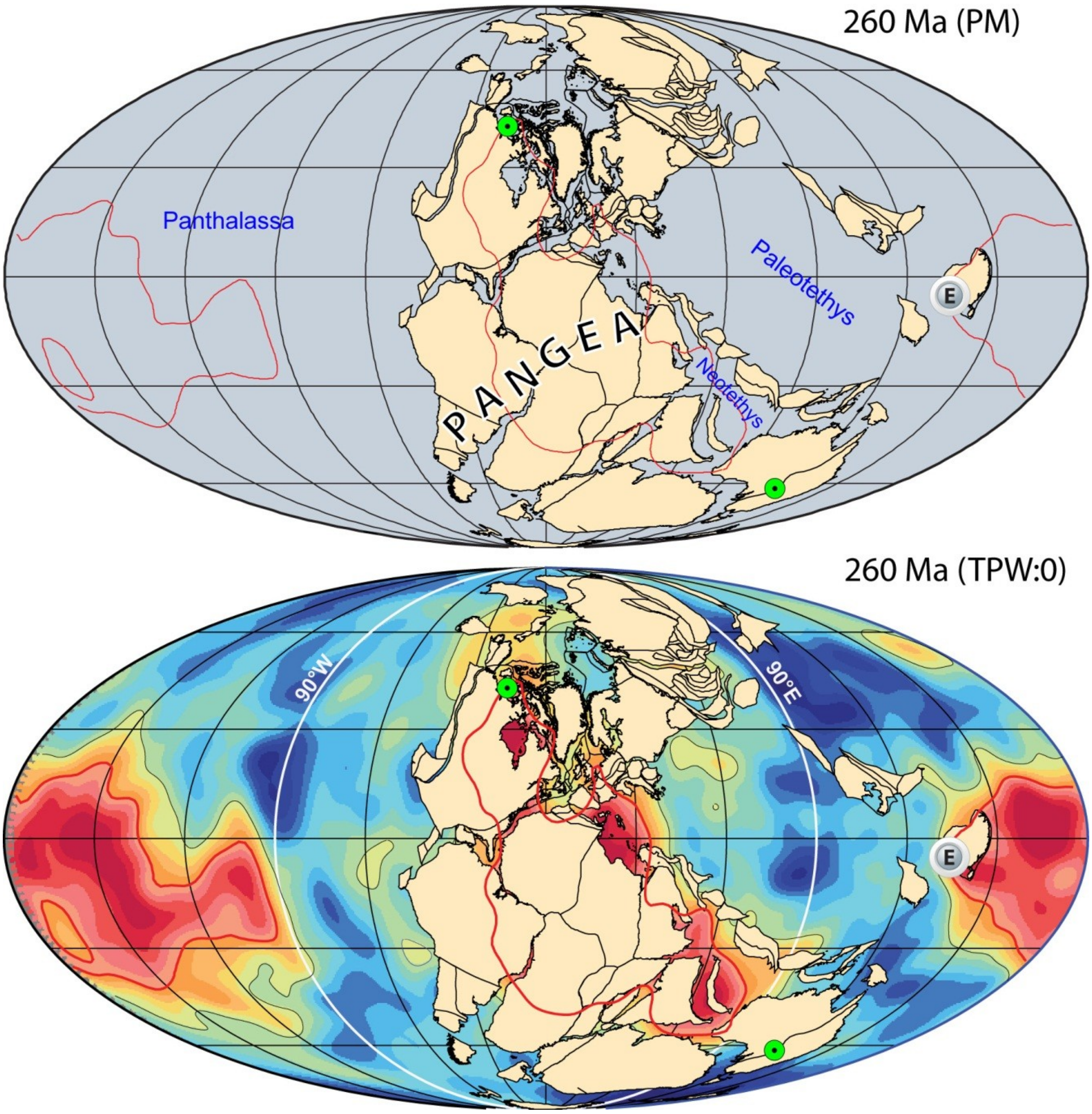

Fig. S35. Late Permian reconstruction. E, Emeishan LIP (~258 Ma) in South China (29, 4). See Figs. S7, S16 & S21 for legend and more information.

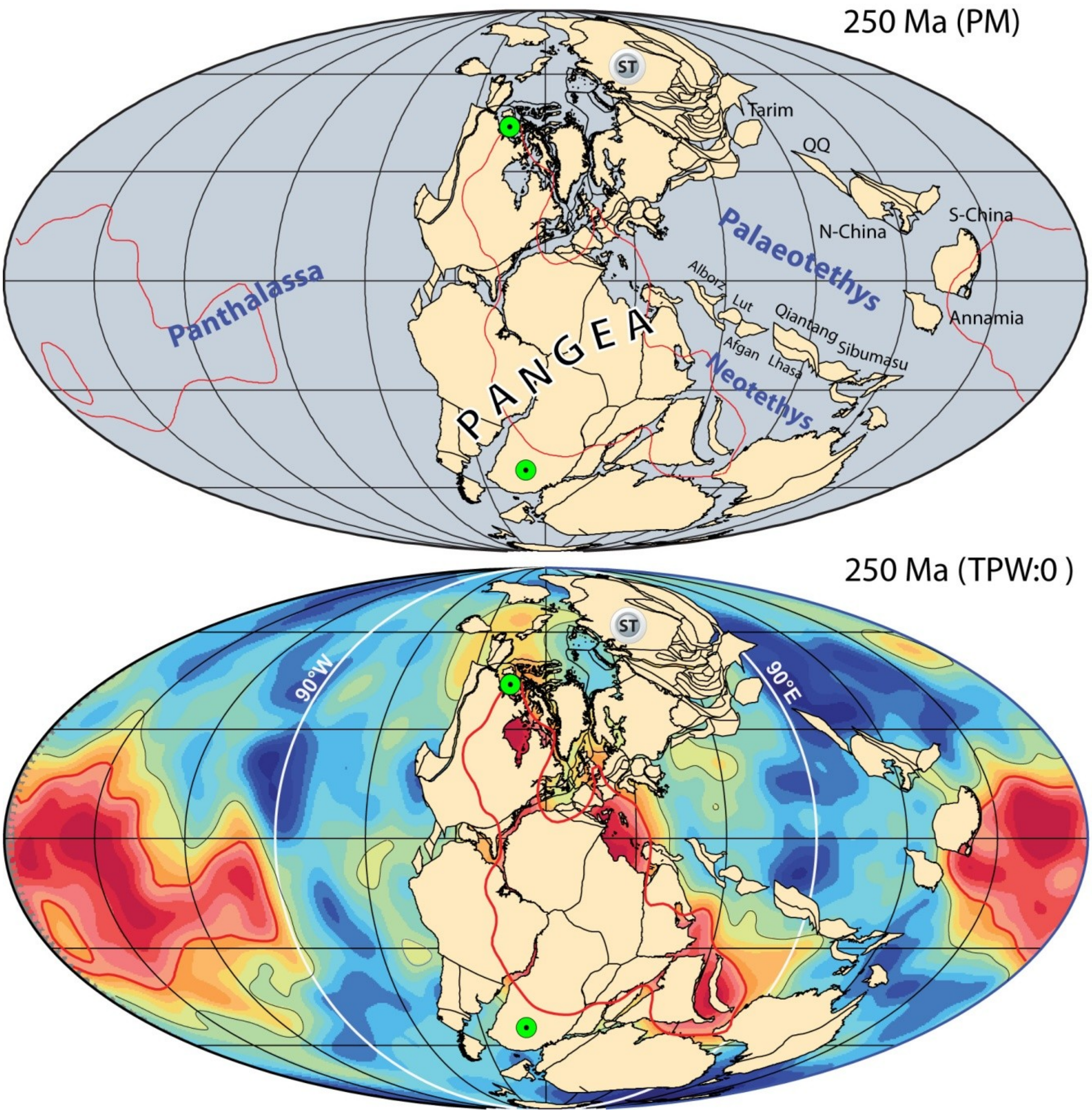

Fig. S36. Early Mesozoic reconstructions. ST, Siberian Traps (~251 Ma) in Siberia (30-32). QQ, Qaidam-Qilian. See Figs. S7, S16 & S21 for legend and more information.

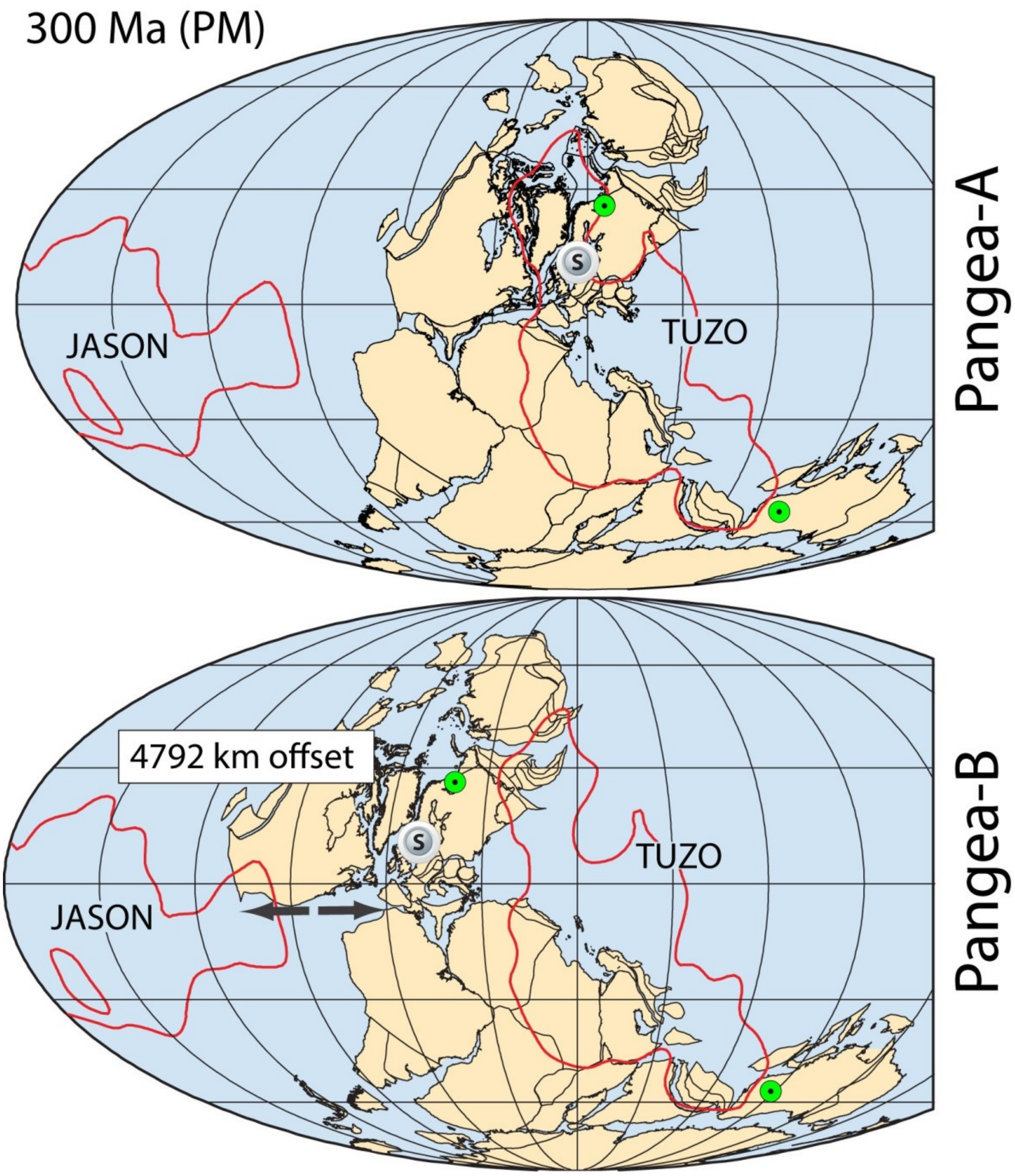

Fig. S37. 300 Ma reconstruction compared with a Pangea B reconstruction (33) where Gondwana and Laurussia are displaced laterally (lower panel) and the transition from a Pangea B to Pangea A fit must accommodate ca. 5000 km dextral strike-slip before the Late Permian. In the Pangea B configuration, Florida would be located south of France and East of Iberia in Late Carboniferous-Early Permian times. In our Pangea B fits we have located Gondwana as in Fig. S31 and moved Laurussia westward to accommodate nearly 5000 km offset. This approach (or alternatively moving Gondwana eastward) generally leads to a poorer correlation between kimberlites and large igneous provinces with a plume generation zone. Reconstructions are in a paleomagnetic frame but the plume generation zones (1% slow in SMEAN model) are rotated according to our true polar wander model (-7^{o} net true polar wander at this time).

Table S1 Relative fits (250-540 Ma) of the most important Paleozoic continents/terranes versus a fixed South Africa in GPlates format (34) (www.gplates.org). South Africa (Plate Id = 701) is listed in a longitude calibrated palaeomagnetic frame (Plate Id = 1, i.e. the spin axis) and our true polar wander (TPW) model is listed in the top 13 rows. At start-up, the GPlates software defaults to a mantle frame (Plate Id = 0) and thus reconstructions will be displayed as TPW corrected (lower panels in Figs. S7-36). In order to show reconstructions with respect to the spin-axis (palaeomagnetic frame) select option "Reconstruction", sub-option "Specify Anchored Plate ID", and type 1.

Plate A	Age	EULER ROTATION POLE			Plate B	Plate A Name (comment)
		Latitude°	Longitude°	Angle°		
1	250	0	0	0	0	Spin Axis (1) to Mantle (0)
1	260	0	0	0	0	Spin Axis (1) to Mantle (0)
1	280	0	11	7	0	Spin Axis (1) to Mantle (0)
1	300	0	11	7	0	Spin Axis (1) to Mantle (0)
1	350	0	11	-22	0	Spin Axis (1) to Mantle (0)
1	380	0	11	-22	0	Spin Axis (1) to Mantle (0)
1	410	0	11	-31	0	Spin Axis (1) to Mantle (0)
1	420	0	11	-31	0	Spin Axis (1) to Mantle (0)
1	430	0	11	-35	0	Spin Axis (1) to Mantle (0)
1	460	0	11	-62	0	Spin Axis (1) to Mantle (0)
1	490	0	11	-62	0	Spin Axis (1) to Mantle (0)
1	520	0	11	-42	0	Spin Axis (1) to Mantle (0)
1	550	0	11	-42	0	Spin Axis (1) to Mantle (0)
101	250	63.19	-13.87	79.87	701	North America
101	320	63.19	-13.87	79.87	701	North America
101	330	52.34	-20.01	81.57	701	North America
101	340	38.73	-15.87	86.18	701	North America
101	350	29.94	-14.54	91.05	701	North America
101	360	17.48	-18.96	111.39	701	North America
101	370	8.9	-21.96	140.86	701	North America
101	380	11.83	-25	141.71	701	North America
101	390	9.6	-25.92	142.03	701	North America
101	400	8.13	-24.99	134.63	701	North America
101	410	4.11	-23.77	122.42	701	North America
101	420	4.12	-22.16	97.99	701	North America
101	430	5.17	-27.94	81.2	701	North America
101	440	7.75	-35.54	97.98	701	North America
101	450	10.43	-38.78	108.64	701	North America
101	460	14.83	-39.68	110.99	701	North America
101	470	21.5	-44.25	93.69	701	North America
101	480	28.05	-46.77	79.07	701	North America
101	490	36.43	-59.04	63.74	701	North America
101	500	39.32	-88.75	43.9	701	North America

101	510	42.98	-66.44	25.65	701	North America
101	520	11.65	-17.25	22.38	701	North America
101	530	9.54	171.92	-43.53	701	North America
101	540	17.95	166.47	-58.08	701	North America
102	250	60.48	1.42	69.4	701	Greenland
102	320	60.48	1.42	69.4	701	Greenland
102	330	49.11	-7.55	72.39	701	Greenland
102	340	34.84	-5.18	79.73	701	Greenland
102	350	26.21	-4.67	86.48	701	Greenland
102	360	15.62	-10.41	108.92	701	Greenland
102	370	9.2	-14.45	139.77	701	Greenland
102	380	12.19	-17.49	139.67	701	Greenland
102	390	10	-18.45	140.4	701	Greenland
102	400	8.05	-17.33	133.48	701	Greenland
102	410	3.19	-15.82	122.4	701	Greenland
102	420	1.13	-13.39	98.39	701	Greenland
102	430	0.26	-18.34	81.08	701	Greenland
102	440	4.75	-26.71	96.33	701	Greenland
102	450	8.42	-30.38	105.95	701	Greenland
102	460	13.06	-31.35	107.23	701	Greenland
102	470	18.31	-35.23	88.29	701	Greenland
102	480	23.49	-36.87	72.31	701	Greenland
102	490	30.43	-48.19	54.68	701	Greenland
102	500	28.98	-78.43	32.94	701	Greenland
102	510	18.7	-45.13	16.64	701	Greenland
102	520	16.91	-178.45	-24.96	701	Greenland
102	530	21.03	-176.1	-49.28	701	Greenland
102	540	25.04	177.14	-64.58	701	Greenland
108	250	63.19	-13.87	79.87	701	Acadia
108	320	63.19	-13.87	79.87	701	Acadia
108	330	52.34	-20.01	81.57	701	Acadia
108	340	38.73	-15.87	86.18	701	Acadia
108	350	29.94	-14.54	91.05	701	Acadia
108	360	17.48	-18.96	111.39	701	Acadia
108	370	8.9	-21.96	140.86	701	Acadia
108	380	11.83	-25	141.71	701	Acadia
108	390	9.6	-25.92	142.03	701	Acadia
108	400	8.13	-24.99	134.63	701	Acadia
108	410	4.11	-23.77	122.42	701	Acadia
108	420	4.12	-22.16	97.99	701	Acadia
108	430	5.17	-27.94	81.2	701	Acadia
108	440	11.2	-36.86	92.54	701	Acadia
108	450	21.39	-34.56	92.86	701	Acadia
108	460	29.19	-31.83	96.56	701	Acadia
108	470	36.62	-25.68	91.32	701	Acadia

108	480	41.64	-10.31	83.37	701	Acadia
108	490	43.38	-3.41	78.61	701	Acadia (Peri-Gondwana)
108	540	43.38	-3.41	78.61	701	Acadia (Peri-Gondwana)
109	250	63.19	-13.87	79.87	701	Florida
109	540	63.19	-13.87	79.87	701	Florid (Peri-Gondwana)
201	250	50	-32.5	55.08	701	Amazonia (Core Gondwana)
201	540	50	-32.5	55.08	701	Amazonia (Core Gondwana)
202	250	47.51	-33.3	56.2	701	Parana (Core Gondwana)
202	540	47.58	-33.3	56.2	701	Parana (Core Gondwana)
290	250	47.5	-33.3	57.3	701	Colorado (Core Gondwana)
290	540	47.5	-33.3	57.3	701	Colorado (Core Gondwana)
291	250	47.5	-33.3	63	701	Patagonia (Peri-Gondwana)
291	260	49.12	-30.35	62.28	701	Patagonia (Peri-Gondwana)
291	270	50.68	-27.15	61.66	701	Patagonia (Peri-Gondwana)
291	540	50.68	-27.15	61.66	701	Patagonia (Peri-Gondwana)
302	250	46.04	3.89	58.2	701	Baltica
302	320	46.04	3.89	58.2	701	Baltica
302	330	34.1	-2.57	64.85	701	Baltica
302	340	20.86	0.32	76.07	701	Baltica
302	350	13.46	1.19	85.23	701	Baltica
302	360	6.41	-3.38	110.96	701	Baltica
302	370	3.38	-6.5	143.63	701	Baltica
302	380	6.45	-9.32	142.86	701	Baltica
302	390	4.42	-10.34	144.34	701	Baltica
302	400	1.82	-9.42	138.07	701	Baltica
302	410	4.01	171.62	-128.59	701	Baltica
302	420	8.73	173.11	-105.51	701	Baltica
302	430	11.72	167.67	-89.36	701	Baltica
302	440	14.27	168.23	-84.07	701	Baltica
302	450	19.32	167.39	-72.49	701	Baltica
302	460	28.57	168.91	-58.33	701	Baltica
302	470	46.54	174.95	-47.21	701	Baltica
302	480	75.11	-170.2	-47.4	701	Baltica
302	490	77.58	37.73	-69.4	701	Baltica
302	500	65.26	33.54	-105.39	701	Baltica
302	510	64.93	10.76	-113.77	701	Baltica
302	520	65.74	-22.11	-118.37	701	Baltica
302	530	63.24	-35.9	-135.01	701	Baltica
302	540	59.6	-37.67	-150.78	701	Baltica
303	250	46.04	3.89	58.2	701	Scotland
303	320	46.04	3.89	58.2	701	Scotland
303	330	34.1	-2.57	64.85	701	Scotland
303	340	20.86	0.32	76.07	701	Scotland
303	350	13.46	1.19	85.23	701	Scotland
303	360	6.41	-3.38	110.96	701	Scotland

303	370	3.38	-6.5	143.63	701	Scotland
303	380	6.45	-9.32	142.86	701	Scotland
303	390	4.42	-10.34	144.34	701	Scotland
303	400	1.82	-9.42	138.07	701	Scotland
303	410	4.01	171.62	-128.59	701	Scotland
303	420	8.73	173.11	-105.51	701	Scotland
303	430	11.72	167.67	-89.36	701	Scotland
303	440	4.92	160.65	-103.44	701	Scotland (Peri-Laurentia)
303	450	0.07	157.66	-111.91	701	Scotland (Peri-Laurentia)
303	460	4.54	-22.97	111.71	701	Scotland (Peri-Laurentia)
303	470	7.08	-26.86	91.69	701	Scotland (Peri-Laurentia)
303	480	8.92	-28.65	74.6	701	Scotland (Peri-Laurentia)
303	490	10.71	-38.96	55.83	701	Scotland (Peri-Laurentia)
303	500	1.5	115.95	-36.25	701	Scotland (Peri-Laurentia)
303	510	28.48	139.21	-27.03	701	Scotland (Peri-Laurentia)
303	520	43.27	175.34	-38.79	701	Scotland (Peri-Laurentia)
303	530	37.42	-175.86	-62.13	701	Scotland (Peri-Laurentia)
303	540	37.2	179.43	-78.39	701	Scotland (Peri-Laurentia)
304	250	51.77	67.88	3.42	701	Iberia
304	320	51.77	67.88	3.42	701	Iberia
304	330	10.76	-166.02	-15.09	701	Iberia
304	340	14.04	-154.13	-33.63	701	Iberia
304	350	12.65	-153.64	-41.98	701	Iberia
304	360	9.43	-164.23	-64.97	701	Iberia
304	370	28.2	-144.2	-64.1	701	Iberia
304	380	-48.1	83.3	58.9	701	Iberia
304	390	47.3	-44.6	-88.9	701	Iberia
304	400	44.8	-26.3	-101.8	701	Iberia
304	410	40.5	-11.6	-113.9	701	Iberia (Peri-Gondwana)
304	420	39.51	-6.66	-116.57	701	Iberia (Peri-Gondwana)
304	540	39.5	-6.73	-116.57	701	Iberia (Peri-Gondwana)
305	250	46.04	3.89	58.2	701	Armorica
305	320	46.04	3.89	58.2	701	Armorica
305	330	34.1	-2.57	64.85	701	Armorica
305	340	20.86	0.32	76.07	701	Armorica
305	350	17.03	0.83	82.86	701	Armorica
305	360	11.58	-5.17	104.92	701	Armorica
305	370	-2.6	175.9	-99.8	701	Armorica
305	380	-7.2	174.1	-83.7	701	Armorica
305	390	10.6	-4.8	61.1	701	Armorica
305	400	16.9	2.5	39.5	701	Armorica
305	410	-39.4	-155.5	-23.3	701	Armorica (Peri-Gondwana)
305	420	54.59	38.4	21.52	701	Armorica (Peri-Gondwana)
305	540	54.33	38.43	21.52	701	Armorica (Peri-Gondwana)
315	250	46.04	3.89	58.2	701	England -Brabant

315	320	46.04	3.89	58.2	701	England -Brabant
315	330	34.1	-2.57	64.85	701	England -Brabant
315	340	20.86	0.32	76.07	701	England -Brabant
315	350	13.46	1.19	85.23	701	England -Brabant
315	360	6.41	-3.38	110.96	701	England -Brabant
315	370	3.38	-6.5	143.63	701	England -Brabant
315	380	6.45	-9.32	142.86	701	England -Brabant
315	390	4.42	-10.34	144.34	701	England -Brabant
315	400	1.82	-9.42	138.07	701	England -Brabant
315	410	4.01	171.62	-128.59	701	England -Brabant
315	420	8.73	173.11	-105.51	701	England -Brabant
315	430	11.72	167.67	-89.36	701	England -Brabant
315	440	14.27	168.23	-84.07	701	England -Brabant
315	450	4.5	170.29	-76.72	701	England -Brabant
315	460	-5.19	172.56	-73.27	701	England -Brabant
315	470	11.17	-0.94	62.97	701	England -Brabant
315	480	13.41	16.78	53.14	701	England -Brabant (Peri-Gondwana)
315	490	12.5	25.18	48.51	701	England -Brabant (Peri-Gondwana)
315	540	12.5	25.18	48.5	701	England -Brabant (Peri-Gondwana)
373	250	49.08	2.28	60.6	701	Novaya -Semya
373	320	49.08	2.28	60.6	701	Novaya -Semya
373	330	37.14	-4.34	66.5	701	Novaya -Semya
373	340	23.59	-1.42	76.85	701	Novaya -Semya
373	350	15.87	-0.56	85.51	701	Novaya -Semya
373	360	8.01	-5.21	110.69	701	Novaya -Semya
373	370	4.25	-8.41	143.1	701	Novaya -Semya
373	380	7.31	-11.26	142.52	701	Novaya -Semya
373	390	5.25	-12.27	143.85	701	Novaya -Semya
373	400	2.77	-11.31	137.41	701	Novaya -Semya
373	410	2.88	169.79	-127.55	701	Novaya -Semya
373	420	7.08	171.38	-104.19	701	Novaya -Semya
373	430	9.66	165.98	-87.82	701	Novaya -Semya
373	440	12.06	166.58	-82.38	701	Novaya -Semya
373	450	16.76	165.82	-70.49	701	Novaya -Semya
373	460	25.55	167.54	-55.82	701	Novaya -Semya
373	470	43.7	174.15	-43.9	701	Novaya -Semya
373	480	74.27	-168.07	-43.47	701	Novaya -Semya
373	490	77.14	32.21	-65.66	701	Novaya -Semya
373	500	64.91	30.45	-102	701	Novaya -Semya
373	510	64.49	7.64	-110.52	701	Novaya -Semya
373	520	65.09	-25.16	-115.19	701	Novaya -Semya
373	530	62.67	-38.71	-131.95	701	Novaya -Semya
373	540	59.19	-40.36	-147.88	701	Novaya -Semya
390	250	46.04	3.89	58.2	701	Urals (Peri-Baltic arcs)
390	320	46.04	3.89	58.2	701	Urals (Peri-Baltic arcs)

390	330	34.1	-2.57	64.85	701	Urals (Peri-Baltic arcs)
401	250	47.59	3.1	59.38	701	Siberia (peri - Siberia)
401	260	48.22	2.61	60.09	701	Siberia (peri - Siberia)
401	270	48.84	2.13	60.82	701	Siberia (peri - Siberia)
401	280	49.44	1.64	61.55	701	Siberia (peri - Siberia)
401	290	50.23	1.07	62.42	701	Siberia (peri - Siberia)
401	300	50.99	0.49	63.3	701	Siberia (peri - Siberia)
401	310	51.74	-0.09	64.2	701	Siberia (peri - Siberia)
401	320	52.46	-0.67	65.1	701	Siberia (peri - Siberia)
401	330	39.38	-3.08	62.59	701	Siberia (peri - Siberia)
401	340	22.43	4.98	67.01	701	Siberia (peri - Siberia)
401	350	21.45	3.04	68.86	701	Siberia (peri - Siberia)
401	360	20.9	-4.62	76.42	701	Siberia (peri - Siberia)
401	370	20.47	-9.82	98.57	701	Siberia (peri - Siberia)
401	380	28.43	-13.96	96.64	701	Siberia (peri - Siberia)
401	390	35.05	-11.14	91.83	701	Siberia (peri - Siberia)
401	400	36.84	-6.25	92.28	701	Siberia (peri - Siberia)
401	410	41.82	2.43	86.66	701	Siberia (peri - Siberia)
401	420	57.21	22.75	75.91	701	Siberia (peri - Siberia)
401	430	68.26	50.31	64.91	701	Siberia (peri - Siberia)
401	440	76.32	16.57	52.8	701	Siberia (peri - Siberia)
401	450	70.32	-42.78	43.22	701	Siberia (peri - Siberia)
401	460	52.14	-37.70	46.13	701	Siberia (peri - Siberia)
401	470	60.25	-20.27	48.07	701	Siberia (peri - Siberia)
401	480	76.95	11.23	52.64	701	Siberia (peri - Siberia)
401	490	71.96	149.46	47.95	701	Siberia (peri - Siberia)
401	500	61.81	145.39	43.87	701	Siberia (peri - Siberia)
401	510	56.69	100.51	46.8	701	Siberia (peri - Siberia)
401	520	46.16	63.47	47.05	701	Siberia (peri - Siberia)
401	530	27.04	50.1	47.5	701	Siberia (peri - Siberia)
401	540	3.59	45.81	55.49	701	Siberia (peri - Siberia)
501	250	29.93	42.29	-60.47	701	India (Core Gondwana)
501	540	29.93	42.29	-60.47	701	India (Core Gondwana)
503	250	37.11	17.11	-8.86	701	Arabia (Core Gondwana)
503	540	37.11	17.11	-8.86	701	Arabia (Core Gondwana)
504	250	37.07	17.13	-8.83	701	Taurides (Turkey) (Peri-G.)
504	540	37.07	17.13	-8.83	701	Taurides (Turkey) (Peri-G.)
505	250	52.83	-11.13	7.73	701	Alborz (Iran) (Peri-Gondwana)
505	260	18.37	32.21	-3.18	701	Alborz (Iran) (Peri-Gondwana)
505	270	35.34	17.69	-7.89	701	Alborz (Iran) (Peri-Gondwana)
505	540	35.34	17.69	-7.89	701	Alborz (Iran) (Peri-Gondwana)
506	250	25.23	69.03	-55.07	701	Afghan (Peri-Gondwana)
506	260	26.61	60.32	-61.61	701	Afghan (Peri-Gondwana)
506	270	27.04	55.58	-66.03	701	Afghan (Peri-Gondwana)
506	280	27.08	53.73	-67.75	701	Afghan (Peri-Gondwana)

506	290	27.09	52.84	-68.62	701	Afghan (Peri-Gondwana)
506	540	27.09	52.84	-68.62	701	Afghan (Peri-Gondwana)
563	250	27.91	45.28	-58.22	701	Tethys Himalayan(GI)
563	270	28.24	44.8	-58.56	701	Tethys Himalayan(GI)
563	280	-28.88	-136.11	59.25	701	Tethys Himalayan(GI)
563	290	-29.12	-136.58	59.59	701	Tethys Himalayan(GI)
563	540	-29.12	-136.58	59.59	701	Tethys Himalayan(GI)
564	250	-29.93	-137.71	60.46	701	Lesser Himalayan(GI)
564	540	-29.93	-137.71	60.46	701	Lesser Himalayan(GI)
581	250	-37.06	-162.86	8.82	701	Pontides (Turkey)
581	540	-37.06	-162.86	8.82	701	Pontides (Turkey)
582	250	-52.83	168.86	-7.73	701	Sanand (Iran)
582	260	-18.38	-147.79	3.17	701	Sanand (Iran)
582	270	-35.35	-162.28	7.89	701	Sanand (Iran)
582	540	-35.35	-162.28	7.89	701	Sanand (Iran)
583	250	31.56	-105.38	-105.38	701	Lut
583	260	-30.15	-121.24	112.63	701	Lut
583	270	-29.41	-123.44	116.35	701	Lut (Peri-Gondwana)
583	540	-29.41	-123.44	116.35	701	Lut (Peri-Gondwana)
599	250	14.56	110.76	48.2	701	Sibumasu south
599	260	5.02	105.57	68.7	701	Sibumasu south
599	270	-1.95	-76.03	-79.45	701	Sibumasu south (Peri-Gondwana)
599	540	-1.95	-76.03	-79.45	701	Sibumasu south (Peri-Gondwana)
601	250	23.87	130.2	-71.99	701	North China
601	260	31.33	124.88	-76.03	701	North China
601	270	37.09	120.13	-87.45	701	North China
601	280	44.71	117.46	-98.11	701	North China
601	290	43.96	112.1	-103.25	701	North China
601	300	43.2	109.46	-106.39	701	North China
601	310	47.21	108.32	-110.85	701	North China
601	320	50.76	111.26	-121.28	701	North China
601	330	52.88	111.21	-122.52	701	North China
601	340	-58.02	-61.02	123.54	701	North China
601	350	57.23	122.22	-121.37	701	North China
601	360	54.77	130.04	-122.23	701	North China
601	370	54.81	149.28	-130.31	701	North China
601	380	50.98	146.36	-130.91	701	North China
601	390	52.34	145.65	-128.95	701	North China
601	400	53.08	139.49	-121.55	701	North China
601	410	55.94	130.09	-118.91	701	North China
601	420	50.14	118.18	-118.36	701	North China
601	430	44.63	110.81	-127.58	701	North China
601	440	45.01	110.02	-144.79	701	North China
601	450	46.54	113.3	-158.29	701	North China
601	460	-49.64	-58.18	161.48	701	North China

601	470	50.05	125.75	-153.16	701	North China
601	480	46.76	120.48	-144.04	701	North China
601	490	36.08	109.76	-148.18	701	North China
601	500	32.54	105.78	-151.47	701	North China
601	510	40.37	104.68	-146.81	701	North China
601	520	50.59	100.5	-153.98	701	North China
601	530	54.17	88.76	-168.61	701	North China
601	540	58.81	81.38	-175.06	701	North China
602	250	53.52	-99.21	37.09	701	South China
602	260	41.85	-103.27	40.51	701	South China
602	270	60.25	-175.17	39.8	701	South China
602	280	60.92	164.36	30.78	701	South China
602	290	56.92	168.31	31.11	701	South China
602	300	53.62	164.62	29.94	701	South China
602	310	49.96	161.26	28.91	701	South China
602	320	45.23	141.21	25.42	701	South China
602	330	42.25	140.57	25.53	701	South China
602	340	39.29	140	25.7	701	South China
602	350	38.76	128.78	23.61	701	South China
602	360	37.38	120.92	22.89	701	South China
602	370	35.4	113.01	22.45	701	South China
602	380	24.03	126.78	22.48	701	South China
602	390	11.3	132	22.9	701	South China
602	400	19.34	140.65	25.56	701	South China
602	410	19.95	152.09	29.24	701	South China
602	420	1.97	-20.64	-19.18	701	South China
602	430	14.35	-17.5	-18.47	701	South China (Peri-Gondwana)
602	440	29.81	-15.31	-17.97	701	South China (Peri-Gondwana)
602	450	44.95	-12.35	-18.8	701	South China (Peri-Gondwana)
602	460	57.92	-8.17	-20.79	701	South China (Peri-Gondwana)
602	470	53.67	62.99	-39.62	701	South China (Peri-Gondwana)
602	480	45.57	77.14	-64.03	701	South China (Peri-Gondwana)
602	540	45.57	77.14	-64.03	701	South China (Peri-Gondwana)
603	250	16.73	112.1	46.74	701	Sibumasu North
603	260	6.44	106.22	66.93	701	Sibumasu North
603	270	3.17	104.43	77.56	701	Sibumasu North (Peri-Gondwana)
603	540	3.17	104.43	77.56	701	Sibumasu North (Peri-Gondwana)
606	250	25.38	68.23	-30.37	701	Lhasa (S Tibet)
606	260	36.14	44.61	-35.02	701	Lhasa (S Tibet)
606	270	34.53	37.26	-43.97	701	Lhasa (S Tibet)
606	280	30.73	41.85	-54.31	701	Lhasa (S Tibet) (Peri-Gondwana)
606	290	29.19	43.42	-59.6	701	Lhasa (S Tibet) (Peri-Gondwana)
606	540	29.19	43.42	-59.6	701	Lhasa (S Tibet)
616	250	25.38	68.23	-30.37	701	Qiantang (N Tibet)
616	260	36.14	44.61	-35.02	701	Qiantang (N Tibet)

616	270	34.53	37.26	-43.97	701	Qiantang (N Tibet)
616	280	30.73	41.85	-54.31	701	Qiantang (N Tibet)
616	290	29.19	43.42	-59.6	701	Qiantang (N Tibet) (Peri-Gondwana)
616	540	29.19	43.42	-59.6	701	Qiantang (N Tibet) (Peri-Gondwana)
701	250	-2.78	150.08	45.34	1	South Africa (Core Gondwana)
701	260	-3.81	148.98	45.87	1	South Africa (Core Gondwana)
701	270	7.4	-35.85	-51.9	1	South Africa (Core Gondwana)
701	280	-7.21	143.43	58.41	1	South Africa (Core Gondwana)
701	290	-14.93	137.7	60.97	1	South Africa (Core Gondwana)
701	300	20.57	-47.73	-64.52	1	South Africa (Core Gondwana)
701	310	19.53	-53.66	-67.86	1	South Africa (Core Gondwana)
701	320	11.5	-60.73	-74.46	1	South Africa (Core Gondwana)
701	330	7.86	-66.19	-73.18	1	South Africa (Core Gondwana)
701	340	13.52	-74.58	-76.26	1	South Africa (Core Gondwana)
701	350	1.55	-69.58	-72.48	1	South Africa (Core Gondwana)
701	360	8.81	115.68	77.64	1	South Africa (Core Gondwana)
701	370	18.89	126.95	89.51	1	South Africa (Core Gondwana)
701	380	15.33	120.65	88.91	1	South Africa (Core Gondwana)
701	390	-15.29	-62.94	-81.53	1	South Africa (Core Gondwana)
701	400	-14.06	-67.19	-72.25	1	South Africa (Core Gondwana)
701	410	-9.35	-75.71	-64.06	1	South Africa (Core Gondwana)
701	420	5.99	-92.66	-67.78	1	South Africa (Core Gondwana)
701	430	14.65	-107.1	-82.48	1	South Africa (Core Gondwana)
701	440	9.11	-108.91	-96.15	1	South Africa (Core Gondwana)
701	450	6.94	-110.79	-111.15	1	South Africa (Core Gondwana)
701	460	11.07	-118.2	-124.37	1	South Africa (Core Gondwana)
701	470	12.77	-115.52	-129.29	1	South Africa (Core Gondwana)
701	480	18.3	-120.15	-135.48	1	South Africa (Core Gondwana)
701	490	23.06	-130.91	-148.84	1	South Africa (Core Gondwana)
701	500	26.66	-140.67	-154.56	1	South Africa (Core Gondwana)
701	510	31.24	-144.41	-146.64	1	South Africa (Core Gondwana)
701	520	30.22	-139.72	-127.55	1	South Africa (Core Gondwana)
701	530	25.12	-136.31	-109.38	1	South Africa (Core Gondwana)
701	540	20.18	-135.59	-94.43	1	South Africa (Core Gondwana)
702	250	14.74	137.62	-15.64	701	Madagascar (Core Gondwana)
702	540	14.74	137.62	-15.64	701	Madagascar (Core Gondwana)
706	250	33.65	26.02	2.34	701	Oran Meseta (Core Gondwana)
706	540	33.65	26.02	2.34	701	Oran Meseta (Core Gondwana)
709	250	9.89	143	-0.22	701	Somalia (Core Gondwana)
709	540	9.89	142.99	-0.22	701	Somalia (Core Gondwana)
712	250	9.89	143	-0.22	701	Lake Victoria (Core Gondwana)
712	540	9.89	142.99	-0.22	701	Lake Victoria (Core Gondwana)
714	250	33.65	26.02	2.34	701	Northwest Africa (Core Gondwana)
714	540	33.65	26.02	2.34	701	Northwest Africa (Core Gondwana)
715	250	40.45	-61.4	-0.7	701	Northeast Africa (Core Gondwana)

715	540	40.41	-61.4	-0.7	701	Northeast Africa (Core Gondwana)
801	250	19.57	117.9	-56.42	701	Australia (Core Gondwana)
801	540	19.57	117.9	-56.42	701	Australia (Core Gondwana)
802	250	10.44	148.74	-58.41	701	East Antarctica (Core Gondwana)
802	540	10.44	148.74	-58.41	701	East Antarctica (Core Gondwana)
854	250	10.44	148.74	-58.41	701	Dronning Maud Land (Core Gondwana)
854	540	10.44	148.74	-58.41	701	Dronning Maud Land (Core Gondwana)

Table S2 ΔPGZ, great circle distance from reconstructed large igneous provinces (LIPs) and kimberlites to a plume generation zone (PGZ; 1% slow contour in SMEAN) or the seismic 'voting' map contours as defined in Lekic et al. (35). We note that although ΔPGZ is always positive, and hence its distribution is not truly Gaussian, we nevertheless use the normal definition of standard deviation as a simple means of describing the variance. Map contour 4 best fits the distribution of large igneous provinces (LIPs) and kimberlites. True polar wander corrected paleomagnetic reference frame.

Contour	**LIPS (N=7)**		**Kimberlites (N=231)**	
	ΔPGZ	**% within 10^{o}**	**ΔPGZ**	**% within 10^{o}**
PGZ: 1% Slow SMEAN contour	8.9 ± 12.8	71%	2.8 ± 4.1	98
	4.4 ± 4.7	83% (Siberian Traps excluded, N=6)		
Map Contour 5	4.5 ± 3.4	86	3.5 ± 4.4	97
Map Contour 4	**3.3 ± 3.7**	**100**	**2.6 ± 3.8**	**97**
Map Contour 3	3.9 ± 4.3	86	3.2 ± 3.7	97
Map Contour 2	6.1 ± 5.5	71	4.4 ± 4.2	97
Map Contour 1	9.1 ± 7.7	57	6.7 ± 4.3	87

GPlates Data File

Download the supplementary file (http://www.earthdynamics.org/data/Data_Torsvik.zip) and unzip all files to a common subdirectory. The GPlates Data contains three main files:

(1) Palaeozoic_SAfrica_Frame_2014.rot
(2) Palaeozoic_Plates_Simple.shp (*and other extensions*)
(3) SMEANSLOW1_ID1.shp (*and other extensions*)

File 1 is a standard format GPlates rotation file (Supplementary Table S1) but all fits (for a selection of continents and smaller blocks) are relative fits versus a longitude-calibrated South Africa (Plate Id = 701) between 250 and 540 Ma. The header (top 13 lines) includes our true polar wander (TPW) model. At GPlates start-up, select all the three unzipped files. GPlates defaults to a mantle frame at start-up (Plate Id = 0) and reconstructions will be displayed as TPW corrected (like the lower panels in Figs. S7-36) because of our header in the rotation file. To show reconstructions with respect to the spin-axis (i.e. a palaeomagnetic frame) select in GPlates option "Reconstruction", then sub-option "Specify Anchored Plate ID" and type 1.

File 2 is an ARC-GIS shape that contains some selected continent outlines, whilst file 3 is an ARC-GIS shape file of the 1% SMEAN slow contour.

References

1. Gubanov AP, Mooney WD (2009) New global maps of crustal basement age. *Eos Trans. AGU* 90, Fall Meet. Suppl., Abstract T53B-1583.
2. Torsvik TH, Burke K, Steinberger B, Webb SC, Ashwal LD (2010) Diamonds sourced by plumes from the core mantle boundary. *Nature* 466:352-355.
3. Burke K, Steinberger B, Torsvik TH, Smethurst MA (2008) Plume Generation Zones at the margins of Large Low Shear Velocity Provinces on the Core-Mantle Boundary. *Earth Planet. Sci. Lett.* 265:49-60.
4. Torsvik TH, Steinberger B, Cocks LRM, Burke K (2008) Longitude: Linking Earth's ancient surface to its deep interior. *Earth Planet. Sci. Lett.* 276:273-283.
5. Becker TW, Boschi L (2002) A comparison of tomographic and geodynamic mantle models. *Geochem. Geophys. Geosys.* 3:doi:2001GC000168.
6. Torsvik TH, Smethurst MA, Burke K, Steinberger B (2006) Large Igneous Provinces generated from the margins of the Large Low Velocity Provinces in the deep mantle. *Geophys. J. Intern.* 167:1447-1460.
7. Leat PT, Dean AS, Millar IL, Kelley SP, Vaughan APM, Riley TR (2005) In Terrane Processes at the Margins of Gondwana (eds. A.P.M. Vaughan, P.T.Leat & R.J. Pankhurst). *Geological Society of London Special Publication* 246:359-380.
8. Eldholm O, Coffin MF (2000) Large Igneous Provinces and plate tectonics, in: MA Richards, RG Gordon, RD van der Hilst (Eds.), The History and Dynamics of Global Plate Motions, American Geophysical Union, Washington, pp. 309– 326.
9. Torsvik TH, Smethurst MA, Burke K, Steinberger B (2008) Long term stability in Deep Mantle structure: Evidence from the ca. 300 Ma Skagerrak-Centered Large Igneous Province (the SCLIP). *Earth Planet. Sci. Lett.* 267:444-452.
10. Chauvet F, *et al.* (2008) Geochemistry of the Panjal Traps basalts (NW Himalaya): records of the Pangea Permian break-up. *Bull. Soc. Géol. Fr.* 179:383-395.
11. Kuzmin MI, Yarmolyuk V, Kravchinsky VA (2010) Phanerozoic hot spot traces and paleogeographic reconstruction of the Siberian continent based on interaction with the African large low shear velocity province. *Earth-Science Reviews* 102:29-59.
12. Torsvik, TH, *et al.* (2012) Phanerozoic polar wander, paleogeography and dynamics. *Earth-Sci. Rev.* 114:325-368.
13. Steinberger B., Torsvik TH (2008) Absolute plate motions and true polar wander in the absence of hotspot tracks. *Nature* 452:620-623.
14. Gradstein FM, Ogg JG, Smith AG (Eds.) (2004) *A Geologic Time Scale 2004*. Cambridge University Press, Cambridge, 589 pp.
15. Van der Voo R (1993) Paleomagnetism of the Atlantic, Tethys and Iapetus Oceans. *Cambridge University Press*, 411 pp.
16. Torsvik TH, Cocks LRM (2011) The Palaeozoic palaeogeography of central Gondwana. In: Van Hinsbergen, DJJ, Buiter, SJH, Torsvik, TH, Gaina, C, Webb, SJ (eds.) The Formation and Evolution of Africa: A Synopsis of 3.8 Ga of Earth History. *Geological Society London Special Publications* 357:137–166.
17. Torsvik TH, Cocks LRM (2013) GR focus review: Gondwana from top to base in space and time. *Gondwana Research* doi.org/10.1016/j.gr.2013.06.012).
18. Cocks LRM, Fortey RA (2009) Avalonia: a long-lived terrane in the Lower Palaeozoic? *Geological Society London Special Publications* 325:141–155.
19. Cocks LRM, Torsvik TH (2011). The Palaeozoic geography of Laurentia and western Laurussia: a stable craton with mobile margins. *Earth-Science Reviews* 106:1–51.
20. Glass LM, Phillips D (2006) The Kalkarindji continental flood basalt province: a new Cambrian Large Igneous Province in Australia with possible links to faunal extinctions. *Geology* 34:461–464.

21. Torsvik TH, Paulsen TS, Hughes NC, Myrow PM, Ganerød M (2009) The Tethyan Himalaya: palaeogeographical and tectonic constraints from Ordovician palaeomagnetic data. *J. Geol. Soc. Lond.* 166:679-687.
22. Zhang H-F, *et al.* (2001) Geochemical significance of a garnet lherzolite from the Dahongshan kimberlite, Yangtze Craton, southern China. *Geochemical Journal* 35:315-331.
23. Liu G-L, Wang X-W, Lü X-M (1983) Dahongshan Lamproites. Geological Publishing House, Beijing, 186 pp. (in Chinese with English abstract).
24. Li Q-L, Wu F-Y, Li X-H, Qiu Z-L, Liu Y, Yang Y-H, Tang G-Q (2011) Precisely dating Paleozoic kimberlites in the North China Craton and Hf isotopic constraints on the evolution of the subcontinental lithospheric mantle. *Lithos* 126**:**127-134.
25. Torsvik TH, Rehnström EF (2003) The Tornquist Sea and Baltica-Avalonia docking. *Tectonophysics* 362:67-82.
26. Domeier M, Torsvik TH (2014) Focus Review Paper: Plate kinematics of the Late Paleozoic. *Geoscience Frontiers:*10.1016/j.gsf.2014.01.002 (in press).
27. McInnes BIA, Evans NJ, McDonald BJ, Kinny PD, Jakimowicz J (2009) Zircon U-Th-Pb-He double dating of the Merlin kimberlite field, Northern Territory, Australia. *Lithos* 112S:592-599.
28. Lapierre, H, *et al.* (2004) The Tethyan plume: geochemical diversity of Middle Permian basalts from the Oman rifted margin. *Lithos* 74:167-198.
29. Zhou M-F, *et al.* (2002) A temporal link between the Emeishan Large Igneous Province (SW China) and the end-Guadalupian mass extinction. *Earth Planet. Sci. Lett.* 196:113–122.
30. Bowring SA, Erwin DH, Jin YG, Martin MW, Davidek K, Wang W (1998) U/Pb zircon geochronology and tempo of the End-Permian mass extinction. *Science* 280 :1039–1045.
31. Reichow MK, *et al.* (2009) The timing and extent of the eruption of the Siberian Traps large igneous province: Implications for the end-Permian environmental crisis. *Earth Planet. Sci. Lett.* 277:9–20.
32. Svensen H, Planke S, Polozov AG, Schmidbauer N, Corfu F, Podladchikov YY, Jamtveit B (2009) Siberian gas venting and the end-Permian environmental crisis. *Earth Planet. Sci. Lett.* 277:490–500.
33. Muttoni G, Gaetani M, Kent DV, Sciunnach D, Angiolini L, Berra F, Garzanti E, Mattei M, Zanchi A (2009) Opening of the Neo-Tethys Ocean and the Pangea B to Pangea A transformation during the Permian. *GeoArabia* 14:17-48
34. Boyden JA, Müller RD, Gurnis M, Torsvik TH, Clark JA, Turner M, Ivey-Law H, Watson RJ, Cannon JS (2011) Next-generation plate-tectonic reconstructions using GPlates, in G.R. Keller & C. Baru (eds.): *Geoinformatics: Cyberinfrastructure for the Solid Earth Sciences*, Cambridge University Press, 95-113.
35. Lekic V, Cottar S, Dziewonski A, Romanowicz B (2012) Cluster analysis of global lower mantle tomography: A new class of structure and implications for chemical heterogeneity. *Earth Planet. Sci. Lett.* 357:68-77.